SYNTHESIS, CHARACTERIZATION AND CATALYTIC ACTIVITY OF SILICOALUMINOPHOSPHATE (SAPO) AND METAL ALUMINOPHOSPHATE (MEAPO) MOLECULAR SIEVES

A THESIS

SUBMITTED TO THE

UNIVERSITY OF POONA

FOR THE DEGREE OF

DOCTOR OF PHILOSOPHY

(IN CHEMISTRY)

BY

ANIL KUMAR SINHA

CATALYSIS DIVISION

NATIONAL CHEMICAL LABORATORY

PUNE - 411 008, INDIA

JANUARY 1999

CERTIFICATE

Certified that the work incorporated in the thesis **"Synthesis, Characterization and Catalytic Activity of Silicoaluminophosphate (SAPO) and Metal Aluminophosphate (MeAPO) Molecular Sieves"** submitted by **Mr. Anil Kumar Sinha**, for the degree of **Doctor of Philosophy**, was carried out by the candidate under my supervision in the Catalysis Division, National Chemical Laboratory, Pune, India. Materials obtained from other sources have been duly acknowledged in the thesis.

Dr. S. SIVASANKER 21/1/99

(Research Guide)

ACKNOWLEDGMENTS

I wish to express my sincere gratitude to Dr. S. Sivasanker, Deputy Director, National Chemical Laboratory, Pune for his invaluable guidance, thought provoking discussions and the help rendered throughout the course of this investigation without which I would not have completed this thesis successfully.

I wish to offer my sincere thanks to Dr. A.V. Ramaswamy, Head, Catalysis Division for providing me all the facilities to conduct research.

I am grateful to Drs. B.S. Rao, P.R. Rajmohanan, Nalini Jacob, A. Behlekar, G. Sainkar, H.S. Soni, K.R. Kamble, Bokade, Kavedia, R. Vetrivel, D. Srinivas, C.V.V.Satyanarayana, S.P. Mirajkar, S.V. Awate, M. Agashe, A.J. Chandwadkar; Mr. Ramakrishnan, Mr. Manna Katti, Mr. Madhusudan and all other scientific and non-scientific staff of the Catalysis Division, NCL, Pune, for extending their cooperation in all ways to complete my research work successfully.

I would be failing in my duty if I do not thank my friends, especially, Sindhu for helping and encouraging me in all ways throughout my work, Raghavan, Rajaram, Karuna, Priyabrata, Rajesh Pandey, Sanjay, Sabde, Suhas, Suresh, Patric, Subho, my seniors, Venkatathri, Debasis, Tapan, Naval and Tapas for encouraging me and providing a friendly working environment.

I am indebted to my brothers Sunil and Akhilesh and sisters, Meena and Neelam, nephew Rahul and all the other relatives who gave full support and encouragement during the course of my research work.

I thank the Director, NCL, Pune, Dr. P. Ratnasamy, for permitting me to submit this work in the form of a thesis, and the Council of Scientific and Industrial Research, New Delhi for providing me a research fellowship.

Anil Sinha

Anil Kumar Sinha

Place: Pune

Date: 21/1/99

.... TO MY PARENTS

CONTENTS

V. CATALYTIC ACTIVITIES OF SAPOs, MEAPOs and MeAPSOs

CHAPTER I

INTRODUCTION

1.1 GENERAL INTRODUCTION

Molecular sieves were first defined by McBain (1932) [1] as materials which separate components of a mixture on the basis of molecular size and shape differences. Two important classes of molecular sieves are zeolites (aluminosilicates) and aluminophosphates ($AlPO_4$s). These materials have generated interest as potential catalysts and as supports for catalytically active metals, resulting in extensive research on the synthesis of new zeolites and $AlPO_4$s during the last 50 years. Even though the synthesis of aluminophosphate hydrates (including variscite and metavariscite) was reported in 1961 [2] it was the discovery of the electroneutral aluminophosphates in 1982 [3] and the possibility of tailoring their acidity and catalytic activity by incorporating Si (SAPOs) [4] or other metal ions (MeAPOs, MeAPSOs) [5-11] that spurred a great interest in this class of molecular sieves.

1.2 ALUMINOPHOSPHATE MOLECULAR SIEVES

In all microporous crystalline aluminophosphate structures there is a three-dimensional network of one to one combination of alternating P (V) and Al (III) with an oxo-bridge between them resulting in an electroneutral framework. Cloverite, $AlPO_4$-12 [12], JDF-20 [13] with interrupted frameworks and $AlPO_4$-14A with Al-O-Al bonds [14] are the only exceptions to this $AlPO_4$ concept. Higher electronegativity of P than Al [15] in $AlPO_4$ framework results in permanent Al $\dashrightarrow$ P dipoles giving rise to polarity which is more pronounced in $AlPO_4$ structures with tubular pores (ATV, AEL, AFO, AFI, AET and VFI topologies) where P and Al atoms of the individual 2-D nets are positioned in discrete parallel planes.

As synthesized $AlPO_4$ structures can be subdivided according to aluminium coordination, into four classes :

(i) Four coordinated $AlPO_4$s ($AlPO_4$-5, -11, -12, JDF-20) where all framework aluminium are four coordinated (Al^{IV}). They are thermally and hydrothermally most stable.

(ii) $AlPO_4$ hydrates (variscite, metavariscite, $AlPO_4$-8, -H3, VPI-5, H1) with some framework Al atoms at specific framework positions which are six coordinated (Al^{VI}) and have two aquo-ligands in addition to the four oxo bridges to framework P atoms. They undergo phase transition on heating and dehydration.

(iii) In $AlPO_4$ hydroxides ($AlPO_4$-15, -14, -14A, -12, -21, -EN3, -17, -18, -31, -20) some specific Al atoms are five or six coordinated depending on whether these atoms are linked either to one hydroxo ligand (Al^{V}), one hydroxo ligand and one aquo ligand or to two hydroxo ligands (Al^{VI}).

(iv) $AlPO_4$ phosphates ($AlPO_4$-22) where a phosphate anion not belonging to the framework has its oxygens occupying a fifth coordination site of Al^{V} atoms.

$AlPO_4$s are synthesized by the hydrothermal treatment of reactive aluminophosphate gels (prepared from psuedoboehmite or aluminium isopropoxide as Al source and orthophosphoric acid as P source) with a general composition: $1Al_2O_3$: 1 P_2O_5 : 1R : x H_2O (x = 30 - 70; R = an organic amine or quarternary ammonium salt) in the preferred temperature range of 397 - 473 K and a gel pH range of 3 to 6.5.

As in the case of zeolites, $AlPO_4$s can be classified on the basis of their pore size into small (8 membered ring, 3-4.3 Å), medium (10 membered ring, 6 - 6.5 Å), large (12 membered ring, 7-8 Å) and mesoporous (18 membered ring, 12 Å).

1.3 ALUMINOPHOSPHATE FORMATION

Preparation of aluminophosphate molecular sieves entails the hydrothermal treatment of an aqueous gel containing a template amine or quartenary ammonium species. Some structures can only be obtained with a specific template, such as JDF-20 [16], which can be synthesized only with triethylamine as the template. In contrast, others such as $AlPO_4$-5 [17] can be made in the presence of any of more than 23 amines.

In recent years, significant progress has been made on the developement of mechanisms of formation of zeolites and aluminophosphate molecular sieves. Some models account for the final framework structures by postulating various building blocks, such as four-rings, six-rings and other small secondary building units (SBUs), similar to those believed to be involved in zeolite formation [18, 19]. More recently, the role of the organic template has been examined by Lewis *et al.* [20, 21]. Their calculations were performed on aluminophophate, metal-substituted aluminophosphate and zeolite frameworks. Davis *et al.* have also made thermochemical calculations of both microporous and dense phase aluminophosphates [22]. These results have led to a better understanding of the synthesis of aluminophosphate framework structures.

Other older models for the formation of aluminophosphates are based on chain species such as the narsarsukite, double-crankshaft [23, 24] and triple-crankshaft chains [25] that run through the structure parallel to the main channel system. Although these species can be identified in the frameworks, there is no direct evidence that they participate in the assembly process. Furthermore, double- or triple-crankshafts are rather complex and are difficult to envisage as stable species in the solution. It has also been suggested that psuedoboehemite is intercalated by

polyphosphate, which forms an amorphous aluminophosphate layer either directly [26, 27] or via molecular species that are present in the aluminophosphate solution [28, 29]. The disordered layered material is proposed to undergo a solid-state transformation to give the crystalline framework.

Recently a new self assembly model for the formation of aluminophosphates ha been developed by Oliver *et al.* [30] in which a progenitor chain is introduced, which accounts for the formation and structures of a family of one dimensional (1D) chain, two dimensional (2D) porous layer and three dimensional (3D) open-framework aluminophosphate materials. The building block (progenitor chain) for this model is a linear chain aluminophosphate, which is the first species to crystallize from the synthesis system. Structural, stereochemical, charge and chemical information present in the chain precursor can be transcribed, under a particular set of experimental conditions, to allow the formation of other chain types through a hydrolysis-condensation self-assembly pathway. The sibling aluminophosphate chains can be crystallized from the system or condense further to more complex porous layer or open-framework aluminophosphate structures.

1.4 ISOMORPHOUS SUBSTITUTION

Replacement of an element in a crystal lattice by another element with similar cation radius and coordination number is called isomorphous substitution. Generally, the atom to be incorporated into the framework is added to the synthesis gel before crystallization. Isomorphic substitution mechanism can be classified broadly into three types [31, 32]:

(1) Substitution of Al atoms (SM I); this can be further subdivided according to the valency of the elements introduced: monovalent elements (SM I_a), bivalent elements (SM I_b) and trivalent elements (SM I_c).

(2) Substitution of P atoms (SM II); this can be further subdivided as: SM II_a when a tetravalent element is incorporated and SM II_b when a pentavalent element is incorporated.

(3) Substitution of a pair of adjacent Al and P atoms (SM III) which has so far been observed only with silicon.

Substitution mechanisms of type SM I_a, SM I_b and SM II_a lead to a negative charged framework and have the potential for Bronsted acidity and cation exchange after removing the organic template from the framework. Substitutions that lead either to a positively charged framework or to an excessive negative charge density are unlikely [32]. Four coordinated $AlPO_4$s are most susceptible to isomorphic substitution [31,32]. Since the positively charged template acts as the charge compensating ion, the template to framework stoichiometry dictates the maximum degree of substitution. So smaller template molecules will lead to higher substitution than a bigger one for the same framework structure.

For $AlPO_4$ hydroxides, the template balances the anionic ligands (OH^-); so, for isomorphic substitution, the framework should be stable even after the OH^- is removed and the template should balance the negative charge created by isomorphic substitution. $AlPO_4$ hydrates are least susceptible to isomorphic substitution.

1.4.1 Silicoaluminophosphates (SAPOs)

The composition of anhydrous SAPOs can be represented as $aR.(Si_xAl_yP_z)O_2$ where R is the occluded template and 'a' its molar ratio. Their adsorption properties,

pore size and thermal / hydrothermal stability resembles those of the $AlPO_4$ molecular sieves. They possess weak to strong acidities depending on the silicon concentration and structure type.

Si incorporation can take place by SM II_a which results in a net negative charge which is compensated by a proton (after calcination) resulting in acidity. Si substitution by SM III mechanism on adjacent Al and P atoms will give rise to Si-O-P linkage which is not feasible [32]. So SM III can apply only in an hetrogeneous way (SM III he) wherein Si replaces Al and P right from the surface to a certain region in the framework so that there is no Si-O-P linkage but there is an $AlPO_4$ layer with a topotactic SiO_2 overlayer and no net charge is generated. In addition, Si can be incorporated by a combination of SM II_a and SM III mechanisms. The relative contribution of the two mechanisms depends on various synthesis parameters like Si content [33-43], nature of template [38, 44, 45], pH [33], crystallization time and temperature [43], amine/Al_2O_3 and P_2O_5/Al_2O_3 ratio in the synthesis mixture [46]. Generally, the Si atoms are initially incorporated by SM II_a mechanism but beyond certain Si concentrations, SM III also comes into play resulting in Si patches in which some Al atoms may also be present resulting in aluminosilicate regions with negative charge.

1.4.2Metal Aluminophosphates (MeAPOs) and Metal silicoaluminophosphates (MeAPSOs)

Around 13 elements have been incorporated in the neutral $AlPO_4$ framework [16]. These elements include, monovalent Li (SM I_a); divalent Be, Mg, Co, Fe Mn and Zn (SM I_b); trivalent B, Ga and Fe (SM I_c); tetravalent Ge and Ti (SM II_a); pentavalent As (SM II_b). Among these SM I_c and SM II_b types of substitution do not

generate framework charge. All the other types of substitution generate negative charge in the framework which is responsible for acidity. In addition, combinations of these elements as well as combinations of these elements with Si in the framework are possible.

The structure directing role of these incorporated elements can be seen from the fact that structures of type SAPO-37 and SAPO-40 have been prepared only in silicon-containing system. The acidity of these materials is both structure and metal dependent [47]. Some of these materials could be suitable for catalysing reactions requiring moderate acidity like the isomerization of n-alkanes. The thermal and hydrothermal stability of these materials is lower than that of the parent $AlPO_4$ and SAPO molecular sieves.

1.5 ACIDITY OF SAPOS, MeAPOS AND MeAPSOS

Acidity of SAPOs, MeAPOs and MeAPSOs is less than that of aluminosilicate zeolites because only a part of the silicon/metal incorporated generate acid sites in the framework. It is only the Si going to the P sites (SM II_a) that generates negative charge and acidity. Likewise, divalent metals substituting at Al sites (SM I_b) generate acidity (Fig. 1.1). Therefore, much effort has been devoted to tailoring the crystallization conditions to favour Si incorporation mainly at P sites [48-50]. Similarily, it is possible to find the conditions that favour divalent metal substitution at Al sites.

1.6 Shape Selectivity

Several authors have discussed in detail the basic concept of shape selectivity [51-53]. Chen *et al.* [54] have underlined the impact of shape selective zeolite catalysis in the petroleum and petrochemical industries. The preferential

isomerization of long chain n-alkanes on medium pore Pt/SAPO-11 and the preferential hydrocracking over large pore Pt/SAPO-5 catalysts [55] have been explained on the basis of the concept of shape selectivity [56-58]. The different types of shape selectivities observed in zeolites are discussed below.

1.6.1 Reactant Shape Selectivity

Reactant shape selectivity occurs when only some of the reactant molecules in the reaction mixture are small enough to diffuse through the zeolite pores and are thus converted to products while the other molecules are excluded. Chen *et al.*[59] have explained reactant shape selectivity on the basis of Coulombic interaction between the reactant and zeolite. An important application of reactant shape selectivity is in the dewaxing of petroleum oils to lower their "pour point" by selectively cracking/ isomerizing the long chain waxy paraffin molecules while "sieving" out branched molecules which enhance the quality of the lube oils.

1.6.2 Product Shape selectivity

Product shape selectivity occurs when one or more of the products formed within the pores or cavities diffuse out faster than the other products, leaving behind the bulkier molecules which are either converted to less bulky molecules that can diffuse out of the pore network or eventually form coke and deactivate the catalyst [60]. Product shape selectivity has been suggested to be responsible for the higher yields of the p-isomer during the isomerization of m-xylene over medium pore zeolites [61].

1.6.3 Restricted Transition State Shape Selectivity

Restricted transition state shape selectivity depends upon the size and the shape of the transition state complex formed during catalytic transformations inside the cavities of the molecular sieves. The products which result from the transition states that can be acomodated inside the pores are preferentially produced. The resistance of ZSM-5 and SAPO-11 to deactivation by coke deposition has been attributed to the fact that large "coke molecules" cannot be formed inside the pores due to restricted transition state selectivity. Additionally, the chemical nature of the active sites, the strength of the acid sites and electronic as well as thermodynamic effects have also been found to influence the overall selectivity pattern in certain reactions [62]. It has been found that the restricted transition state shape selectivity does not always guide the reaction path in molecular sieves, but electronic as well as thermodynamic effects predominate over steric effects [63].

1.6.4 Molecular Traffic Control

According to this concept, in the case of zeolites with more than one type of intersecting channels, the reactant molecules preferentially enter through one type of channel, while the products diffuse out through the other one minimising counter diffusion. Derouane and Gabelica [64] explained the concept of molecular traffic control in the conversion of methanol over H-ZSM-5. the smaller reactant molecules (methanol) enter through the sinusoidal circular channels, while the larger product molecules exit from the straight elliptical channels. However the existance of molecular traffic control is not yet experimentally confirmed.

1.6.5 Molecular Orbital Induced Shape Selectivity

Recently the role of the chemical nature of the reactant in directing selectivity has been interpreted by Corma *et al.* [65] on the basis of Pearson's principle of soft and hard acids and bases (SHAB). The SHAB principle can be extended to show that the energy levels of HOMO and LUMO orbitals play an important role in determining the path of the reaction [65]. The principle can also be used to explain the preferential position of attack (ortho, meta, para) of electrophiles on substituted aromatic compounds during electrophilic aromatic substitution and the ortho/para ratios of the products.

1.7 PHYSICOCHEMICAL CHARACTERIZATION TECHNIQUES

1.7.1 X-ray diffraction (XRD)

XRD is the most important technique to identify crystalline solids and to study the kinetics and mechanism of zeolite crystallization [66]. Variation in lattice parameters and framework symmetry [67, 68], collapse of crystal structure and the presence of alien phases are also detected by x-ray diffraction measurements.

1.7.2 Scanning electron microscopy (SEM)

SEM is a technique used to measure the particle size distribution and morphology of the crystals. The amorphous material present can be detected by scanning electron micrographs.

1.7.3 Infra red spectroscopy (IR)

Infrared spectroscopy is an important technique for the investigation of zeolite framework vibrations and is complementary to X-ray structure analysis. The fundamental vibrations of AlO_4/SiO_4 tetrahedra are in the mid infra red region (200 - 1300 cm^{-1}) and these have been used in conjunction with XRD to identify zeolite

structures [69]. It is found that the main Si-O, Al-O vibrational bands occur at about 1100 cm^{-1} and is related to the Si/Al ratio in the zeolite framework [70]. Crystallization of the zeolites during the synthesis has been studied by monitoring the changes in the framework IR vibrational frequencies and comparing these with those of the reactants [71]. It is also possible to study the progressive incorporation of the organic cation into the zeolite lattice by measuring the intensity of the bands characteristic of the organic cation. The IR technique has been extensively used to distinguish the different types of structural hydroxyl groups. The hydroxyl groups are characterized by adsorption bands in the region 3500 - 3750 cm^{-1}. IR is also used for detection and estimation of acid sites by absorption of bases.

1.7.4 Thermal analysis

This technique has been used [72,73] to obtain information on the synthesis mechanism as well as the thermal behaviour of the synthesized zeolites and identification of template decomposition products. Various physicochemical changes occuring during the thermal treatment are reflected in the DTA/TG/DTG profiles. Dehydration of adsorbed water, decomposition of the occluded organic cations and dehydroxylation at higher temperatures to produce Lewis acid sites are reflected in these thermoanalytical curves.

1.7.5 Adsorption studies

The void pore volume and surface areas of zeolite solids are often determined by low temperature (77 K) N_2 sorption. Analysis of such sorption isotherms have been found useful in determining the pore volume and pore size distribution of composite materials containing molecular sieves [74, 75].

1.7.6 Nuclear Magnetic Resonance Spectroscopy (NMR)

High resolution solid state MAS NMR spectroscopy has emerged as a powerful tool for the investigation of zeolite lattice structures and the location of various isomorphously substituted metal ions [76]. NMR is very sensitive to the local ordering and geometry. Till date, about 20 NMR active nuclei in zeolites [77] have been studied by this technique. It is also used to investigate Si and Al ordering [78] in the zeolite framework and to identify the crystallographically equivalent [79] and non-equivalent [80] Si and Al ions at various sites. It has also been used to calculate framework Si/Al ratios [81] and the coordination number of Si [82] and Al [83].

1.7.7 X-ray photoelectron spectroscopy (XPS)

XPS is an important tool for the characterization of surface properties of zeolites and related materials [84]. It yields information on the surface elemental composition, the oxidation state of elements and on the dispersion of one phase over another.

1.7.8 TPD of adsorbed pyridine

Temperature programmed desorption of adsorbed pyridine conditions [85] is used to determine the acid site distribution in many materials.

1.8 CATALYSIS USING SAPOS, MeAPOS AND MeAPSOS

Aluminophosphate molecular sieves have acidic activities and find catalytic applications in the conversion of hydrocarbons. As acid catalysts, they promote olefin isomerization and oligomerization but they are less effective at the competing hydride transfer and cracking reactions. In reactions involving aromatics, they are effective for skeletal isomerization but show low ethyl group disproportionation activity. As acid components of bifunctional catalysts, they are selective for paraffin and

cycloparaffin isomerization with low cracking activity. In general, medium pore SAPOs are more selective for olefin and paraffin isomerization than zeolites. They are also more resistant to coking.

The activity and selectivity for olefin oligomerization and the isomerization of C_8 aromatics is enhanced by the introduction of transition metals (MeAPOs and MePSOs). This could be attributed to uniquely located acid sites along with unexpected spatial effects in MeAPOs and MeAPSOs.

Some of the most promising applications, a few of which are expected to become commercial in the near future, are enumerated below:

(i) Dewaxing by isomerization:

While in conventional catalytic dewaxing, zeolites crack the paraffins to lighter olefinic materials, medium pore aluminophosphate compositions show outstanding selectivity in the catalytic dewaxing of heavy petroleum products [86, 87] through isomerization of the long-chain n-paraffins to non-waxy hydrocarbons of similar molecular weight resulting in incremental yield advantage and high product quality.

(ii) Production of p-xylene:

High catalytic activity and outstanding resistance to coke formation of these materials in the isomerization of ethylbenzene containing C_8 aromatics mixture to give high xylene yields provides an opportunity to commercially use these in the production of p-xylene [87].

(iii) Isomerization of olefins:

Isomerization of n-butenes to iso-butene and such other skeletal isomerization rections of olefins with low coking has been proved to be viable on SAPOs, MeAPOs and MeAPSOs [88].

(iv) Methanol to light olefin conversion:

High selectivity for ethylene and propylene and longer life-time than zeolitic catalysts for SAPO-34 like molecular sieves has been reported. The ethylene selectivity can be enhanced by the use of MeAPSO compositions [89].

(v) Alkylation of aromatics with methanol:

Medium pore aluminophosphate catalysts have been found to be highly selective for p-xylene production by shape selective alkylation of toluene with methanol [90].

(vi) Octane -boosting application:

Aluminophosphate based catalysts can be used as catalyst additives in FCC and hydrocracking as they show high selectivity for iso-alkanes when processing paraffins and olefins [91].

1.9 STRUCTURES OF SOME SAPOS

SAPO-11, SAPO-31 and SAPO-39 are aluminophosphate molecular sieves with medium and small pore openings. The typical structural properties of these silicoaluminophosphates are described below.

1.9.1 SAPO-11, MeAPO-11, MeAPSO-11

They have the framework topology of $AlPO_4$-11. The framework consists of unidimensional sheets of six ring - six ring - four ring units (6R-4R-4R)[92].

Unit cell Composition : $Al_{20}P_{20}O_{80}$, Symmetry : Orthorhombic; Space group : I_{cmm}

Unit cell constants : a = 13.5 Å; b = 18.5 Å; c = 8.4 Å

Pore Structure : 6.7 x 4.4 Å; Unidimensional.

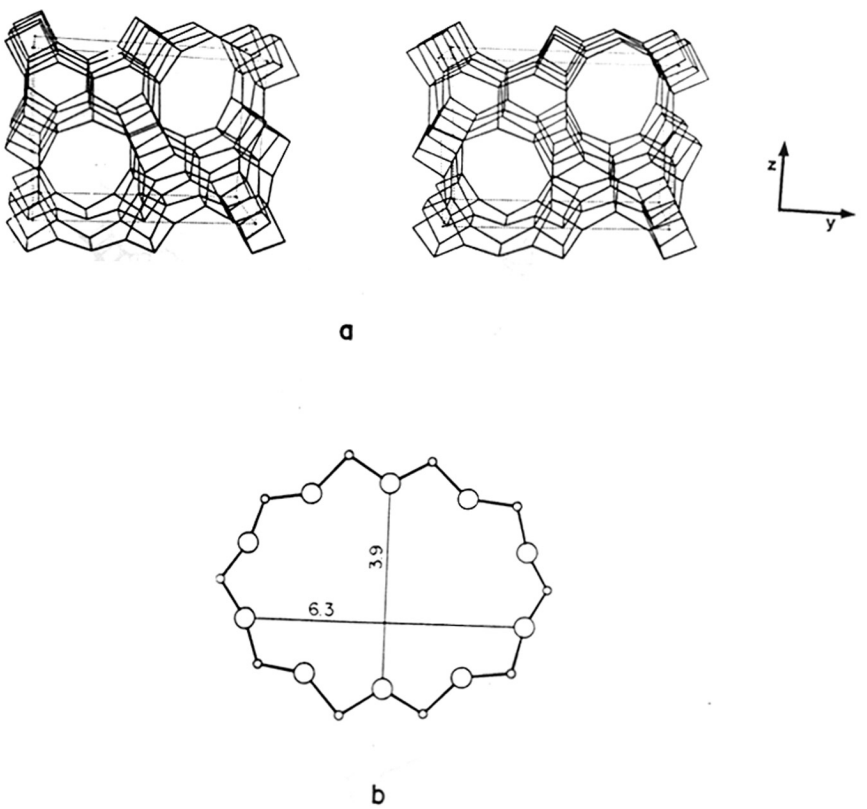

Figure 1.1. Structure of $AlPO_4$-11 [92]. (a) framework viewed along [001]; (b) 10 membered ring viewed along [100].

1.9.2 SAPO-31

It has the framework topology of $AlPO_4$-31. It consists of non-planar layers of D4R-D6R. 12-rings linked with staggered four rings. Entry into the structure is through 12-membered rings [93].

Unit cell composition : $Al_{18}P_{18}O_{72}$

Symmetry : Hexagonal

Space group : R3

Unit cell constants : a = b = 20.3 Å

c = 5.0 Å

Pore Structure : 5.4 Å; unidimensional.

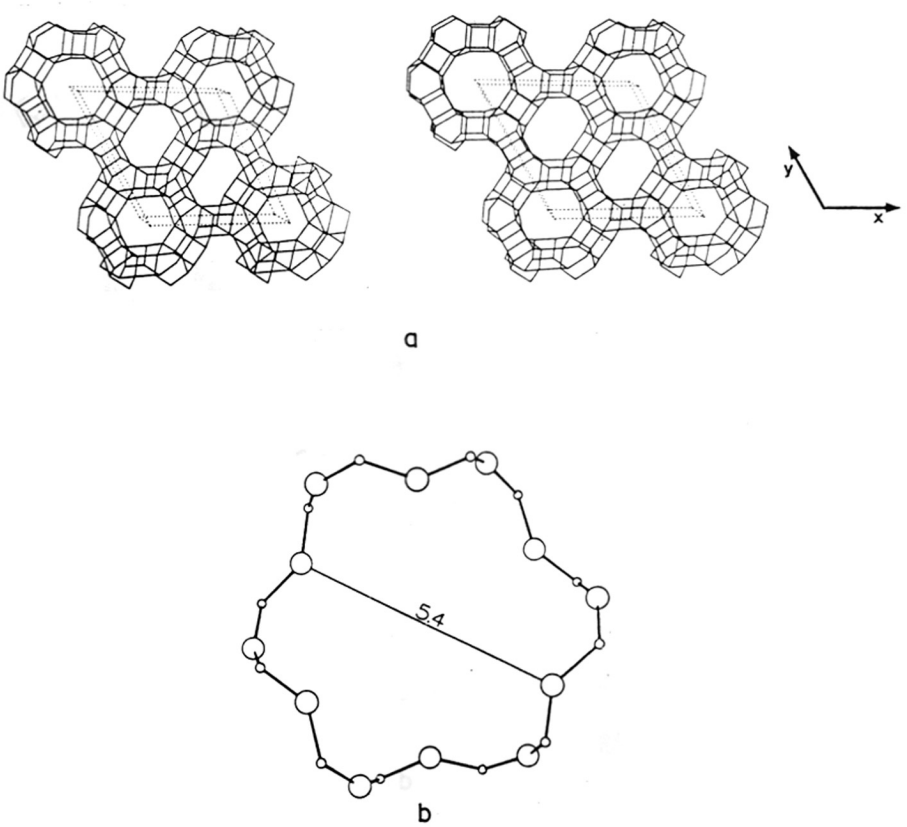

Figure 1.2. Structure of $AlPO_4$-31 [93]. (a) framework viewed along [001]; (b) 10 membered ring viewed along [100].

1.9.3 SAPO-39

It has the framework topology of $AlPO_4$-39. It is a small pore molecular sieve with eight-ring pore openings. It has eight member rings and cancrinite six-member rings [94].

Chemical Composition : $Al_8P_8O_{32}$

Unit cell constants : a = 13.09 Å

c = 5.18 Å

Pore Structure : 4.0 Å; unidimensional.

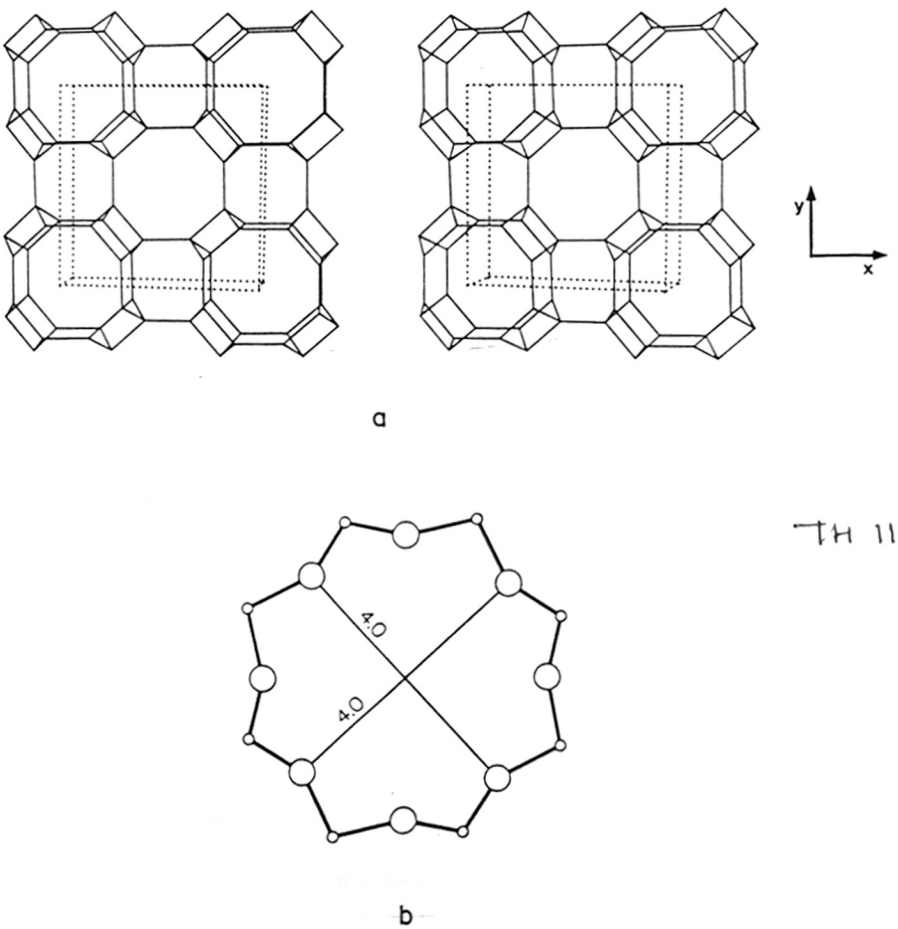

Figure 1.3. Structure of $AlPO_4$-39 [94]. (a) framework viewed along [001]; (b) 10 membered ring viewed along [100].

1.10 ISOMERIZATION OF N-ALKANES

Hydroisomerization of n-paraffins to branched paraffins is one of the main routes to produce high octane gasoline blending components [95], to improve the low temperature performance of diesel [96] and to obtain high viscosity index lube oils [97]. These isomerization reactions are generally carried out over bifunctional catalysts containing metallic sites for hydrogenation/ dehydrogenation and acidic sites for skeletal isomerization via carbenium ions [98]. The requirement of acid sites with high selectivity for desired products via shape selective reactions [58] has spurred a widespread interest in identifying new molecular sieves (zeolite and silicoaluminophosphate) - based catlysts for hydroisomerization.

During the isomerization of n-paraffins, shape selective molecular sieves suppress the formation of multibranched isomers [99], which are more susceptible to hydrocracking, thereby leading to high isomerization selectivities [100]. In general, methyl branching increases with decreasing pore width of the zeolite, whereas ethyl and propyl branched isomers are obtained from wide pore openings and large cavities. In the isomerization of n-decane, bifunctional 10-membered ring zeolites (ZSM-5 and ZSM-22) produce very little di- and tri-branched isomers. In addition, the formation of 4-methylnonane and 5-methylnonane were low when compared with that of the 2-methyl isomer [101-104]. Also, the isomerization of n-heptadecane over ZSM-22 resulted in the preferential formation of certain dimethyl isomers [105]. These results have been explained on the basis of a pore mouth catalysis mechanism operative when the reactant is a long chain n-alkane. Again, Pt-ZSM-22 (0.45 x 0.55 nm) showed a preferential central hydrocracking of n-decane different from that over the medium pore Pt-ZSM-5 (0.52 x 0.54 and 0.51 x 0.55 nm) [104].

1.11 SCOPE OF THE THESIS

SAPO molecular sieves have developed into industrially important catalysts [106]. They have been found to be effective catalysts in n-alkane isomerization p-xylene production, olefin oligomerization and isomerization, conversion of methanol to light olefins and alkylation of aromatics.

Si^{4+} incorporation at isolated P^{5+} sites in the framework results in maximum amount of acid sites. Insufficient and non-specific incorporation of Si in $AlPO_4$ lattice and poor crystallinity of the SAPOs [107-109] are major problems faced during the synthesis of SAPOs. Numerous efforts have been made in the past to overcome these problems [48-50] through modifications in synthesis methods such as the use of biphasic medium [110] and novel structure directing templates [111].

Hydroisomerization of n-paraffins is one of the major routes to produce high octane gasoline blending components, to increase the low temperature performance of diesel and to obtain high viscosity index lube oils. Due to their moderate acidities medium pore SAPO-11 and SAPO-31 have acquired considerable importance in these reactions. The aim of this work was to search for synthesis methods which would lead to materials with more Si present as isolated species in the framework resulting in more number of medium strength acid sites. Medium pore SAPO-11 and SAPO-31 were synthesized using two novel synthesis methods, using a non-aqueous synthesis medium and a rapid crystallization method. The influence of variation of synthesis method on the properties of the various samples was studied using various physicochemical characterization techniques such as SEM, XRD, TGA/DTA, MAS-NMR, TPD of adsorbed pyridine and XPS. The isomerization of n-hexane, n-octane,

n-hexadecane and m-xylene isomerization nreactions were used as test reactions to study the influence of synthesis methods on the catalytic activity and selectivity.

Small pore molecular sieves such as SAPO-34 and SAPO-44 have been reported to be efficient catalysts in the methanol to olefin conversion reaction. Keeping this in view, small pore SAPO-39 was synthesized (for the first time). It was characterized by XRD, TGA/DTA, SEM and FTIR of adsorbed NH_3. Further, the activity and selectivity of the samples were tested in the conversion of methanol to olefins.

To examine the influence of metal incorporation in the aluminophosphate framework on catalytic activity in the isomerization of n-hexane and m-xylene, Zn, Co, Mn and Mg containing $AlPO_4$-11 and SAPO-11 catalysts were synthesized and compared for their activities and selectivities in the said reactions.

MnAPO-11 synthesized from aqueous and non-aqueous media was characterized by SEM, TGA/DTA and ESR to study the influence of the synthesis medium on its physicochemical properties.

This work is presented in five more chapters.

The **second chapter** provides a description of the various experimental techniques adopted in the hydrothermal synthesis of the microporous materials under investigation and the various characterization techniques used in the present study. The methods adopted for the evaluation of the catalytic properties of the samples are also described.

In the **third chapter** the use of dipropylamine template in the synthesis of silicoaluminophosphate molecular sieves from aqueous and non-aqueous media and by a rapid crystallization method are described. The kinetics of crystallization of the different SAPOs are also presented. The conditions for the synthesis of SAPOs from

non-aqueous medium and a rapid synthesis method were optimised resulting in samples with higher crystallinities than those of the samples synthesized from aqueous medium. Besides the synthesis of MeAPO-11 and MeAPSO-11 is also discussed.

Chapter four presents the results of the characterization of SAPO-11, SAPO-31, SAPO-39, MeAPO-11 and MeAPSO-11 molecular sieves by different physicochemical methods. Elemental analysis provided the chemical composition of the synthesized materials. X-ray diffraction measurements were used to identify the phase purity of the synthesized materials and their stabilities on calcination. Phase purity was also determined by scanning electron microscopy. Acidity of SAPO-39 was studied by adsorption of NH_3 using IR spectroscopy, while that of SAPO-11 and SAPO-31 was studied by the TPD of adsorbed pyridine. The thermal properties of the samples were analyzed by TGA/DTA. Incorporation of Si in the SAPO-11 and SAPO-31 was examined by ^{29}Si MAS-NMR. Location of Mn in MnAPO-11 was studied using ESR spectroscopy.

Chapter five presents the details of the various reactions carried out over SAPO-11, SAPO-31, SAPO-39, MeAPO-11 and MeAPSO-11. Isomerization reactions of n-hexane, n-octane, n-hexadecane and m-xylene were carried out over SAPO-11 and SAPO-31 molecular sieves. Methanol to olefins conversion was carried out over the small pore SAPO-39 and compared with MAPO-39. Isomerization of n-hexane and m-xylene was carried out over MeAPO-11 and MeAPSO-11 and compared with the results obtained over SAPO-11 molecular sieves.

Finally, a summary of the above studies is presented in **chapter VI**

REFERENCES

1. McBain, J.W., "The sorption of Gases and Vapors by Solids", Rutledge and Sons, London, **Ch. 5**, (1932).
2. d'Yvoire, F., *Bull. Soc. Chim. Fr.* 1762 (1961).
3. Wilson, S.T., Lok, B.M. and Flanigen, E.M., *U.S. Patent* 4, 310, 440 (1982); Wilson, S.T., Lok, B.M., Messina, C.A., Cannan, T.R. and Flanigen, E. M., *J. Am. Chem. Soc.*, **104,** 1146 (1982).
4. Lok, B.M., Messina, C.A., Patton, R.L., Gajek, R.T., Cannan, T.R. and Flanigen, E.M., *U.S. Patent* 4,40,871 (1984); *J. Am. Chem. Soc.*, **106,** 6092 (1984).
5. Messina, C.A., Lok, B.M. and Flanigen, E. M., *U.S. Patent*, 4,544,143 (1985).
6. Wilson, S.T. and Flanigen, E.M., *Eur. Pat. Appl.* 132,708 (1985); U.S. Patent 4,567, 029 (1986).
7. Lok, B.M., Marcus, B.K., Flanigen, E.M., *U.S. Patent*, 4500 651 (1985).
8. Wright, L.J., Milestone, N.B., *Eur. Pat. Appl.* 0141662 (1985).
9. Pyke, D.R., Whitney, P., Houghton, H., *Appl. Catal.* **18**, 173 (1985).
10. Bond, G.C., Gelsthrope, M.R., Sing, K.S., *J. Chem. Soc., Chem. Commun.*, 1056 (1985).
11. Flanigen, E.M., Lok, B.M., Patton, R.L., Wilson, S.T., *Pure and Appl. Chem.*, **58 (10)**, 1351 (1986).
12. Parise, J.B., *J. Chem. Soc., Chem. Commun.*, 1449 (1984).
13. Huo, Q., Xu, R., Li, S., Xu, Y., Ma, Z., Thomas, J.M., Chippendale, *J. Chem. Soc., Chem. Commun.* 320 (1992).
14. Pluth, J.J. and Smith, J.V., *Acta Crystallogr.* **C43**, 866 (1987).
15. Uytterhoeven, L., Mortier, W.J. and Geerlings, P., *J. Phys. Chem.*, **16**, 50 (1989)

16. (a) Huo, Q., Xu, R., Li, S., Xu, Y., Ma, Z., Thomas, J.M., Chippendale, *J. Chem. Soc., Chem. Commun.* 875 (1992).

(b) Jones, R.H., Thomas, J.M., Chen, J., Xu, R., Huo, Q., Li, S., Ma, Z., Chippendale, A.M., *J. Solid State Chem.*, **102**, 204 (1993).

17. Szostak, R., "Handbook of Molecular sieves", Van Nostrand Reinhold, New York (1992).

18. Szostak, R., "Molecular Sieves: Principles of synthesis and identification", Van Nostrand Reinhold, Toronto (1983).

19. Ferey, G., *J. Flourine Chem.*, **72**, 187 (1995).

20. Lewis, D.W., Catlow, C.R.A., Thomas, J.M., *Chem. Mater.*, **8**, 1112 (1996).

21. Lewis, D.W., Willock, D.J., Catlow, C.R.A., Thomas, J.M., Hutchings, G.J., *Nature*, **382**, 604 (1996).

22. Hu, Y., Navrotsky, A., Chen, C., Davis, M.E., *Chem. Mater.*, 7, 1816 (1995)

23. Richardson, Jr., J.W., Smith, J.V., Pluth, J.J., *J. Phys. Chem.*, **94,** 3365 (1990).

24. Keller, F.B., Meier, W.M., Kirchner, R.M., *Solid State Ionics*, **43,** 93 (1990).

25. Li, H., Davis, M.E., Higgins, J.B., Dessan, R.M., *J. Chem. Soc., Chem. Commun.*, 403 (1993).

26. Jahn, E., Mueller, D., Richter-Mendau, J. "Synthesis of Microporous Materials", Vol. 1: Molecular Sieves (Eds.: Occelli, M.L., Robson, H.E.), Nelson Canada, Scarborogh, P. 248 (1992).

27. He, H., Klinowski, J., *J. Phys. Chem.*, **98,** 1192 (1994).

28. Davis, M.E., Young, D., *Stud. Surf. Sc. Catal.*, **60**, 53 (1991).

29. Davis, M.E., Murray, B.D., Narayana, M., *ACS Symp. Ser.*, **437**, 48 (1990).

30. Oliver, S., Kuperman, A., Ozin, G.A., *Angew Chem. Int. Ed.*, **37**, 46 (1998).

31. Flanigen, E.M., Lok, B.M., Patton, R.L. and Wilson, S.T., in 'New Developements

in Zeolite Science and Technology', Proceed. 7th Int. Zeolite Conf. (Eds. Murakami, Y., Lijima, A. and Ward, J.W.) Kodansha/Tokyo, Elsevier/Amsterdam 103 (1986).

32. Flanigen, E.M., R.L. Patton and Wilson, S.T., *Stud. Surf. Sci. Catal.*, **37**, 13 (1988).

33. Mertens, M., Martens, J.A., Grobet, P.J. and Jacobs, P.A., "Guidelines for Mastering the Properties of Molecular sieves", (Eds. Barthomeuf, D., Derouane, E.G. and Holderich, W.) NATO ASI, Ser. B, vol. 221, Plenum Press, New York, London, 1990, p.1.

34. Martens, J.A., Grobet, P.J. and Jacobs, P.A., *J. Catal.*, **126**, 299 (1990).

35. Hasha, D., Saldarriaga, L.S., Saldarriaga, C., Hathaway, P.E., Cox, D.F. and Davis, M.E., *J. Am. Chem. Soc.*, **110**, 2127 (1988).

36. Blackwell, C.S. and Patton, R.L., *J. Phy. Chem.*, **92**, 3965(1988).

37. Tapp, N.J., Milestone, N.B. and Bibby, D.M., *Stud. Surf. Sci. Catal.*, **37**, 393 (1988).

38. Janchen, J., Penchev, V., Loffler, E., Parlitz, B. and Stach, H., *Collect. Czech. Chem. Commun.*, **57**, 826 (1992).

39. Rajic, N., Stojakovic, D., S. Hocevar, Kancic, V., *Zeolites*, **13**, 384 (1992).

40. Man, P.P., Briend, M., Peltre, M.J., Lamy, A., Beaunier, P. and Barthomeuf D., *Zeolites*, **13**, 384 (1992).

41. Corma, A., Fornes, V., Franco, M.J., Melo, F., Perez-Pariente, J. and Sastre, E., Proceed. 9th International Zeolite Conference Vol. II (Eds. Von Ballmoos R., Higgins, J.B. and Treacy, M.M.J.) Butterworth - Heinemann, Stoneham, 1993, p. 343.

42. Makarova, M.A., Ojo, A.F., Al-Ghefaili, K.M. and Dwyer, J., Proceed. 9th

International Zeolite Conference Vol. II (Eds. Von Ballmoos R., Higgins, J.B. and Treacy, M.M.J.) Butterworth - Heinemann, Stoneham, 1993, p. 259.

43. Young, D. and Davis, M.E., *Zeolites*, **11**, 277 (1991).

44. Waug, R., Lin, C.F., Ho, Y.S., Len, L.J. and Chao, K.J., *Appl. Catal.*, **72**, 39 (1991).

45. Biaglow, A.L., Adamo, A.T., Kokotailo, G.T. and R.J. Gorte, *J. Catal.*, 131 (1991).

46. Jahn, E., Muller, D. and Becker, K., *Zeolites*, **10**, 151 (1990).

47. Flanigen, E.M., Report, Int. Symp. on Innovation in Zeolite Material Science. Nieuwpoort, Belgium, 6 Sept. 1987.

48. Singh, P.S., Bandyopadhyay, R. and Rao, B.S., *J. Chem. Soc., Far. Trans.*, **92**, 2017 (1996).

49. Vomscheid, R., Briend, M., Peltre, M.J., Man, P.P. and Barthomeuf, D., *J. Phys. Chem.*, **98**, 9614 (1995).

50. Herreros, B., and Klinowski, J., *J. Phy. Chem.*, **99**, 9514 (1995).

51. Chen, N.Y., Weisz, P.B., *Chem. Eng. Progr. Symp. Ser.*, **63**, 86 (1967).

52. Csicsery, S.M., *ACS Monograph*, **171**, 680 (1976).

53. Derouane, E.G., "Interrelation Chemistry" (Eds.Whittingham, M.S. and Jacobson, A.J.), p.101, Academic Press, New York, 1982.

54. Chen, N.Y. in "Shape Selective Catalysts in Industrial Applications", Marcel Dekker, Inc., New York, 1989.

55. Campelo, J.M., Lafont, F. and Marinas, J.M., *J. Chem. Soc., Faraday Trans.*, **91**, 1551 (1995).

56. Weisz, P.B., Frilette, V.J., Maatman, R.W. and Mower, E.B., *J. Catal.* **1**, 307 (1962).

57. Weisz, P.B., *Pure Appl. Chem.*, **52**, 2091 (1980).

58. Csicsery, S.M., *Zeolites*, **4**, 202 (1984).

59. Chen, N.Y. and Garwood, W.E., *Catal. Rev. Sci. Eng.*, **28**, 1 (1986).

60. Weisz, P.B., *Stud. Surf. Sci. Catal.*, **7A**, 3 (1981).

61. Dewing, J., *J. Mol. Cat.*, **27**, 25 (1984).

62. Lerchert, L., *React. Kinet. Catal. Let.* **46,** 153 (1992).

63. Weisz, P.B., Frilette, V.J., Matman, R.W. and Momer, E.B., *J. Catal.*, **1**, 307 (1962).

64. Derouane, E.G. and Gabelica, Z., *J. Catal.*, **65**, 486 (1980).

65. Corma, A., "Guidelines for Mastering the properties of Molecular Sieves" NATO Series, p.221.

66. Chao, K.J., Tasi, T.C., Chen and Warg, I.J., *J. Chem. Soc. Faraday Trans. I*, **77,** 547 (1981).

67. Denpsey, E., Kuhl, G.H. and Olson, D.H., *J. Phy. Chem.*, 387 (1969).

68. Smith, J.V., *Acta Cryst.*, **15**, 835 (1962).

69. Flanigen, E.M., Khatami, H., Symanski, H.A., 'Molecular Sieve Zeolites', Adv. Chem. Ser. 101, Amer. Chem. Soc., Washington DC, p. 201 (1971).

70. Lohodny-Sorac., D. and White, J.L., *J. Phy. Chem.*, **75**, 1408 (1971).

71. Whyte, J.R. and Della Betta, R.A., *Cat. Rev. Sci. Eng.*, **24**, 580 (1982).

72. Derouane, E.G., Detremmerie S., Gabelica, Z. and Blom, N., *Appl. Catal.*, **1**, 20 (1981).

73. Barrer, R.M., and Langloy, D.A., *J. Chem. Soc.*, **1817,** 3804 (1988).

74. Hung-Xin, Li, Martins, T.A., Jacobs, P.A., "Innovation in Zeolite Material Science" (Ed. Gribet, P.J.) p.75 (1987).

75. Tapp, N.J., Milestone, N.B. and Biby, D.M., ibid, p. 393.

76. Lippmann, E., Magi, M., Samoson, A., Engelhardt, A. and Grimmer, A.R., *J. Am. Chem. Soc.*, **102**, 4889 (1980).

77. Nagy, J.B. and Derouane, A.E.G., *ACS Symp.*, **368,** 2 (1988).

78. Lippmann, E., Magi, M., Samoson, A., Taramak, M. and Engelhardt, G., *J. Am. Chem. Soc.*, **103**, 4992 (1981).

79. Fyfe, C.A., Gobbi, G.C., Klinowski, J., Thomas, J.M. and Ramdas, S., *Nature*, **296,** 530 (1982).

80. Fyfe, C.A., Gobbi, G.C., Klinowski, J., Thomas, J.M., *J. Phy. Chem.*, **86**, 1247 (1982).

81. Engelhardt, G., Lohse, U., Lippmaa, E., Tarmak, M., Magi, M.Z., *Anorg. Allg. Chem.* **482**, 49 (1981).

82. Mastikhin, V.M. and Zmaraev, K.I.Z., *Phy. Chemie*, **152**, 332 (1987).

83. Muller, D., Garsenev, W., Behrens, H.J. and Scheler, G., *Chem. Phy. Lett.*, **79**, 59 (1981).

84. Stocker, M., *Microporous Materials*, **6**, 235 (1996).

85. Choudhary, V.R., Nayak, V.S., *Appl. Catal. A: Gen*, **4**, 31 (1983).

86. Pellet, R.J., Coughlin, P.K., Long, G.N. and Rabo, J.A., *US Patent*, 4880,760 (1989).

87. Gortsema, F.P., Springer, A.R., Long, G.N., US Patent, 4,880,700 UOP (1989).

88. Pellet, R.J., Coughlin, P.K., Long, G.N. and Rabo, J.A., US Patent, 4,859,314 (1989).

89. Pellet, R.J., Coughlin, P.K., Stainiulis, M.T., Rabo, J.A. and Long, G.N., US Patent, 4,791,083 (1988).

90. Gortsema, F.P., Pellet, K.J., Springer, A.R., Rabo, J.A. and Long, G.N., US Patent, 4,913,799 (1990).

91. Gortsema, F.P., Springer, A.R., Rabo, J.A. and Long, G.N., US Patent, 4,818,739 (1989).

92. Bennet, J.M., Cohen, J.P., Flanigen, E.M., Pluth, J.J. and Smith, J.V., *Am. Chem. Soc. Symp. Ser.*, **218**, 109 (1983).

93. Bennet, J.M. and Kirchner, R., *Zeolites,* **12**, 338 (1992).

94. McCusker, L.B., Brunner, G.D. and Ojo, A.F., *Acta Crystalogr. A* , **46**, C59 (1990).

95. Cusher, N.A.; Greenouch, P., Rolfe, J.R.K., Weiszmann, J.A., UCC (Shell) Hysomer Process; "Handbook of Petroleum Refining Process", (Ed. Meyers, R.A.) Mcgraw-Hill, New York (1986).

96. Miller, S.J., *Stud. Surf. Sci. Catal.*, **84 C**, 2319 (1994).

97. Miller, S.J., *Microporous Materials*, **2**, 439 (1994).

98. Alvarez, F., Ribuiro, F.R., Gianetto, C., Chevalier, F., Perot, C. and Guisnet, M., *Stud. Surf. Sc. Catal.*, **44**, 1339 (1989).

99. Ernst, S., Weitkamp, J., Martens, J.A., Jacobs, P.A., *Appl. Catal. A: Gen*, **48**, 137 (1989).

100. Martens, J.A., Jacobs, P.A., Weitkamp, J., Appl. Catal. A: Gen., **20**, 239 (1986).

101. Martens, J.A., Tielen, M., Jacobs, P.A., Weitkamp, J., Zeolites, **4,** 98 (1984).

102. Jacobs, P.A., Uytterhoeven, J.B., Steyns, M., Forment, G., Weitkamp, J., Proc. 5th Int. Zeolites Conf., Rees, Lovat, Heyden V.C., Naples, Italy, June 1980, Heyden, London, 1980, 397.

103. Jacobs, P.A., Martens, J.A., Weitkamp, J., Beyer, H.K., *Faraday Discuss. Chem. Soc.*, **72**, 353 (1982).

104. Weitkamp, J., Jacobs, P.A., Martens, J.A., *Appl. Catal. A: Gen.*, **8**, 123 (1983).

105. Martens, J.A., Jacobs, P.A., *Angew. Chem. Int. Ed. Engl.*, **34, No. 22**, 2528 (1995).

106. Miller, S.J., *US Patent*, 4,859,311 (1989).

107. Blackwell C.S., and Patton, R.L., *J. Phy. Chem.*, **92**, 3965 (1988).

108. Lohse, U., Vogt, F., Richter-Mendau, J., *Cryst. Res. Technol.*, **28**, 1101 (1993).

109. Barrett, P.A., Jones, R.H., Thomas, J.M., Sankar, G., Shannon, I.J., Catlow, C.R.A., *J. Chem. Soc. Chem. Commun.*, 2001 (1996).

110. Montoya-Urbina, M., Cardoso, D., Perez-Pariente, J., Sastre, E., Blasco, T. and Fornes, V., *J. Catal.*, **173**, 501 (1998).

111. Gao, Q., Li, S., and Xu, R., *J. Chem. Soc. Chem. Comm.*, 1465 (1994).

CHAPTER II

EXPERIMENTAL

2.1 INTRODUCTION

Synthesis of aluminophosphate based molecular sieves was carried out using reactive sources of alumina, orthophosphoric acid, templating agent, silica / metal source and heating the gel under hydrothermal conditions at autogeneous pressure. The sources of raw materials, the synthesis procedures adopted and the methods adopted for the chemical analysis of the samples are discussed in this section. The different instrumental techniques employed in the elucidation of structural features and properties of the synthesized products are also described.

2.2 SYNTHESIS

$AlPO_4$ based molecular sieves were synthesized hydrothermally using the reactants listed in table 2.1. In a typical synthesis procedure, an aluminium source (psuedoboehmite or aluminium isopropoxide) was stirred well mechanically with a solvent (water or ethylene glycol). Orthophosphoric acid was added dropwise to the mixture and further stirred well to get an aluminophosphate gel. To this gel, the required template was added and stirred. A silica source (fumed silica or silica sol) or (and) a metal source (as the acetate salt) was (were) next added (if necessary, to obtain SAPO, MeAPO or MeAPSO molecular sieves). Crystallization was carried out using a teflon lined stainless steel autoclave (Fig. 2.1) at 423 - 473 K for 1 - 15 days at autogeneous pressure. the final product was filtered, washed well with distilled water several times and dried at 393 K. The gel molar composition and duration of crystallization used for various SAPOs, MeAPOs and MeAPSOs are given in table 2.2. The exact synthesis procedure adopted for the different materials are presented in chapter 3.

Table 2.1 Specifications of the reactants used in the synthesis.

S. No.	Chemical Name (Supplier)	Chemical Formula	Purity (%)
1.	Aluminium isopropoxide (Aldrich)	$Al(OC_3H_7)_3$	98
2.	Pseudoboehmite (Vista)	Al_2O_3	74.2 (25.8% H_2O)
3.	Fumed silica (Fluka)	SiO_2	99.5
4.	Orthophosphoric acid (s.d. fine, India)	H_3PO_4	85 (15% H_2O)
5.	Dipropylamine (Aldrich)	$(C_3H_7)_2NH$	99
6.	Ethylene Glycol (s.d. fine, India)	$CH_2(OH)CH_2(OH)$	99
7.	Magnesium acetate (Loba, India)	$Mg(CH_3COO)_2.4H_2O$	99.5
8.	Zinc acetate (s.d. fine, India)	$Zn(CH_3COO)_2.2H_2O$	99.5
9.	Cobalt acetate (s.d. fine, India)	$Co(CH_3COO)_2.4H_2O$	99.5
10.	Manganese acetate (s.d. fine, India)	$Mn(CH_3COO)_2.2H_2O$	99.5

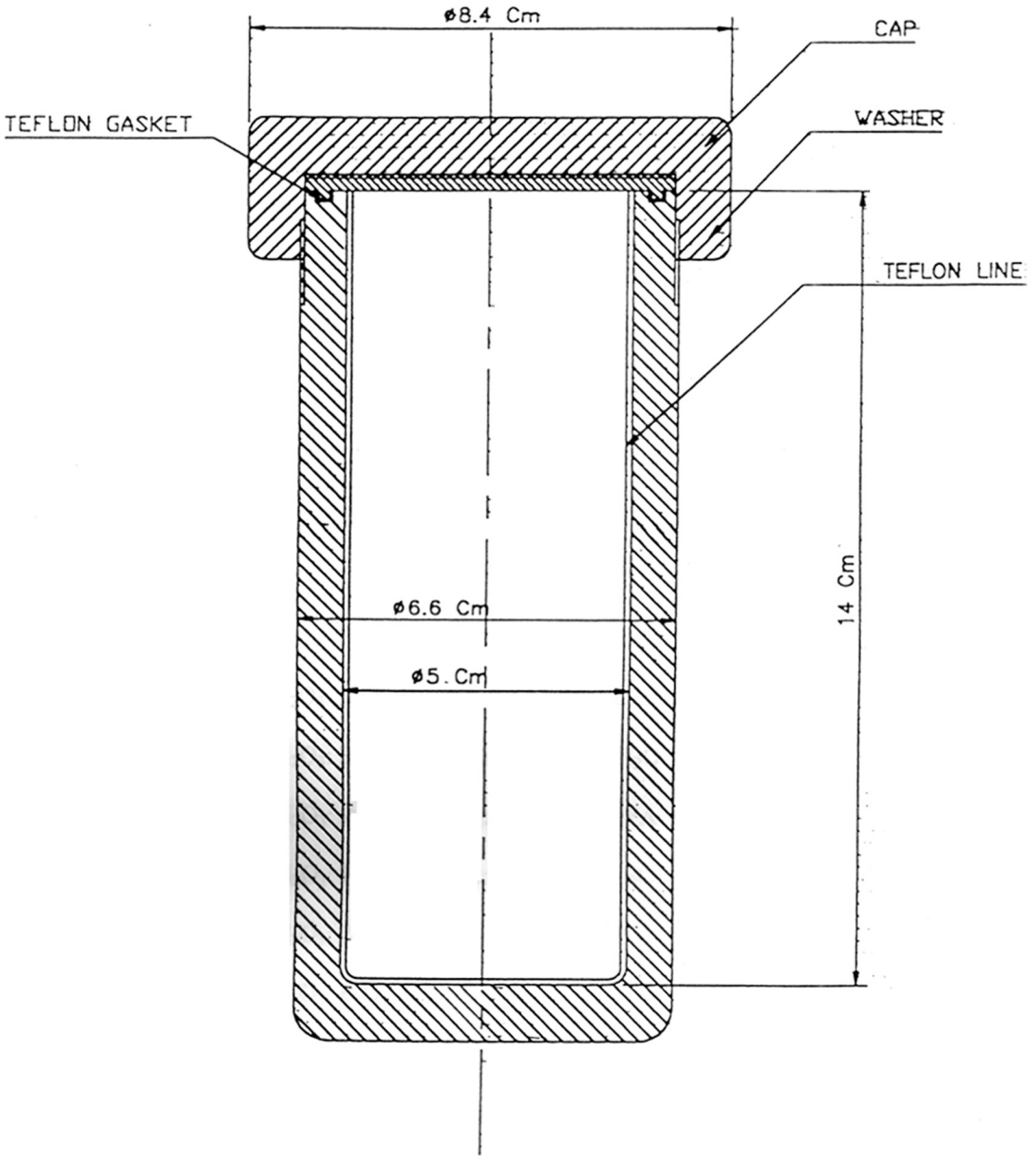

Figure 2.1. Stainless-steel autoclave with teflon gasket and liner for hydrothermal synthesis.

Table 2.2 Gel molar composition and duration of crystalization for SAPOs, MeAPOs and

MeAPSOs.

Structure	Gel composition	crystallization time
SAPO-11(a)	Al_2O_3: P_2O_5: 0.2SiO_2: 1 DPA :50 H_2O	24 h
SAPO-11(na)[a]	Al_2O_3: P_2O_5: 0.2 SiO_2: 5 DPA :60 EG	144 h
SAPO-31(a)	Al_2O_3:P_2O_5: 0.2 SiO_2: 1 DPA:50 H_2O	24 h
SAPO-31(na)[a]	Al_2O_3: P_2O_5: 0.2 SiO_2: 5 DPA :60 EG	72 h
SAPO-11(r)[b]	Al_2O_3:1.1P_2O_5:1.5DPA:0.2SiO_2: 40H_2O	2 h
SAPO-5 (r)[b]	Al_2O_3:1.1P_2O_5:1.5DPA:0.6SiO_2: 40 H_2O	0 h
SAPO-31 (r)[b]	Al_2O_3:1.1P_2O_5:1.5DPA:0.2SiO_2:40 H_2O	4 h
MgAPO-11	Al_2O_3: P_2O_5: 0.2MgO: 1 DPA :50 H_2O	24 h
MgAPSO-11	Al_2O_3: P_2O_5: 0.1SiO_2:0.1 MgO: 1 DPA :50 H_2O	24 h
MnAPO-11	Al_2O_3: P_2O_5: 0.2MnO: 1 DPA :50 H_2O	24 h
MnAPSO-11	Al_2O_3: P_2O_5: 0.1SiO_2: 0.1MnO:1 DPA :50 H_2O	24 h
CoAPO-11	Al_2O_3: P_2O_5: 0.2CoO: 1 DPA :50 H_2O	24 h
CoAPSO-11	Al_2O_3: P_2O_5: 0.1SiO_2:0.1CoO:1 DPA :50 H_2O	24 h
ZnAPO-11	Al_2O_3: P_2O_5: 0.2ZnO: 1 DPA :50 H_2O	24 h
ZnAPSO-11	Al_2O_3: P_2O_5: 0.1SiO_2:0.1ZnO: 1 DPA :50 H_2O	24 h
MnAPO-11(na)[a]	Al_2O_3: P_2O_5: 0.2 MnO: 5 DPA :60 EG	

a: Synthesized in ethylene glycol medium; all other samples were synthesized in aqueous medium.

b: Programmed gradual heating to 473 K; Crystallization temperature = 473 K

2.3 PRETREATMENT PROCEDURE

2.3.1 Calcination

All the above SAPOs, MeAPOs and MeAPSOs contained organic templates inside the channels in the as-synthesized form. For the characterization and application of these molecular sieves in catalytic reactions, it was necessary to remove the organic material from the pores of these molecular sieves. The as-synthesized material was placed in a petridish and calcined in a flow of air by slowly raising the temperature to 823 K and keeping at this temperature for 12 h. The temperature of the furnace was raised at the rate of 1.5 K/min.

2.3.2. Pt loading of samples

Pt was loaded on the SAPOs, MeAPOs and MeAPSOs by wet impregnation with an aqueous solution of $Pt(NH_3)_4Cl_2$. The resulting materials were dried at 393 K for 4 h and calcined at 723 K for 3 h in air.

2.3.3 Na-exchange of MnAPO-11

MnAPO-11(a) or MnAPO-11(na) (1 g each) was added to 1M NaCl (100ml) solution and stirred at 343 K for 5 h to exchange any extraframework Mn present with Na^+.

2.4 METHODS USED FOR PHYSICOCHEMICAL CHARACTERIZATION

2.4.1 Chemical Analysis

2.4.1A. *Estimation of aluminium as 8-hydroxy quinolate* $[Al(C_9H_6OH)_3]$

A known quantity of the calcined silicoaluminophosphate or metal alumonophosphate sample was dissolved in a few ml of conc. HCl, diluted and heated to 343-353 K and an appropriate amount (about 40 ml) of the oxime reagent was mixed and a 2 M ammonium acetate solution was then added slowly until a precipitate just appeared. The mixture was heated to boiling and again 25 ml of 2 M

ammonium acetate solution was added dropwise with constant stirring. The precipitate was allowed to cool and filtered through a quantitative filter paper (whatman no. 41) and washed with ice cold water. The precipitate was transferred into a previously weighed platinum crucible, dried, charred, ignited and weighed as Al_2O_3.

2.4.1B. *Estimation of phosphorous as magnesium phosphate ($Mg_2P_2O_7$)*

A known amount of the sample (about 0.5 g) was dissolved in a few ml of conc. HCl, diluted and boiled. A few drops of methyl red indicator was added to check for acid pH necessary to keep the aluminium in solution. Then 25 ml of magnesia mixture was added followed by pure concentrated ammonia solution while stirring vigorously until the indicator turned yellow. The solution was allowed to stand at room temperature for 24 h. The precipitate was then filtered, washed with dilute ammonia solution until the filtrate gave no turbidity with $AgNO_3$ and HNO_3. The precipitate was transferred to a platinum crucible, dried, charred and ignited to a constant weight and weighed as $Mg_2P_2O_7$.

2.4.1C *Estimation of silicon*

About 1 g of the sample was ignited in a platinum crucible to a constant weight. After cooling, it was moistened with a few drops of conc. H_2SO_4 and 5 ml of AR hydroflouric acid was added and slowly evaporated to dryness. The HF treatment was repeated thrice or more till there was no further weight loss. From the loss in weight silica was estimated.

2.4.1E *Estimation of metal ions in MeAPOsand MeAPSOs*

The samples were dissolved in minimum quantity of aqueous HF (~ 1 ml, 38%), followed by dilution to required concentration using double distilled water and the resulting solution was analyzed using AAS (Hitachi).

2.4.2A X-ray photoelectron spectroscopy

The surface chemical composition of the different samples were determined using X-ray photoelectron spectroscopy using Mg-K_α-radiation (ESCA-3-MK (II); (VG Scientific, UK) under evacuation to ca 10^{-8} torr.

2.4.2B X-ray diffraction

All the samples synthesied were analyzed for phase identification by X-ray powder diffraction (Rigaku, Model D/MAX III VC, Japan; Ni filtered Cu-Kα radiation, λ = 1.5404 Å; graphite crystal monochromator, computer assisted automated diffractometer). The X-ray crystallinity of the samples was calculated using the following equation. The most crystalline sample synthesized was taken as the standard.

$$\text{X-ray crystallinity} = \frac{\text{sum of the peak intensities of six major peaks x 100}}{\text{sum of the peak intensities of six major peaks of the standard sample}}$$

2.4.3 Scanning electron microscopy

The morphologies and particle sizes of all the samples synthesized were investigated using a scanning electron microscope (Leica Stereoscan 440 model; Leica Cambridge Ltd., UK). The samples were dusted on the holder, and coated with a thin film of gold to prvent surface charging and to protect the material from thermal damage by the electron beam. In all the analysis, a uniform film thickness of about 0.1 mm was maintained.

2.4.4 Infrared spectroscopy

The infrared spectra of the samples in the framework region (400 - 1300 cm^{-1}) were recorded using a Nicolet 60 SXB FT-IR instrument in the diffuse reflectance mode using 1:20 ratio of the sample to KBr mixture. For the range 1300 - 4000 cm^{-1},

self supported wafers were used. For *in situ* studies, a cell which could be heated to 773 K was used (Fig. 2.2). The cell was connected to a volumetric adsorption apparatus (Micrometrics, USA; model Accusorb-2000E). The sample was pressed under a pressure of 5 ton /inch^2 into a thin pellet (5-6 mg/cm^2) and mounted on the sample holder (SH). It was then placed inside the heating compartment (HC) of the cell and aligned in line with the IR beam. The cell was sealed at both the ends by potassium bromide windows (KW) with the help of elastomer 'O' rings. A thermocouple placed in close vicinity of the sample measured the temperature of the sample. The side tube at the top of the cell was connected to the high vacuum system. Cold water was constantly circulated through the cooling coil provided near the KBr windows. The sample was heated to 673 K at a heating rate of 5 K / min. under vacuum and maintained at this temperature for about 6 h and then cooled down to 323 K in vacuum. The spectra were recorded by averaging more than 100 scans with 2 cm^{-1} resolution. Vapours of ammonia were admitted to the sample through the adsorption manifold of the system..

2.4.5 Thermal Analysis

TG / DTA analysis of the crystalline phases were performed simultaneously on an automatic derivatograph (Setaram TG-DTA 92). The thermograms for the samples were recorded under the following conditions.

Weight of the samples = ~ 30 mg

Heating rate = 10 K/min.

Atmosphere = flowing air or nitrogen.

Preheated and finely powdered α-alumina was used as the reference material. The temperature range studied was from room temperature to 805 K.

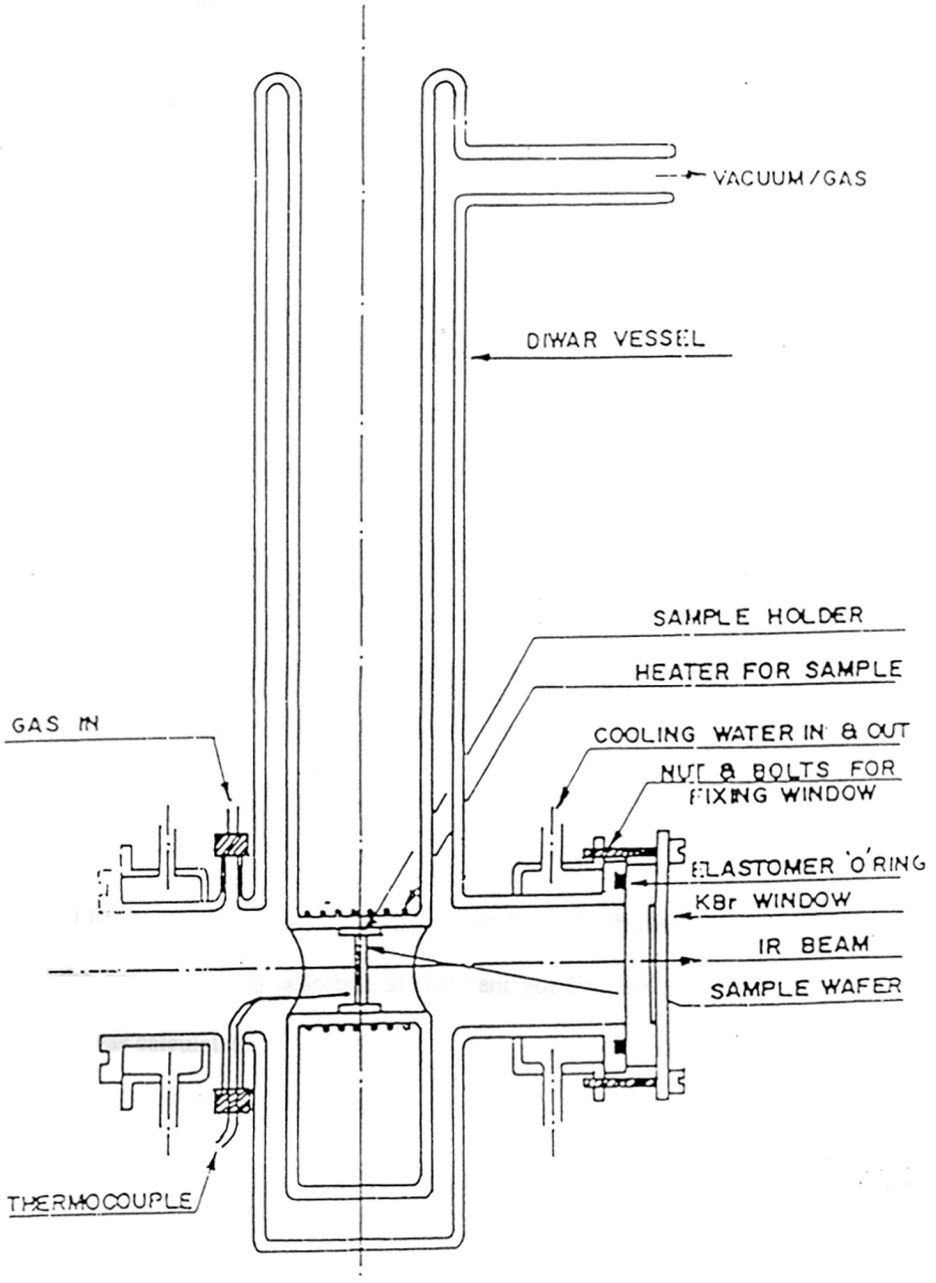

Figure 2.2. Sample cell for FT-IR spectrometer.

2.4.6 Nuclear magnetic resonance spectroscopy

MAS-NMR spectra were recorded in the solid state with a Bruker MSL 300 spectrometer operating at a field of 7 Tesla. ^{27}Al spectra were recorded at a frequency of 78.2 KHz, with a pulse length of 2 μs and a spinning speed of 3-5 KHz. The high resolution ^{29}Si MAS-NMR spectra were recorded at room temperature using "one cycle" type measurements. A 90° pulse with 3 μs delay time was used for ^{29}Si nuclei and chemical shifts (δ) in ppm were measured with respect to tetramethyl silane (TMS) as the external reference. The rotor (sample holder) was spun at the rate of 4.0 KHz.

2.4.7 Surface area measurments

A commercial adsorption unit (Omnisorb 100CX; Coulter Corporation, USA) was used for the measurement of nitrogen adsorption to determine the surface areas. The samples were activated at 673 K for 12 h in high vacuum (~ 10^{-5} mm). After the treatment, the anhydrous weights of the samples were recorded. The samples were then cooled to 94 K in liquid nitrogen and allowed to adsorb nitrogen gas. Finally, knowing the amount of N_2 adsorbed at different equilibrium pressures, the BET surface area was calculated.

2.4.8 Electron spin resonance spectroscopy

Electron spin resonance spectra of the MnAPO-11 samples synthesized from aqueous and non-aqueous media in as synthesized, calcined and Na-exchanged forms were recorded using a Bruker EMX X-band (ν = 9.75 GHz) spectrometer with 100 KHz field modulation. Samples were taken in suprasil quartz tubes and spectra were recorded at 298 and 77 K. Measurements at 77 K were done using a quartz insert Dewar. Spectral simulations and deconvolution were performed using Bruker WINPER and Simfonia packages.

2.4.9 Catalytic properties

Details regarding the different chemicals used in the catalytic reactions are presented in Table 2.3.

2.4.9A m-Xylene isomerization

m-Xylene isomerization and toluene alkylation with methanol were carried out in a fixed bed down flow tubular glass reactor at atmospheric pressure over the calcined samples. The catalyst powder was pelletized, sieved to 10-20 mesh size and 2 g of it was loaded in the reactor. The catalyst was activated at 823 K in air before each run. The reactant was fed using a syringe pump (Sage Instruments, USA). The products of the reaction were collected downstream from the reactor in a cold trap (0°C) and analyzed by a gas chromatograph (Shimadzu; Bentone column; FID detector) at different time intervals.

2.9B Methanol to hydrocarbon conversion reaction

Methanol conversion to hydrocarbons was carried out at different temperatures in a tubular glass reactor using 1.5 g of the catalyst after pelletizing and sieving to 10-20 mesh size. The reaction products were analyzed using a Hewlett-Packard gas chromatograph fitted with a flame ionization detector. A capillary column (50 m x 0.3 mm; HP1, methyl silicone gum; GC 5880A) was used for the separation of the products.

2.9C Isomerization of n-alkanes

The hydroconversion of n-alkanes was carried out in a fixed bed down flow tubular glass reactor at atmospheric pressure in the temperature range of 548 to 648 K, WHSV (h^{-1}) range of 1 to 4 and H_2/hydrocarbon (mole) ratio between 5 to 20. The catalyst powder was pelletized, sieved to 10 - 20 mesh size and 2 g of it was loaded into the reactor. Before activity measurements, the catalyst was activated at

648 K in flowing hydrogen (25 ml/min) for 1 h. The reactants were fed using a syringe pump (Sage instruments, USA). The reaction products were analyzed using a Hewlett-Packard gas chromatograph (5880A) with a flame ionization detector and a capillary column (50 m x 0.2 mm; HP1, cross linked methyl silicon gum). The isomeric products from n-hexadecane reaction were identified by GC-MS (Shimadzu, model QP2000A).

Table 2.3 The reagents used in various catalytic reactions.

S.No.	Chemical (Supplier)	Formula	Purity (%)
1.	n-hexane (s.d. fine-chem, India)	C_6H_{14}	99
2.	n-octane (s.d. fine-chem, India)	C_8H_{18}	99
3.	n-hexadecane (s.d. fine-chem, India)	$C_{16}H34$	99
4.	Methanol (s.d. fine-chem, India)	CH_3OH	99
5.	m-Xylene (Aldrich)	C_8H_8	99
6.	Platinum tetra-ammine dichloride (Aldrich)	$Pt(NH_3)_4Cl_2$	99

CHAPTER III

SYNTHESIS

3.1 INTRODUCTION

The studies carried out on the synthesis of silicoaluminophosphate molecular sieves using a single template, viz., dipropylamine are presented. Variations in synthesis conditions resulted in the synthesis of SAPO-11, SAPO-31, SAPO-5 and SAPO-39. SAPO-11 and SAPO-31 were synthesized from aqueous and non-aqueous meda. Metal containing $AlPO_4$-11 (MeAPO-11) and SAPO-11 (MeAPSO-11) were also synthesized using dipropylamine template.

3.2 SYNTHESIS OF SAPOs USING DIPROPYLAMINE AS TEMPLATE

3.2.1 Syntheis of SAPO-11, SAPO-31 and SAPO-39 by conventional synthesis procedures.

SAPO-11 was prepared according to the reported procedure of Lok et al. [1] from a gel of composition: Al_2O_3 : P_2O_5 : 0.2 SiO_2 : 1.0 Pr_2NH : 50 H_2O. SAPO-31 was also synthesized hydrothermally on the basis of method described by Lok et al. [1] from a reactive gel of composition 1.0 Al_2O_3 : 1.1 P_2O_5 : 0.2 SiO_2 : 1.0 Pr_2NH : 40 H_2O.

During the synthesis of SAPO-11, SAPO-39 was sometimes observed as an impurity phase. So, to get pure SAPO-39 material a single gel composition was used and the crystallization conditions were varied. The typical gel composition used for the crystallization of pure SAPO-39 was: 1.0 Al_2O_3 : 1.0 P_2O_5 : 0.3 SiO_2 : 1.3 Pr_2NH : 50 H_2O. A typical procedure to get pure SAPO-39 was as follows : psuedoboehemite (3.6g) was stirred in 10 g of distilled water for 15 minutes. A solution of 5.75 g of 85% orthophosphoric acid in 10 g of distilled water was added dropwise, and the resulting slurry was stirred for 2 h and aged overnight under slow stirring. Then dipropylamine (2.66 g) mixed with fumed silica (0.47 g) was added

slowly to the aged aluminophosphate gel with continuous stirring for 3h at room temperature. The gel was transferred into a teflon lined stainless steel autoclave and was heated under static conditions for 48 h. The solid product obtained was processed by washing with distilled water and was dried at 393 K for 24 h.

3.2.1.1 Crystallization of SAPO-39

Influence of varying the synthesis parameters during the synthesis of SAPO-39 is presented in table 3.1.

(a) Influence of Al / P ratio

Generally, aluminophosphate molecular sieves are prepared by using equimolar amounts of Al and P. If the gel composition is varied slightly from the mole ratio of 1, then impurity phases are formed. Table 3.1(a) shows the influence of changing the mole ratios of Al and P on the nature of crystalline phase obtained. Keeping all other synthesis parameters constant, increasing the molar ratio of Al in the synthesis gel resulted in co-crystallization of SAPO-11 and SAPO-39. But if the molar ratio of P was increased keeping Al ratio constant, then only SAPO-11 along with some impurity dense phases (crystobalite, trydimite and bernilite) was obtained.

(b) influence of template ratio

Decreasing the template molar ratio in the gel from 1.3 to 1.0 keeping all other synthesis parameters unchanged resulted in pure SAPO-11 material, but if the template ratio was increased from 1.3 to 1.6 it resulted in co-crystallization of SAPO-11 and SAPO-39 along with some dense phases.

Table 3.1(a) Influence of variation in Al/P ratio on the synthesis of SAPO-39.

Expt. #	Gel Composition						crystallization		pH (bc)[a]	pH (ac)[b]	Phase
	Al_2O_3	P_2O_5	SiO_2	Pr_2NH	H_2O	MgO	time	temp. (K)			
1	1.0	1.0	0.3	1.3	50	-	48	473	5.2	8.8	SAPO-39
2	1.1	1.0	0.3	1.3	50	-	48	473	5.0	9.1	SAPO-11+SAPO-39
3	1.2	1.0	0.3	1.3	50	-	48	473	4.8	8.9	SAPO-11+SAPO-39
4	1.0	1.1	0.3	1.3	50	-	48	473	5.0	8.6	SAPO-11 + C, T, B*
5	1.0	1.2	0.3	1.3	50	-	48	473	4.9	8.3	SAPO-11 + C, T, B*

[a]bc = before crystallization,

[b]ac = after crystallization,

*C = crystobalite; T = tridymite; B = Bernilite.

(c) Influence of water content

Variation of the water content in the gel from (50 to 40 or 60) resulted in SAPO-39 but the crystallinity was less than that of the material obtained with 50 molar ratio of water (Table 3.1 (c)).

(d) Influence of added metals

Adding Mg to the synthesis gel instead of Si resulted in pure MAPO-39 with the gel composition of 0.9 Al_2O_3 : 1.0 P_2O_5 : 0.4 MgO : 1.0 Pr_2NH : 40 H_2O in 96 h and at 423 K (table 3.1 (d)).

For the crystallization of pure $AlPO_4$-39 material, it was necessary to have a gel with molar composition 1.0 Al_2O_3 : 1.0 P_2O_5 : 2.0 Pr_2NH : 40 H_2O. Complete crystallization occured only after 48 h and at a crystallization temperature of 423 K.

3.2.1.2. Kinetics of crystallization of SAPO-11, SAPO-31 and SAPO-39

The variation in the crystallinity of the three SAPO materials with crystallization time is presented in Fig. 3.1. While the maximum crystallinity of SAPO-11 and SAPO-31 materials was obtained in 24 h, the most crystalline SAPO-39 was obtained only after 48 h. On extrapolation, the induction period for the three SAPOs was found to be in the decreasing order SAPO-11 < SAPO-31 < SAPO-39.

3.2.2 Synthesis of SAPO-11 and SAPO-31 from non-aqueous medium.

SAPO-11(na) and SAPO-31(na) were also prepared by a similar procedure but using a non-aqueous solvent, ethylene glycol (EG) using a gel with the composition Al_2O_3: P_2O_5: (0.2-0.8) SiO_2: 5 DPA : 60 EG. In a typical procedure for the non-aqueous synthesis, 11.6 g of aluminium isopropoxide was added slowly to 109.7 g of ethylene glycol under stirring and the mixture was stirred further for 1 h. Dipropylamine (14.2 g) was added dropwise to the stirring mixture and further stirred

Table 3.1(b) Influence of variation in template ratio on the synthesis of SAPO-39.

Expt.#	Gel Composition						crystallization		pH(bc)[a]	pH(ac)[b]	Phase
	Al_2O_3	P_2O_5	SiO_2	Pr_2NH	H_2O	MgO	time	temp. (K)			
6.	1.0	1.0	0.3	1.0	50	-	48	473	4.2	8.7	SAPO-11
7.	1.0	1.0	0.3	1.6	50	-	48	473	6.3	9.2	SAPO-11+SAPO-39 + C, T, B*

[a]bc = before crystallization,

[b]ac = after crystallization,

*C = crystobalite; T = tridymite; B = bernilite

Table 3.1(c) Influence of variation in water content on the synthesis of SAPO-39.

Expt. #	Gel Composition						crystallization		pH(bc)[a]	pH(ac)[b]	Phase
	Al_2O_3	P_2O_5	SiO_2	Pr_2NH	H_2O	MgO	time	temp. (K)			
8.	1.0	1.0	0.3	1.3	40	-	48	473	5.1	8.6	SAPO-39
9.	1.0	1.0	0.3	1.3	60	-	48	473	5.4	8.8	SAPO-39

Table 3.1(d). Influence of added metal on the synthesis of SAPO-39.

Expt. #	Gel Composition						crystallization		pH(bc)	pH(ac)	Phase
	Al_2O_3	P_2O_5	SiO_2	Pr_2NH	H_2O	MgO	time	temp. (K)			
10.	1.0	1.0	0.1	1.3	40	0.1	96	473	4.1	8.9	MAPSO-39
11.	0.9	1.0	-	1.0	40	0.4	96	423	3.6	9.2	MAPO-39
12.	1.0	1.0	-	1.3	60	-	48	423	6.0	9.4	AlPO-39

[a]bc = before crystallization, [b]ac = after crystallization.

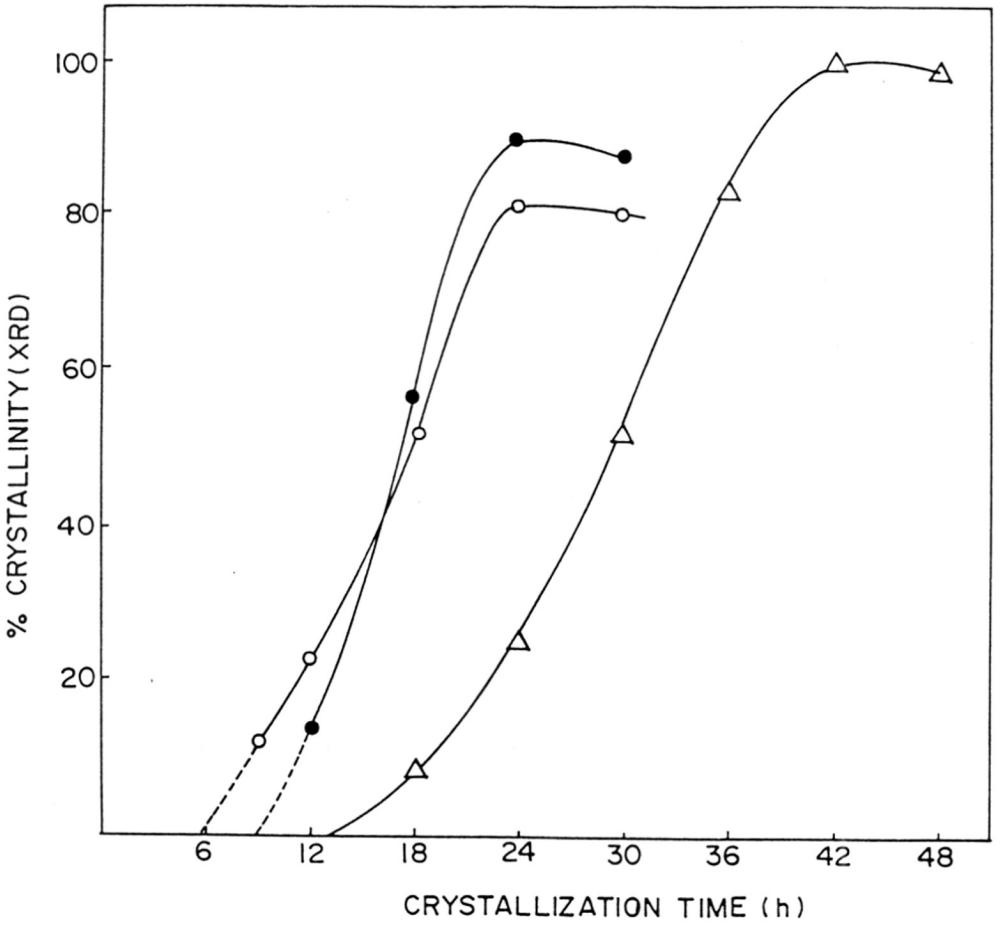

Figure 3.1. Variation in crystallinity with crystallization time. (o) SAPO-11(a), (•) SAPO-31(a) and (Δ) SAPO-39.

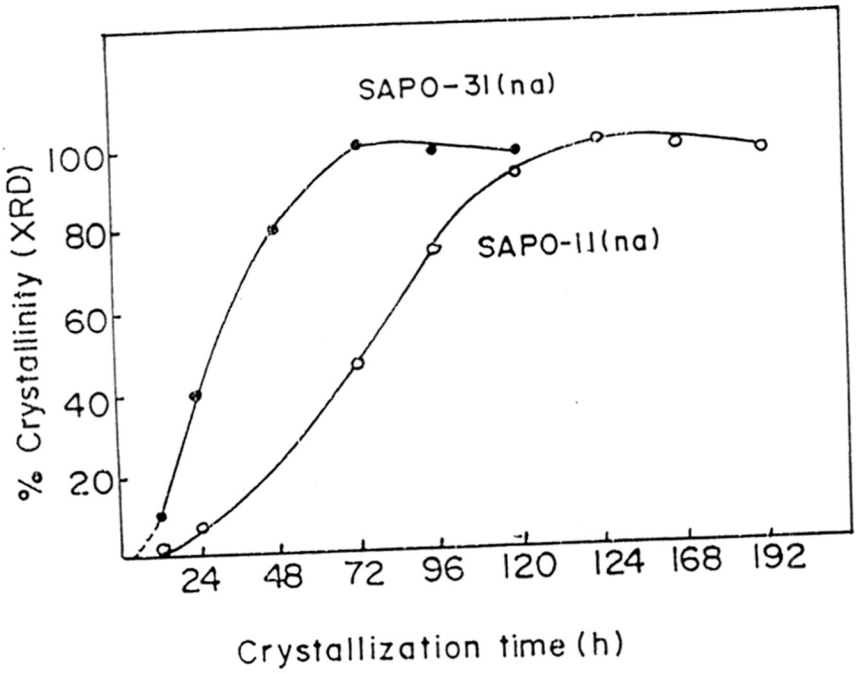

Figure 3.2. Variation in crystallinity with crystallization time. (o) SAPO-11(na) and (•) SAPO-31(na)

for 0.5 h. Then, 11.5 g of orthophosphoric acid was added dropwise and stirred for another 0.5 h. Finally, 0.34 g of fumed silica was added and the final mixture was stirred for 2 h to get a homogeneous gel which was transferred to a stainless steel autoclave and heated at 473 K for different time intervals between 24 h and 15 days. The synthesis products were washed, dried at 393 K for 6 h and examined for crystallinity by XRD. The conditions of synthesis and the kinetics of crystallization are presented in table 3.2 and Fig. 3.2.

It was found that using a gel with a composition different (Expt # 5,6 and 7; Table 3.2) from that used for SAPO-11(na) and SAPO-31(na) resulted in poorly crystalline samples and the XRD of these samples showed impurity peaks. It was also found that when the concentration of orthophosphoric acid or that of dipropylamine in the gel was varied (Expt # 6 and 7; Table 3.2), the gel became too acidic or too alkaline which was probably responsible for the low crystallinity and the presence of impurity peaks in the final product as the synthesis of SAPOs requires a slightly acidic to neutral medium. Kinetics of SAPO-11 synthesis from non aqueous medium showed that the most crystalline sample was obtained after 6 days while the most crystalline SAPO-31 was obtained after 72 h (Fig. 3.2). The sample synthesized in aqueous medium with 0.6 SiO_2 mole ratio, SAPO-11(a2) had only 61.5 % crystallinity which further decreased to 50% on calcination (Expt.#2; Table 3.2). But the sample synthesized from non-aqueous medium with 0.6 mole ratio of SiO_2 had 93% crystallinity even after calcination (Expt.#4; Table 3.2). The XRD patterns of the samples synthesized from the non-aqueous medium were identical to those synthesized from aqueous medium but the crystallinities of the non-aqueous samples were better.

Table 3.2. Synthesis conditions for the SAPO-11 and SAPO-31 from aqueous and non-aqueous media.

Expt. #	Sample	Gel composition	T_c (h)	pH (bc)[a]	pH (ac)[b]	Crystallinity (%)
1.	SAPO-11(a1)	Al_2O_3: P_2O_5: 0.2SiO_2: 1 DPA :50 H_2O	24	5.8	8.2	82
2.	SAPO-11(a2)	Al_2O_3: P_2O_5: 0.6 SiO_2: 1 DPA :50 H_2O	24	6.0	8.5	61.5
3.	SAPO-11(na1)	Al_2O_3: 1.8P_2O_5: 0.2 SiO_2: 5 DPA :60 EG	144	6.8	8.8	100
4.	SAPO-11(na2)	Al_2O_3: 1.8P_2O_5: 0.6 SiO_2: 5 DPA :60 EG	144	6.7	8.7	96.7
5.	SAPO-31(a)	Al_2O_3: P_2O_5: 0.2 SiO_2: 1 DPA : 50 H_2O	24	6.2	8.1	89.3
6.	SAPO-31(na)	Al_2O_3:1.8 P_2O_5: 0.2 SiO_2: 5 DPA :60 EG	72	6.9	8.3	100
7.	SAPO-11(na3)	Al_2O_3: 1.8P_2O_5: 0.6 SiO_2: 2 DPA :60 EG	144	3.8	8.6	SAPO-11+C,B,T*
8.	SAPO-11(na4)	Al_2O_3: 1.8P_2O_5: 0.6 SiO_2: 5 DPA :30 EG	144	7.3	8.9	SAPO-11+C,B,T*
9.	SAPO-11(na5)	Al_2O_3: 1.0P_2O_5: 0.6 SiO_2: 5 DPA :60 EG	144	7.6	8.4	C, B, T*

[a]bc = before crystallization, [b]ac = after crystallization.

* C = crystobalite; T = tridymite; B = Bernilite.

3.2.3 Synthesis of SAPO-11, SAPO-31 and SAPO-5 by programmed heating (rapid crystallization method).

A rapid crystallization method developed for the synthesis of SAPO-5, SAPO-11 and SAPO-31 requires 1-4 h (as opposed to the normally used duration of 1-6 days). A synthesis gel of similar composition with slight variations in the pH and the Si composition was used for the synthesis of the above SAPOs. The novel procedure which leads to samples with better Si distribution involves the controlled hydrothermal heating of a precursor gel with the composition 1.0 Al_2O_3 : 1.1 P_2O_5 : 1.5 DPA : 0.2-0.6 SiO_2 : 40 H_2O enabling the rapid crystallization of pure and highly crystalline SAPO materials. This crystallization procedure is different from that normally reported in the literature [1] which generally involves the preparation of the gel, charging it in an autoclave and placing the autoclave inside an oven preheated to the desired temperature.

In a typical synthesis procedure (present rapid method), a slurry of aluminium isopropoxide (11.6 g, 99%) in water (13.0 g) was stirred mechanically for 45 min., orthophosphoric acid (6.4g, 85 wt%) diluted with water (6.5 g) was added dropwise to the slurry under stirring. The stirring was then continued for 1.5 h. DPA (4.2 g) and fumed silica (or silica sol) were added and the mixture was stirred for another 2 h to get a homogeneous gel. The gel was charged into an autoclave (150 ml) and heated at 1.5 K/ min to 433 K and then at 0.5 K/min to 473 K. The final temperature (473 K) was maintained for a suitable time (1- 4 h) to complete the crystallization. The autoclave was then quenched, the products filtered, washed with distilled water, dried at 383 K and finally calcined at 793 K in air for 8 h.

Some of the typical results of the crystallization kinetics are given in table 3.3. Experiments 1 and 2 (method 1) refer to the synthesis of SAPO-11 and SAPO-31

using DPA and fumed silica following the conventional heating procedure of placing the autoclave inside an oven preheated to the desired temperature. As SAPO-5 was not crystallizable with DPA by the above procedure, triethylamine was used for its synthesis (Expt. 3). Experiments 4 to 7 (method 2) were carried out by crystallization using a slow and programmed heating of the autoclave to 473 K as described above. The interesting aspect of this synthesis is the crystallization of pure SAPO-5 using DPA as the template. This confirms the earlier conclusions of Ojo *et al.*[2] that DPA favours the formation of straight channels. The experiments reveal that the nature of the crystalline phase obtained and its purity depends on the pH of the gel and the source of SiO_2. Very interestingly, the crystalline product was obtained within a few hours of the attainment of the crystallization temperature (473 K). This reduces the overall crystallization time significantly; this is an advantage when synthesizing large volumes of SAPOs for commercial applications.

It was observed that while at SiO_2 contents between 0.3 and 0.4 both SAPO-5 and SAPO-11 were obtained as mixed phases, at a SiO_2 content of 0.4 moles, SAPO-5 was obtained as a pure phase only at pH = 6.8 above which mixed SAPO-5 and SAPO-11 phases were obtained. But at 0.6 - 0.8 SiO_2 molar ratio SAPO-5 was obtained as a pure phase over a wider pH range of 6.8 - 7.1. So it is concluded that SAPO-5 can be obtained as a pure phase over a wide pH range using DPA as the template only when the SiO_2 molar ratio is > 0.4. SiO_2 is found to have a promoter as well as a stabilising effect on the $AlPO_4$-5 structure. The X-ray crystallinity of SAPO-5 sample increased with increasing Si content and was maximum at 0.6 SiO_2 content in the gel. For the SAPO-5 samples, the crystallization time for the most crystalline sample was found to be lower for the samples with higher Si content.

During the synthesis of SAPO-5, the phase purity of the sample was not so much sensitive to the pH of the gel at a high SiO_2 content of 0.6-0.8, but it was very much sensitive to pH at a lower Si content. Under many conditions (Table 3.3) both SAPO-5 and SAPO-11 co-crystallize and there was no phase transformation of one into other even when crystallization was carried out for 12 h. SAPO-5 being the structure of higher simplicity, it crystallised easily over a wider synthesis condition than SAPO-11. It was also observed that when the gel (Expt.# 6) for SAPO-5 synthesis was heated to 443 K at the rate of 1.5 K and kept at 443 K for 1 h, then a lamellar phase with an intense peak at $2\theta = \sim 6.8$ degrees was observed.

When silica sol was used instead of fumed silica and the gel pH was 6.5 (Expt. 7; Table 3.3), a precursor phase similar to the one found in the case of SAPO-5 with a very intense peak at $2\theta = \sim 6.8$ was observed. This is probably a short range ordered lamellar type aluminophosphate phase. the formation of similar precursor lamellar phases during the synthesis of $AlPO_4$s and SAPOs has already been reported [3]. After 2 h crystallization time, SAPO-11 with SAPO-31 impurity phase was observed, which transformed into pure SAPO-31 after 4 h crystallization time. There was a further transformation into pure SAPO-11 after 10 h crystallization time. These successive phase transformations can be written as lamellar→ SAPO-11+SAPO-31→ SAPO-31→ SAPO-11+SAPO-31→ SAPO-11. A similar phase transformation has been recently reported by Lopez et al. [4].

Recently Oliver *et al.* [5] based on various reports have proposed that the

Table 3.3. Synthesis conditions for SAPOs from conventional and rapid synthesis methods[1].

Expt. #	Gel composition	t_c[2] (h)	pH (bc[3])	pH (ac[4])	product	silica source	Crystallinity (%)[5]
	method 1 [conventional (s)]						
1.	Al_2O_3:1.0P_2O_5:1.0DPA:0.2SiO_2	24	5.8	8.6	SAPO-11(s)	fumed silica	83
2.	Al_2O_3:1.0P_2O_5:1.0DPA:0.2SiO_2	24	6.2	8.9	SAPO-31(s)	fumed silica	87
3.	Al_2O_3:1.0P_2O_5:1.0 EA:0.6SiO_2	24	4.8	8.4	SAPO-5(s)	fumed silica	92
	method 2 [rapid (r)]						
4.	Al_2O_3:1.1P_2O_5:1.5DPA:0.2SiO_2	0	6.8	8.3	SAPO-11(r)	fumed silica	82
		2		9.2	SAPO-11(r)	fumed silica	100
		4		8.9	SAPO-11(r)	fumed silica	96
		6		8.6	SAPO-11(r)	fumed silica	91
5.	Al_2O_3:1.1P_2O_5:1.6DPA:0.2SiO_2	2	7.4	9.5	SAPO-11 + SAPO-5	fumed silica	na

Expt. #	Gel composition	t_c[2] (h)	pH (bc[3])	pH (ac[4])	product	silica source	Crystallinity (%)[5]
6.	Al_2O_3:1.1P_2O_5:1.5DPA:0.6SiO_2	0	7.1	9.1	SAPO-5	fumed silica	100
		1		9.2	SAPO-5 + SAPO-11	fumed silica	na
		2		9.2	SAPO-5 + SAPO-11	fumed silica	na
7.	Al_2O_3:1.1P_2O_5:1.5DPA:0.2SiO_2	0	6.5	7.8	lamellar	silica sol	na
		2		8.5	SAPO-11 + SAPO-31	silica sol	na
		4		9.1	SAPO-31(r)	silica sol	100
		6		9.6	SAPO-11 + SAPO-31	silica sol	na
		10		9.5	SAPO-11	silica sol	na

[1]Crystallization temp. = 473 K; [2]t_c = crystallization time; [3]before crystallization; [4]after crystallization;

[5]Relative crystallinity (XRD) = (s)x100/(r); na = not applicable

crystallization of most of the aluminophosphates presumably follows a chain - to - layer transformation process wherein the parent chain is initially hydrolysed in solution leading to the formation of other chain structure types. Further, chain condensation causes cross linking and leads to a porous layer or open-framework structure. Our observations during the synthesis of SAPOs by method 2 could be rationalized by the above mechanism. In the above method where the aluminophosphate precursor gel is gradually heated from room temperature to 473 K, the formation of the parent chain and the hydrolysis to other chain types followed by chain condensation take place slowly in consecutive steps with increasing temperature. In the conventional synthesis procedure (method 1), it is possible that due to the rapid initial heating of the gel, all the three steps overlap and the chain species have more difficulty in undergoing condensation so that not only the crystallization time for porous structure is more but also the particle morphology and size is not uniform. Besides, the crystallinities of the samples are also lower when the heating rate is not controlled. SAPO-5 with the simplest structure is fully crystallized when the gel reaches 473 K (at 0 h) while SAPO-11 and SAPO-31 crystallize fully only after the gel has been kept at 473 K for some time (Table 3.3). Further, SAPO-5 could be crystallized over a broader range of synthesis conditions than SAPO-11 or SAPO-31, the last structure being most sensitive to parameter changes.

3.3A Synthesis of MeAPOs and MeAPSOs

The molar gel composition and the synthesis conditions are given in table 3.4. The synthesis procedures used were according to those of Flanigen and co-workers [6]. In a typical synthesis procedure, a slurry of aluminium isopropoxide (11.6 g) in water was stirred mechanically for 45 min.; orthophosphoric acid diluted with water (6.5 g) was added dropwise to the stirring mixture and was stirred for 30 min. Then

the metal to be incorporated was added as its acetate salt followed by fumed silica (for the MeAPSOs). Finally, 4.2 g of dipropylamine was added dropwise and the final mixture was stirred for 2 h to get a homogeneous gel which was transferred to a stainless steel autoclave and was hydrothermally heated at 473 K for 24 h. The synthesis products were washed, dried at 393 K for 6 h and calcined by slowly heating to 823 K in air and keeping for 8 h. The general gel composition used for the synthesis of metal aluminophosphates was 1.0 Al_2O_3 : 1.0 P_2O_5 : 0.2 MO : 1.0 Pr_2NH : 50 H_2O. (MO = metal oxide) and that for metal silicoaluminophosphates was 1.0 Al_2O_3 : 1.0 P_2O_5 : 0.1 MO : 0.1 SiO_2 : 1.0 Pr_2NH : 50 H_2O.

3.3B Synthesis of MnAPO-11 (from non-aqueous medium)

MnAPO-11(na) was synthesized using ethylene glycol as the non-aqueous medium. In a typical synthesis from non-aqueous medium, aluminium isopropoxide (11.6 g) was added slowly to ethylene glycol (109.7 g) and the mixture was stirred for 1 h. Dipropylamine (14.2 g) was added dropwise to the mixture and further stirred for 1/2 h. Then, 11.5 g of orthophosphoric acid was added dropwise and stirred for another 1/2 h. Finally, 0.34g of manganese(II) acetate was added and the final mixture was stirred for 2 h more to get a homogeneous gel. This was transferred to a stainless steel autoclave and heated at 473 K for 144 h. The synthesis products were washed with water, dried at 393 K for 6 h and calcined at 823 K for 8 h by gradually raising the temperature (2 K/min.)

Table 3.4. Synthesis conditions for MeAPO-11 and MeAPSO-11.

Sample	Gel composition									pH (bc)[a]	pH (ac)[b]
	Al_2O_3	P_2O_5	MnO	MgO	ZnO	CoO	SiO_2	DPA	H_2O		
MnAPO-11	1.0	1.0	0.2	-	-	-	-	1.0	50	6.3	9.1
MnAPSO-11	1.0	1.0	0.1	-	-	-	0.1	1.0	50	6.9	9.3
MgAPO-11	1.0	1.0	-	0.2	-	-	-	1.0	50	7.0	8.9
MgAPSO-11	1.0	1.0	-	0.1	-	-	0.1	1.0	50	7.1	9.1
ZnAPO-11	1.0	1.0	-	-	0.2	-	-	1.0	50	6.2	8.7
ZnAPSO-11	1.0	1.0	-	-	0.1	-	0.1	1.0	50	6.8	8.9
CoAPO-11	1.0	1.0	-	-	-	0.2	-	1.0	50	6.5	9.4
CoAPSO-11	1.0	1.0	-	-		0.1	0.1	1.0	50	6.3	9.1

[a]bc = before crystallization, [b]ac = after crystallization.

REFERENCES

1. Lok, B.M., Messina, C.A., Patton, R.L., Gajek, R.T., Cannan, T.R. and Flanigen, E.M., *US Patent,* 4,440,871 (1984).
2. A.F. Ojo and L.B. McCusker, *Zeolites*, **11,** 460 (1991).
3. N. Venkatathri, S.G. Hegde, V. Ramaswamy and S. Sivasanker, *Microporous and Mesoporous Materials*, **23**, 277 (1998).
4. C.M. Lopez, F.J. Machado, J. Goldwasser, B. Mendez, K. Rodriguez and M.M.R. Agudelo, *Zeolites*, **19,** 133 (1997).
5. S.Oliver, A. Kuperman and G.A. Ozin, *Angew. Chem. Int. Ed.*, **37,** 46 (1998).
6. Messina, C.A., Lok,B.M., Flanigen, E.M., *US Patent*, 4,544,143 (1985).

CHAPTER IV

CHARACTERIZATION

4.1 INTRODUCTION

The usefulness of SAPO molecular sieves in various industrially important reactions requiring moderate acidity has spurred research to find new catalytically active molecular sieves and to improve the catalytic activity of the known SAPOs. In this connection, the characterization of the SAPOs becomes necessary to understand the differences in the catalytic activities of the materials. The results of the characterization studies of the various SAPOs and MeAPOs synthesized in this study are presented in this chapter.

SAPO-11 and SAPO-31 molecular sieves were synthesized using different synthesis procedures, such as synthesis from non-aqueous medium and by programmed heating of the synthesis gel. Incorporation of Si in the $AlPO_4$-39 framework was also done for the first time. The synthesized materials were characterized by many techniques such as chemical analysis, XPS, XRD, SEM, FT-IR, ^{29}Si MAS-NMR, ^{27}Al MAS-NMR and TPD of adsorbed pyridine to establish their physicochemical properties and the nature of Si incorporation in the framework of the samples. Besides, some metal incorporated $AlPO_4$-11 were also synthesized using published procedures and characterized by chemical analysis, XRD and SEM. Mn incorporated $AlPO_4$-11 synthesized from aqueous and non-aqueous media was also characterized by ESR spectroscopy to study the location of Mn ions in the samples.

4.2 CHARACTERIZATION OF SAPO-5, SAPO-11 AND SAPO-31.

4.2.1 Elemental Analysis

The overall elemental (bulk) compositions of the different samples in the calcined form namely, SAPO-11, SAPO-31, SAPO-5, SAPO-11(na), SAPO-31(na), SAPO-11(r), SAPO-31(r) and SAPO-5(r) were determined by chemical analysis and atomic absorption spectroscopy. The surface compositions were determined by XPS.

The chemical composition of the different samples are presented in table 4.1. It is found that Si content in the bulk is less than that at the surface for all the samples. A probable reason is that as the pH of the synthesis gel increases with crystallization time, more Si depolymerizes and gets incorporated into the aluminophosphate framework so that more Si is present in the surface layers formed during the later stages of crystallization.

The higher Si contents in the rapid crystallized samples and those synthesized from non-aqueous medium than in the conventionally synthesized samples suggests that the synthesis conditions for the former are more conducive to silicon depolymerization and incorporation in the framework than the latter. In all the samples (except SAPO-5(a)) the Al/P ratio (bulk) is more than 1 suggesting the preferential occupation of the P sites by Si. More importantly, Si incorporation is more in the samples synthesized in ethylene glycol (na) and by programmed heating (r) than in those prepared from aqueous medium (a) in the case of SAPOs (Table 4.1). This is also confirmed by the larger Al/P ratios for the samples 'na' and 'r' than for the 'a' samples.

4.2.2 X-ray diffraction

The x-ray crystallinities of the SAPOs synthesized from non-aqueous medium was higher than those of the samples synthesized from aqueous medium (Fig. 3.1 and 3.2). Similarily the x-ray crystallinities of the samples prepared by programmed heating of the gel (rapid crystallization) were higher than those of the samples prepared by the conventional method (table 3.3). The XRD patterns of all the samples matched well with the reported patterns [1]. Fig. 4.1(a to f) shows the XRD patterns of the lamellar phase (a), SAPO-11 (b), SAPO-31 (c), SAPO-5 (d), SAPO-11 + SAPO-31 mixed phase (e) and SAPO-11 + SAPO-5 mixed phase (f) and lamellar

Table 4.1. Elemental composition of various SAPOs

Sample	Bulk composition	Surface composition
SAPO-11(a)	$(Al_{0.57}P_{0.38}Si_{0.05})O_2$	$(Al_{0.54}P_{0.39}Si_{0.07})O_2$
SAPO-31(a)	$(Al_{0.56}P_{0.41}Si_{0.03})O_2$	$(Al_{0.42}P_{0.39}Si_{0.19})O_2$
SAPO-5(a)	$(Al_{0.45}P_{0.46}Si_{0.09})O_2$	$(Al_{0.43}P_{0.37}Si_{0.20})O_2$
SAPO-11(na)	$(Al_{0.59}P_{0.32}Si_{0.07})O_2$	$(Al_{0.57}P_{0.26}Si_{0.17})O_2$
SAPO-31(na)	$(Al_{0.61}P_{0.35}Si_{0.04})O_2$	$(Al_{0.55}P_{0.32}Si_{0.13})O_2$
SAPO-11(r)	$(Al_{0.58}P_{0.35}Si_{0.07})O_2$	$(Al_{0.45}P_{0.38}Si_{0.17})O_2$
SAPO-31(r)	$(Al_{0.55}P_{0.39}Si_{0.06})O_2$	$(Al_{0.52}P_{0.34}Si_{0.14})O_2$
SAPO-5(r)	$(Al_{0.50}P_{0.39}Si_{0.11})O_2$	$(Al_{0.46}P_{0.36}Si_{0.18})O_2$

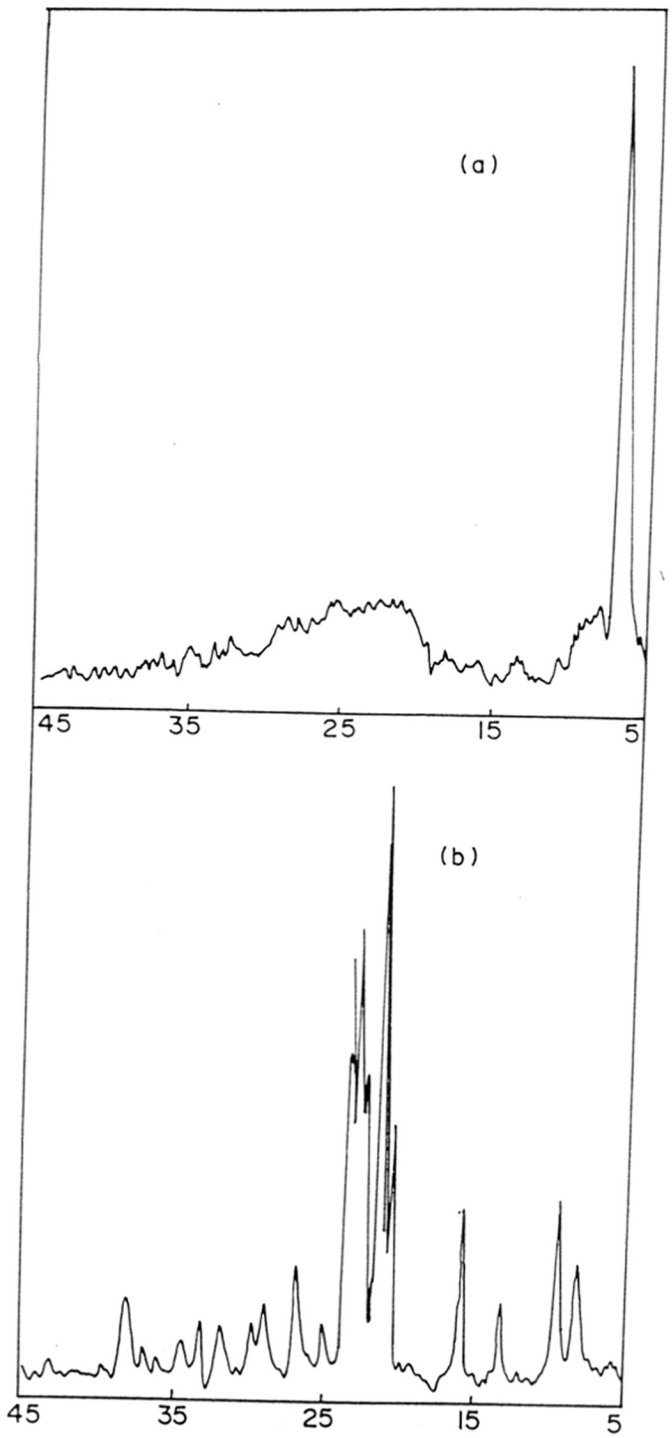

Figure 4.1A. XRD patterns of lamellar phase (a) and SAPO-11(b).

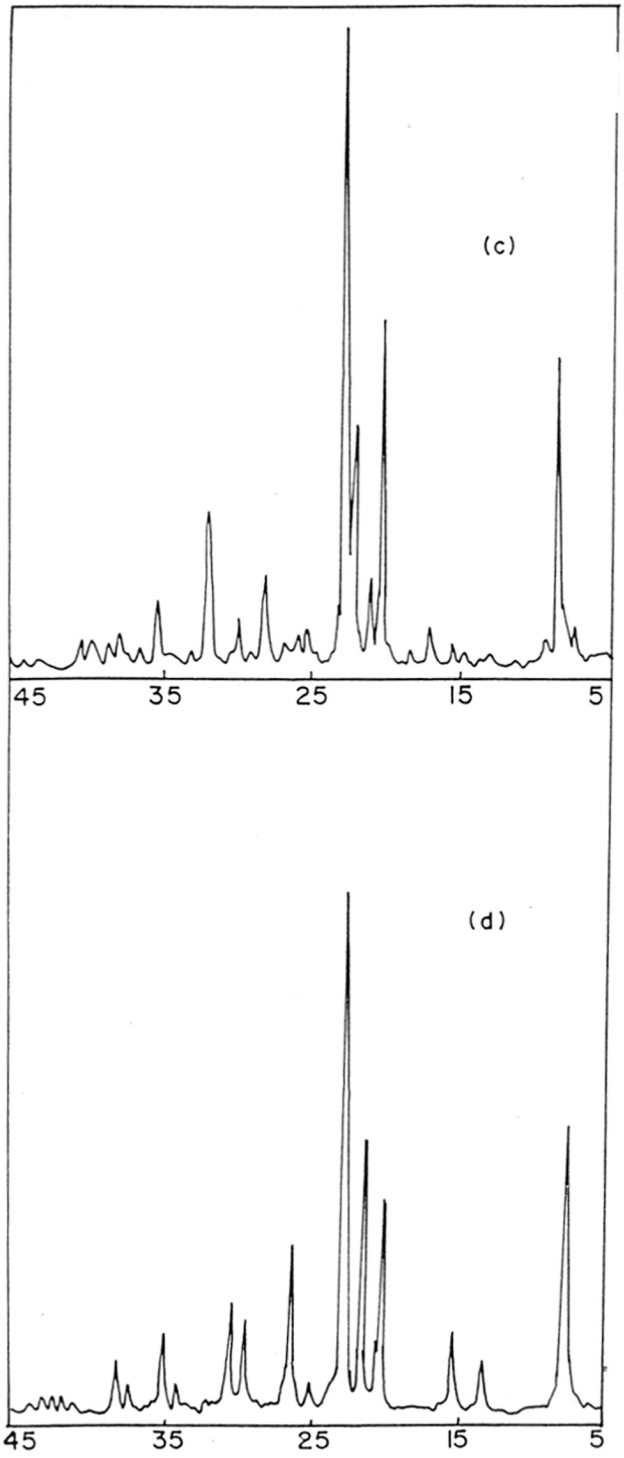

Figure 4.1B. XRD patterns of SAPO-31 (c) and SAPO-5 (d).

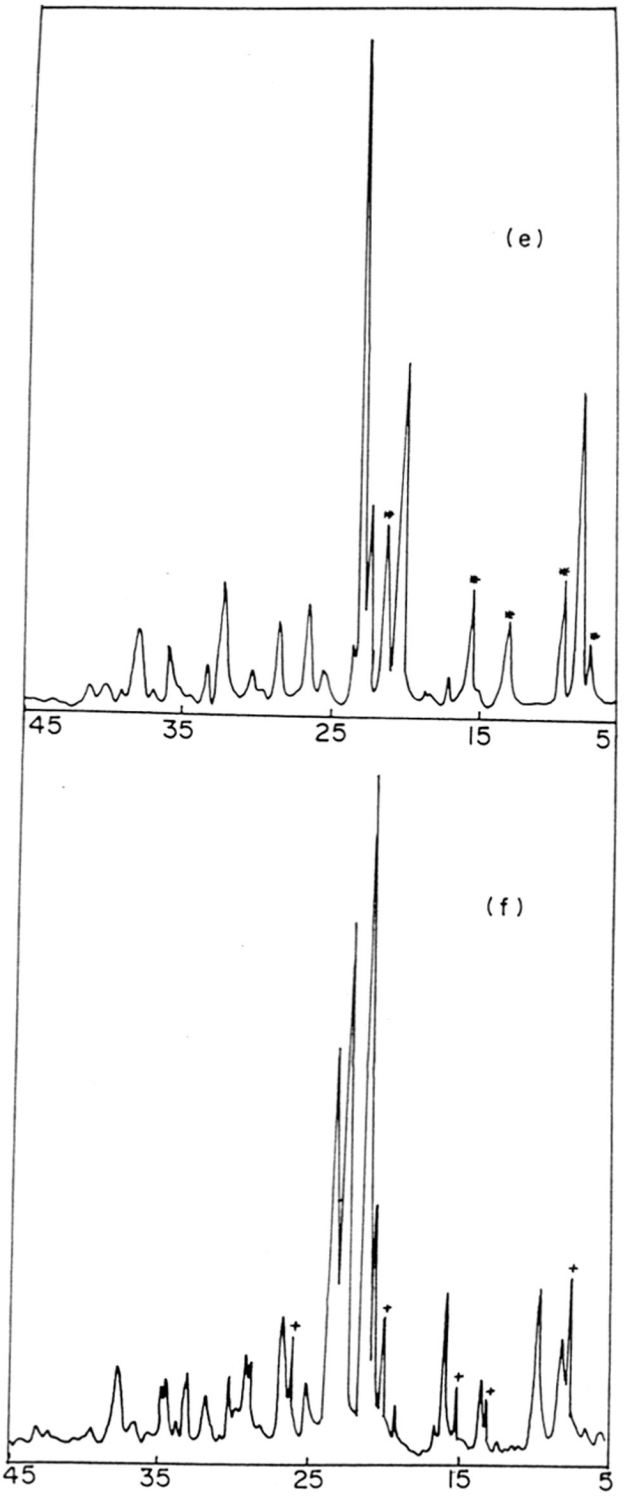

Figure 4.1C. XRD patterns of SAPO-11 + SAPO-31 (*, SAPO-11 peaks) (e) and SAPO-11 + SAPO-5 (+, SAPO-5 peaks) (f).

phase (a)obtained by the rapid crystallization method. These phases were obtained during the various crystallization conditions used in the rapid synthesis method (chapter 3; Table 3.3).

4.2.3 Scanning Electron Microscopy

The morphology and particle size of SAPO-11(a), SAPO-31(a) and SAPO-5(a) made by the conventional method, SAPO-11(na) and SAPO-31(na) from ethylene glycol and SAPO-11(r), SAPO-31(r) and SAPO-5(r) made by the rapid crystallization method are presented in table 4.2. Though the crystallite size of the SAPO-11(na) and SAPO-31(na) samples synthesized from non-aqueous medium were similar to those of the samples synthesized from aqueous medium, the crystallites of the former samples were of more uniform size (Fig. 4.3 (a, b)). SAPO-11(a) synthesized from aqueous medium using the conventional method consisted of crystallites aggregated into spheres (Fig. 4.2 (a)). In contrast, SAPO-11(r) synthesized by rapid synthesis method was in the form of well defined rectangular crystallites of 1.0 x 0.5 μm only partially aggregated into hollow spheroids (Fig. 4.4B). The above sample did not reveal any amorphous component even at a crystallization time of 0 h though the crystallite shape was not well defined (Fig. 4.4A); they were more like irregular jarred elongated plates. After 6 h crystallization time, the crystallites were completely aggregated axially into spheres (Fig. 4.4B). SAPO-31(a) synthesized by the conventional method was made up of rectangular rod like crystals of various sizes in the range 1.0 x 0.5 μm to 3.0 x 0.5 μm (Fig. 4.2 (b)). But the rapid crystallized SAPO-31(r) sample consisted of particles of uniform rhombohedral shape and size (3.0 x 1.0 μm) (Fig. 4.4C). SAPO-5(a) synthesized using conventional method had crystals of different morphologies (Fig. 4.4D). But

Table 4.2 Morphology and size of various SAPOs

Sample	Particle Shape	Particle size (μm)
SAPO-11(a)	spherical	5.0
SAPO-31(a)	rectangular rod	(2.0-6.0) x 1.0
SAPO-5(a)	mixed	5.0 - 8.0
SAPO-11(r), 0 h	jarred plates	~ 1.0 x 0.5
SAPO-11(r), 2 h	rectangular	1.0 x 0.5
SAPO-11(r), 6 h	spherical	5.0
SAPO-31(r)	rhombohedral	3.5 x 1.0
SAPO-5(r)	hexagonal prism	6.0 x 8.0
Lamellar	flake like	-
SAPO-11(na)	spherical	4.0 x 6.0
SAPO-31(na)	rectangular	5.0

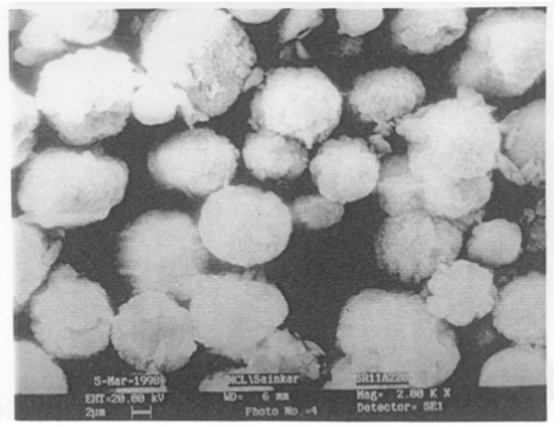

(a)

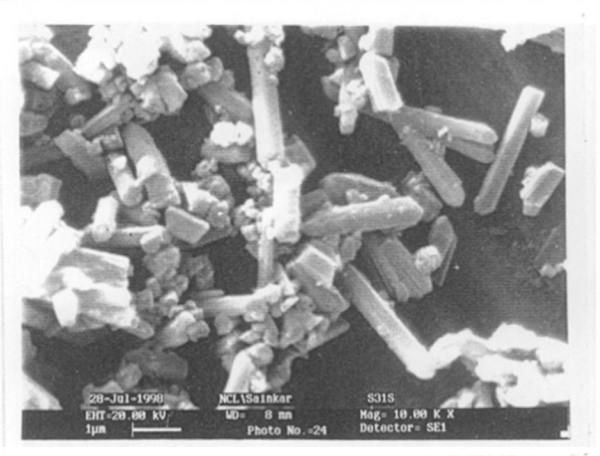

(b)

Figure 4.2. Scanning Electron Micrographs of SAPO-11(a) (a) and SAPO-31(a) (b).

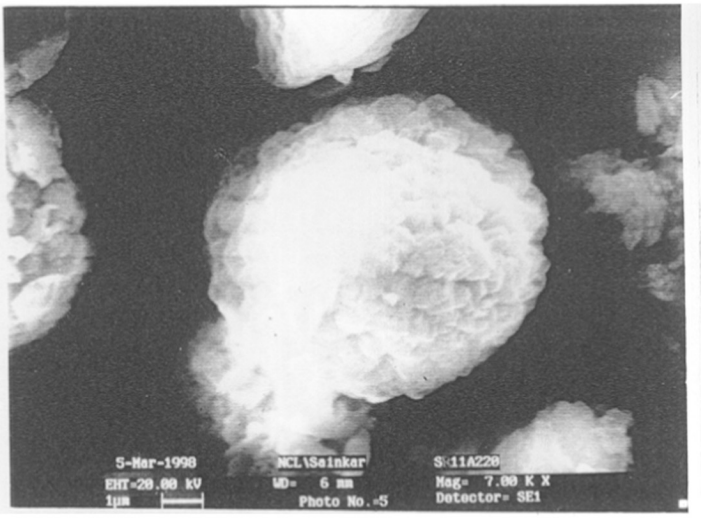

(a)

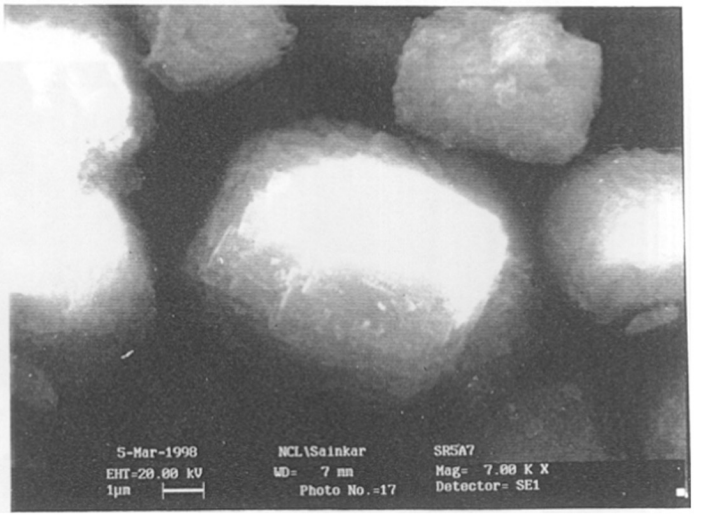

(b)

Figure 4.3. Scanning Electron Micrographs of SAPO-11(na) (a) and SAPO-31(na) (b).

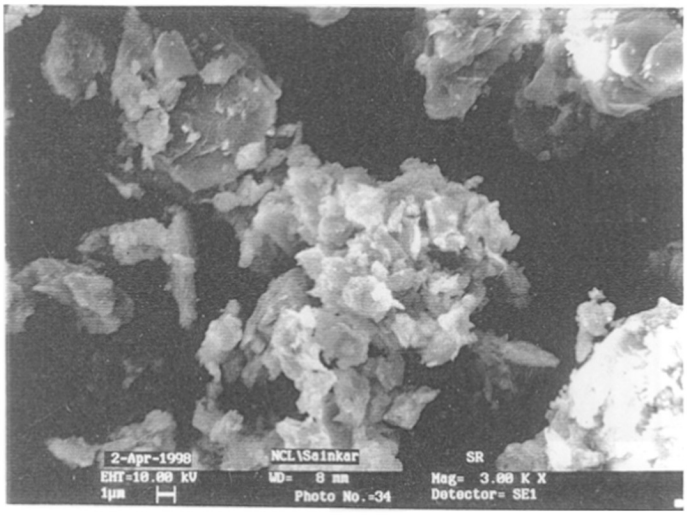

(a)

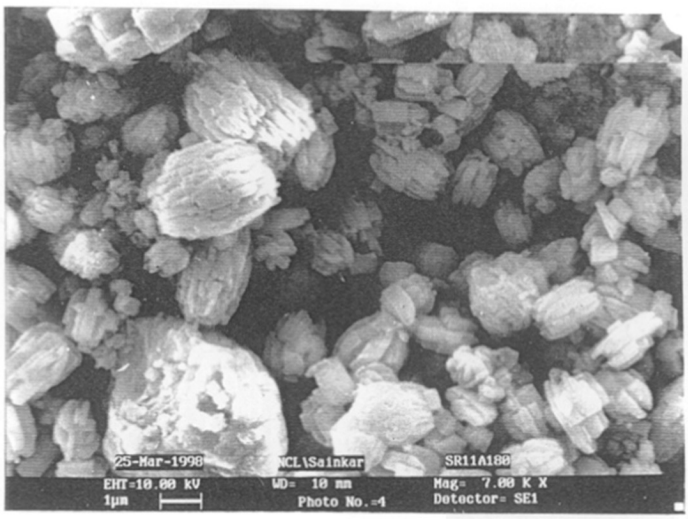

(b)

Figure 4.4A. Scanning Electron Micrographs of Lamellar phase (a) and SAPO-11(r), 0 h (b).

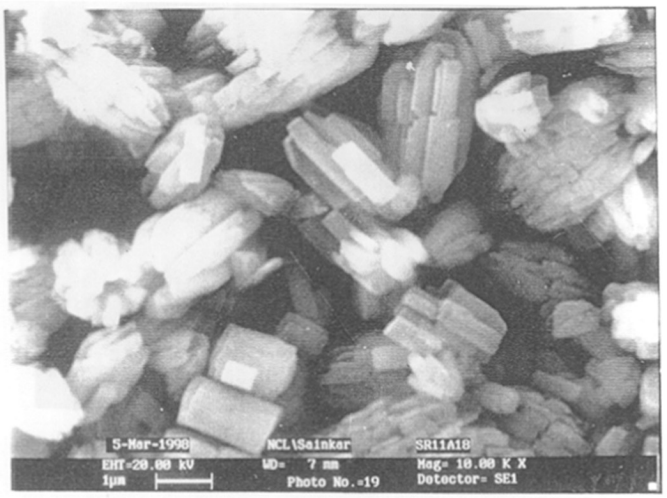

(c)

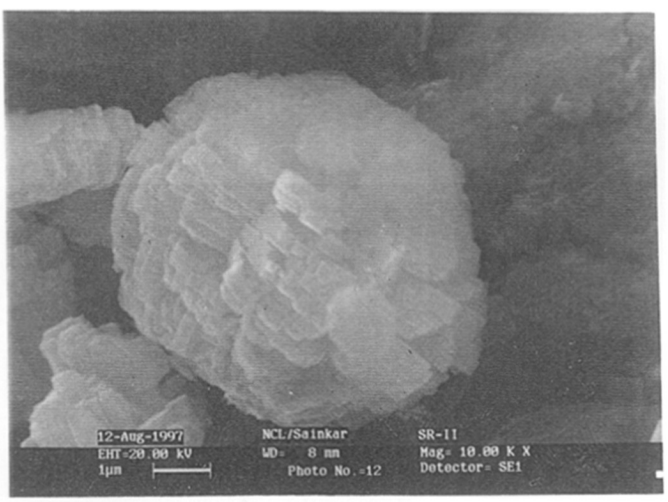

(d)

Figure 4.4B. Scanning Electron Micrographs of SAPO-11(r), 2 h (c) and SAPO-11(r), 6 h (d).

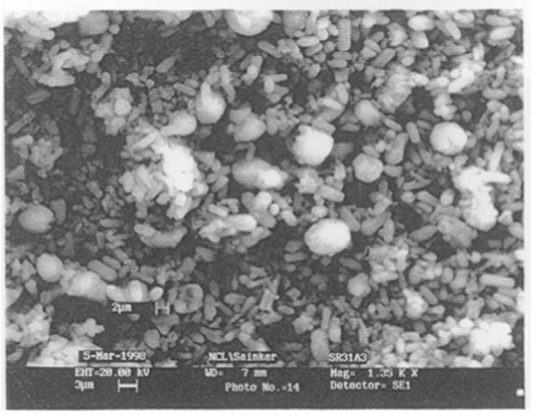

(e)

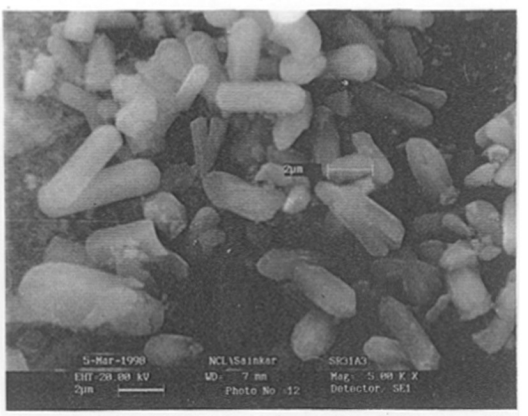

(f)

Figure 4.4C. Scanning Electron Micrographs of SAPO-31(r) + SAPO-11(r) (e) and SAPO-31(r) (f).

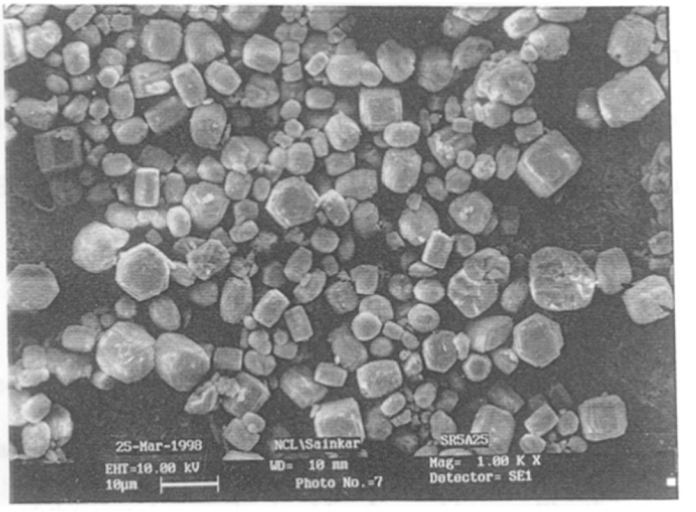

(g)

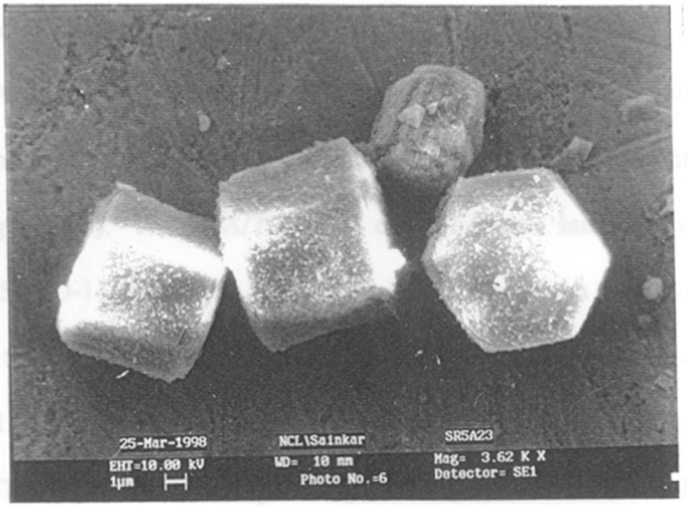

(h)

Figure 4.4D. Scanning Electron Micrographs of SAPO-5(a) (g) and SAPO-5(r) (h).

the SAPO-5(r) synthesized by rapid crystallization method was made up of only hexagonal prism shaped single crystals of 6.0 x 8.0 μm size and no other type of morphology was found (Fig. 4.4 D). So, it can be concluded that synthesis by rapid crystallization method results in particles with well defined uniform morphology and size. The SEM of the lamellar phase which was isolated as an intermediate during the synthesis of SAPOs by the rapid crystallization method revealed flake like particles (Fig. 4.4A).

4.2.4 Surface Area Measurement

Surface areas of different SAPOs are tabulated in table 4.3. It is found that the surface areas of the samples synthesized by the rapid crystallization method and from non-aqueous medium are higher than those of the samples synthesized by conventional method.

4..2.5 Thermal Analysis

TGA profiles for different SAPO samples in oxidizing (air) atmosphere are presented in Fig. 4.5 (A) and 4.6 (A), while the DTA profiles are presented in Fig. 4.5 (B) and Fig. 4.6 (B). The DTA/TGA data of the different samples are presented in Table 4.4 (SAPO-11) and Table 4.5 (SAPO-31). Comparison of the overall weight loss from the different samples shows that it is more in the case of samples synthesized from non-aqueous medium and those synthesized by rapid crystallization method. This is expected due to the higher surface areas of the rapid crystallized samples and the samples synthesized from non-aqueous medium so that they have more amount of occluded water and dipropylamine molecules. TG/DTA results indicate that the decomposition occurs in three stages. In the first stage (table 4.4 and 4.5), the desorption of physisorbed water and dipropylamine from the samples occurs at lower temperatures. In the second and the third stages, weight losses occur due to

Table 4.3 Surface areas of various SAPOs.

SAMPLE	Surface Area (m^2g^{-1})
SAPO-11(a)	140
SAPO-31(a)	207
SAPO-11(na)	183
SAPO-31(na)	221
SAPO-11(r)	208
SAPO-31(r)	218
SAPO-39	134

Table 4.4 TGA and DTA data for as-synthesized SAPO-11 sample (in air).

Sample	Step	Temperature range (K)	Weight loss (%)	Total weight loss (%)	Peak Temp. (K); DTA
SAPO-11(a)	I	298 - 473	5.9	5.9	378 (endo)
	II	473 - 720.5	6.4	12.3	367.5 (exo)
	III	720.5 - 973	7.1	19.4	549 (exo)
SAPO-11(na)	I	298 - 473	6.3	6.3	353 (endo)
	II	473 - 720	6.5	12.8	393 (exo)
	III	720 - 973	8.7	21.5	607 (exo)
SAPO-11(r)	I	298 - 473	6.8	6.8	353 (endo)
	II	473 - 720	6.2	13.0	687.5 (exo)
	III	720 - 973	9.2	22.2	880.5 (exo)

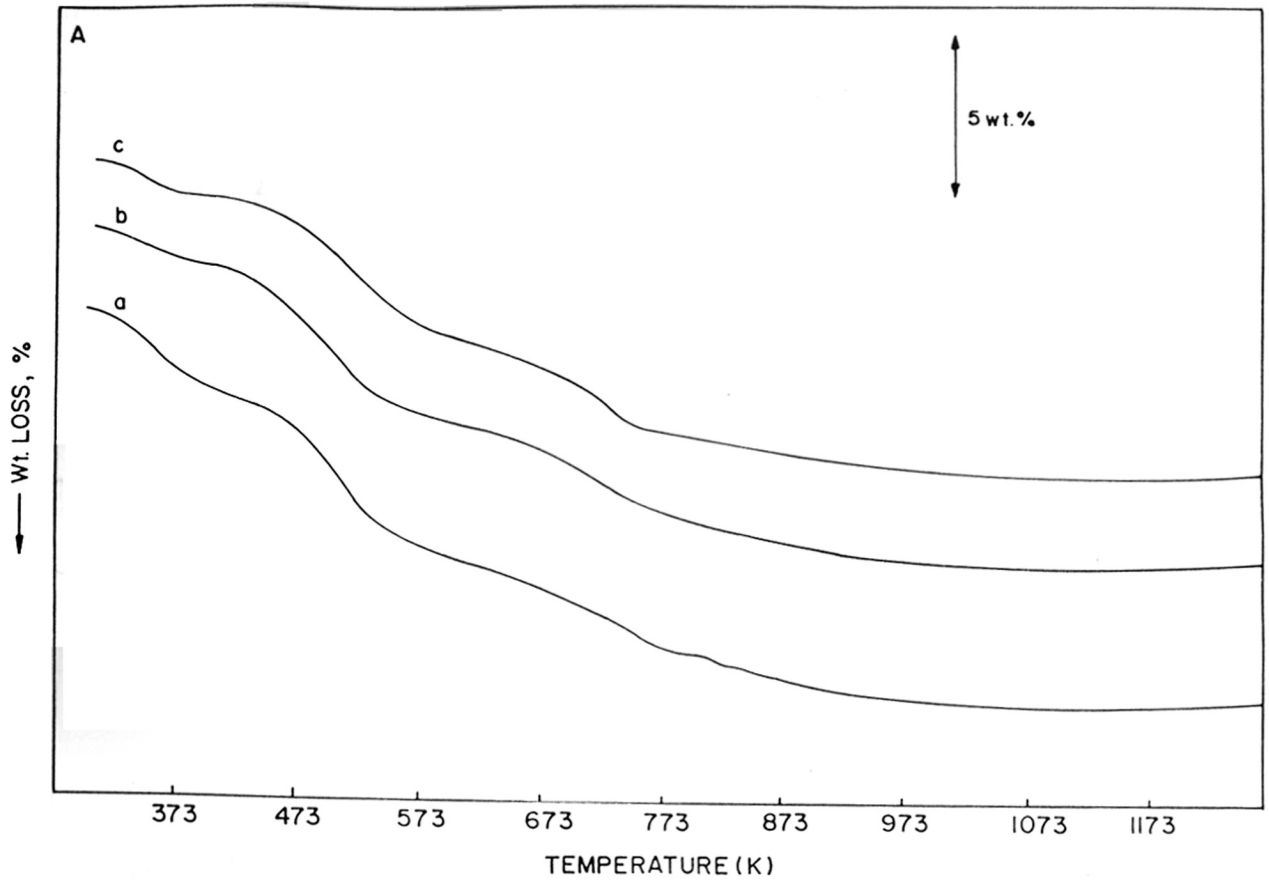

Figure 4.5A. TGA curves of SAPO-11 samples prepared by different procedures.

(a), SAPO-11(a); (b), SAPO-11(na) and (c), SAPO-11(r).

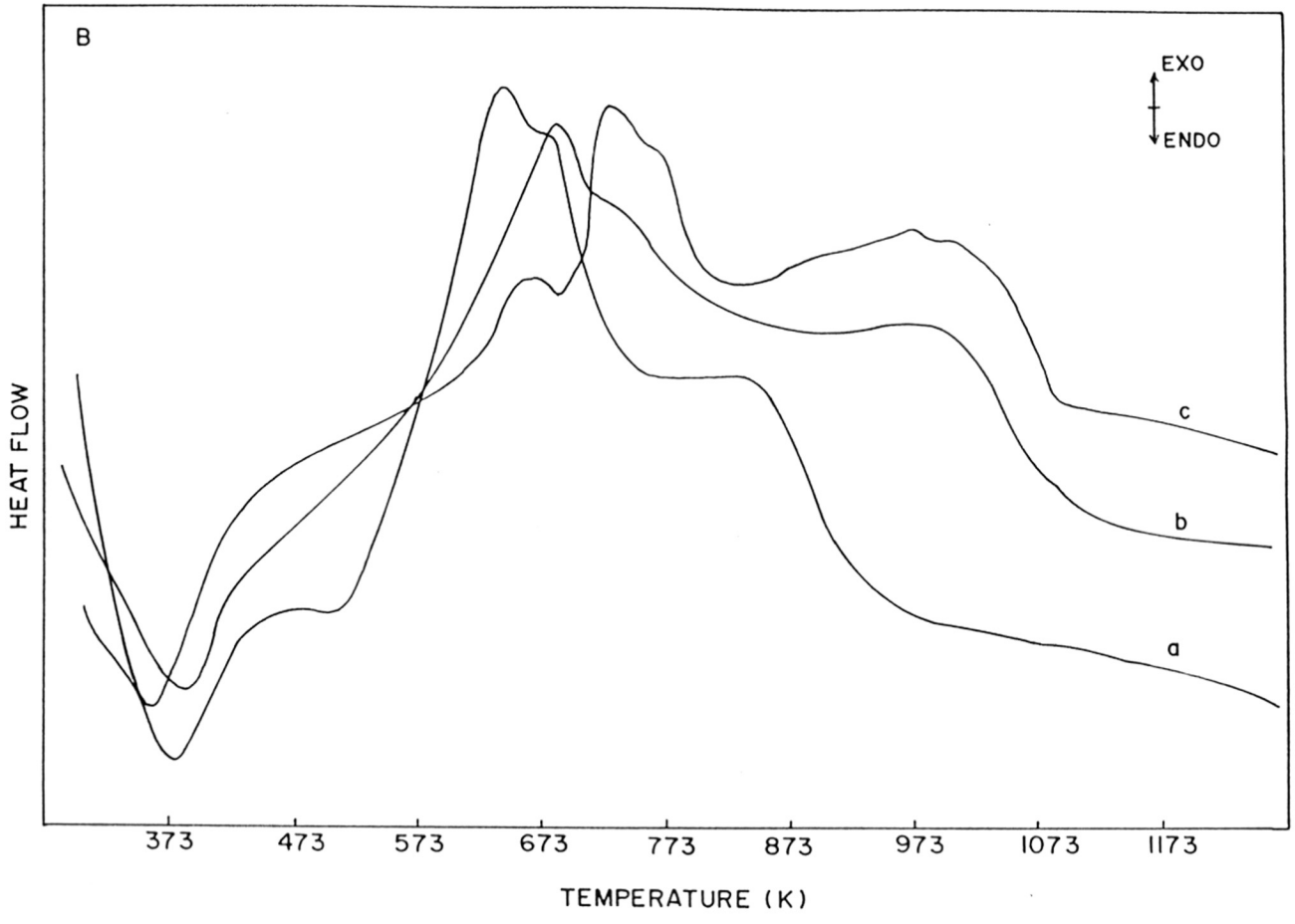

Figure 4.5B. DTA curves of SAPO-11 samples prepared by different procedures.

(a), SAPO-11(a); (b), SAPO-11(na) and (c), SAPO-11(r).

Table 4.5 TGA and DTA data for as-synthesized SAPO-31 samples (in air).

Sample	Step	Temperature range (K)	Weight loss (%)	Total weight loss (%)	Peak Temp. (K); DTA
SAPO-31(a)	I	298 - 473	4.8	4.8	375 (endo)
	II	473 - 694	5.6	10.4	656.5 (exo)
	III	694 - 953	6.7	17.1	844(exo)
SAPO-31(na)	I	298 - 483	5.2	5.2	382 (endo)
	II	483 - 718	5.5	10.7	691 (exo)
	III	718 - 993	7.8	19.5	978 (exo)
	I	298 - 453	5.6	5.6	356 (endo)
	II	453 - 736	6.2	11.8	735 (exo)
	III	736 - 993	8.8	20.6	978.5 (exo)

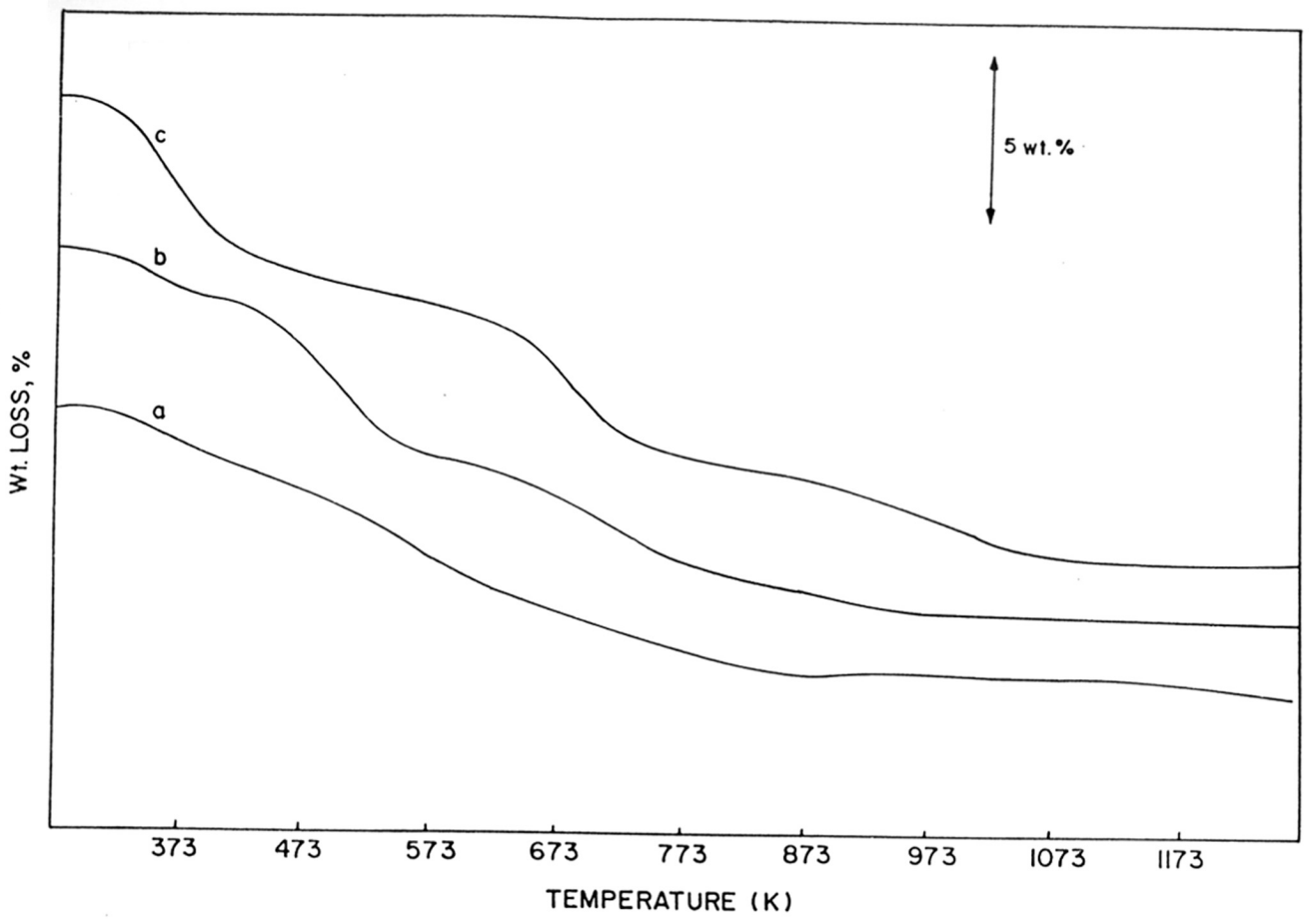

Figure 4.6A. TGA curves of SAPO-31 samples prepared by different procedures.

(a), SAPO-31(a); (b), SAPO-31(na) and (c), SAPO-31(r).

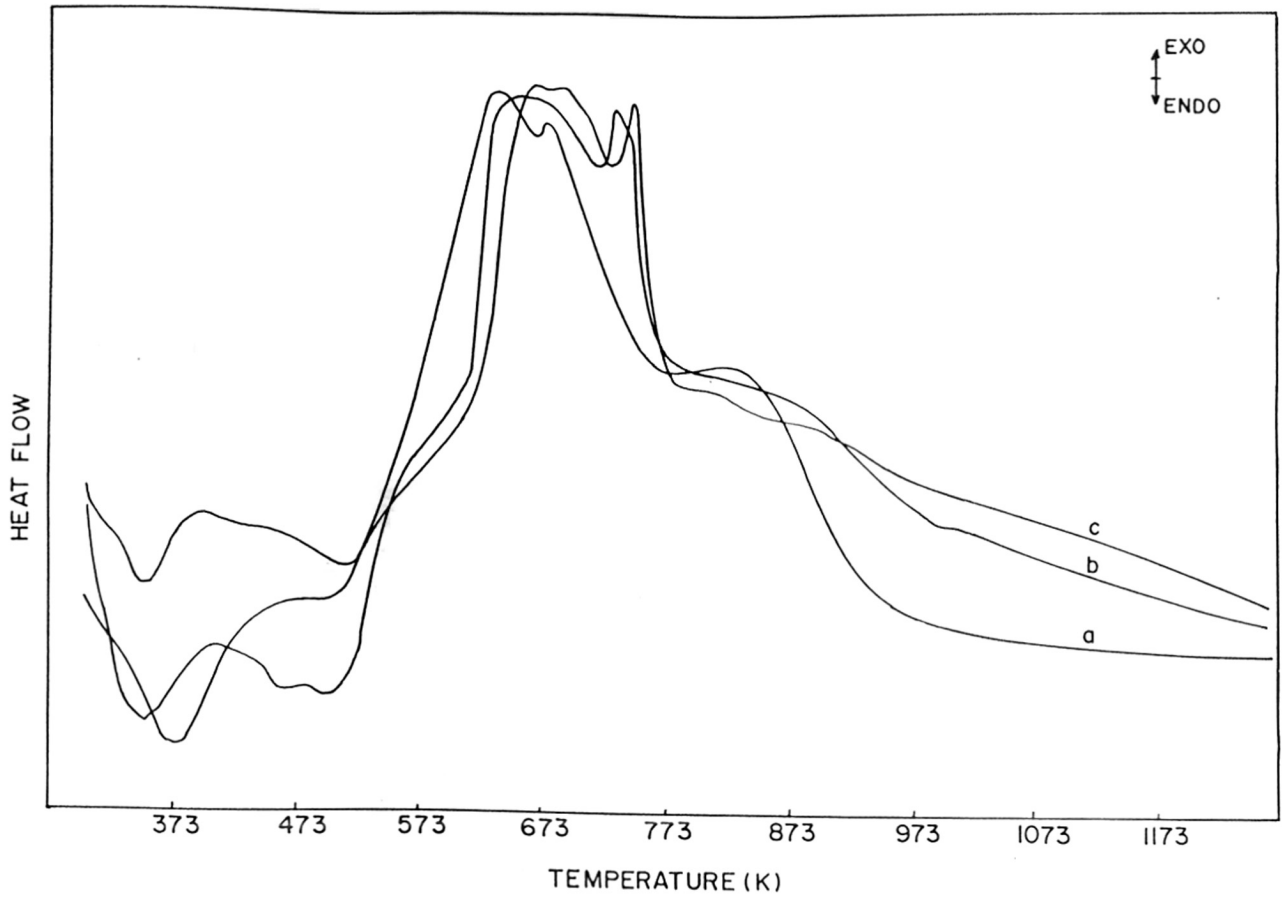

Figure 4.6B. DTA curvesof SAPO-31 prepared by different procedures.

(a) SAPO-31(a); (b) SAPO-31(na); (c) SAPO-31(r).

the oxidative decomposition, which is an exothermic process. The oxidative decomposition is thought to involve the thermal cracking of the occluded dipropylamine, followed by oxidation of the cracked products in the intra- and intercrystalline spaces and also the direct oxidation of dipropylamine within the channels. The exothermic peaks in steps II and III are found to be at higher temperatures for non-aqueous (na) medium synthesized samples and for rapid crystallized samples (r) which could be due to the higher acidities of these samples than conventionally synthesized (s) samples so that the occluded dipropylamine template molecules are strongly held at the acidic sites.

The DTA/TGA curves for the lamellar phase which is obtained during the crystallization of SAPO-11(r), SAPO-31(r) and SAPO-5(r) by the rapid crystallization method is presented in Figure 4.7. The large endothermic weight loss (25% in the temperature range 298-523 K with an endothermic peak at 373 K in the first stage reveals the presence of more water molecules along with the template. The two exothermic peaks at 613 K and 803 K are associated each with a weight loss of 5%. Compared to SAPO molecular sieves the total weight loss is more but the oxidative decomposition occurs at lower temperatures than for SAPO-11 and SAPO-31 molecular sieves.

4.2.6 Nuclear Magnetic Resonance Spectroscopy

^{27}Al MAS-NMR spectra of SAPO-11(s) and SAPO-31(s) are shown in Figure 4.8; those of SAPO-11(r) and SAPO-31(r) are shown in Figure 4.9 and those of SAPO-11(na) and SAPO-31(na) are shown in Figure 4.10. All the spectra consist of an intense peak at δ = +39 ppm typical of tetrahedral aluminium in the framework. Low intensity peaks at around δ = -8 and -12 ppm are found for all the samples

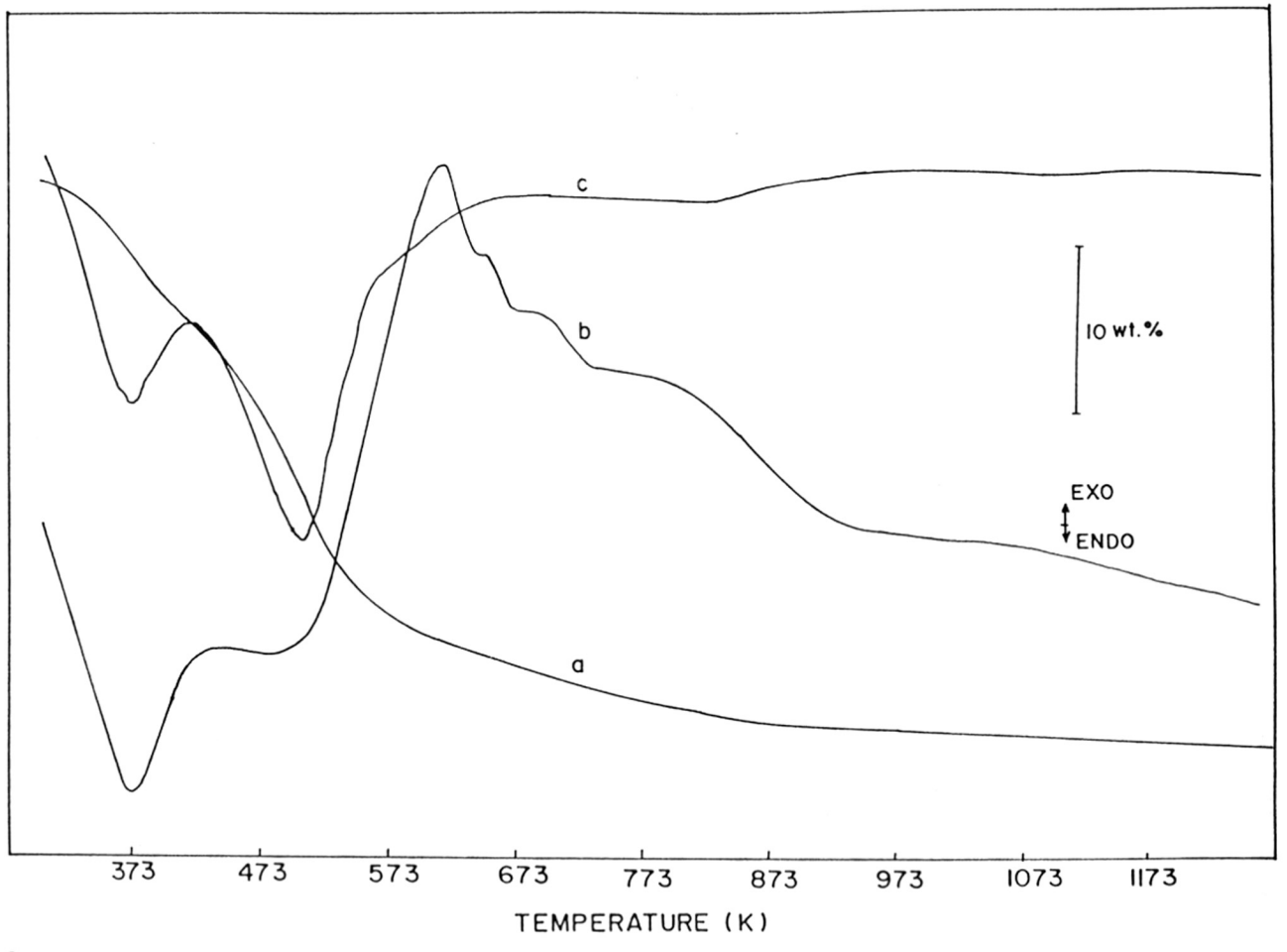

Figure 4.7. DTA, TGA and DTG curves of lamellar phase.

attributable to pentacoordinated and hexacoordinated Al [9-11] due to coordination of tetrahedral framework Al with water molecules.

^{29}Si MAS-NMR spectra of SAPO-11(a) and SAPO-31(a) are shown in Figure 4.11; those of SAPO-11(r) and SAPO-31(r) are shown in Figure 4.12 and that of SAPO-11(na) and SAPO-31(na) are shown in Figure 4.14. Also ^{29}Si MAS-NMR spectra of SAPO-5(a) and SAPO-5(r) are shown for comparison in Figure 4.13. Figure 4.15 shows the ^{29}Si MAS-NMR spectrum of SAPO-11 synthesized from non-aqueous medium using tetraethylorthosilicate as the source of silicon. The conventionally synthesized samples (a) show a broad band in the region of δ = -90 to -110 ppm (Figure 4.11) indicating the presence of large amounts of multiple Si environments and Si island formation. The rapid crystallized samples (r) on the other hand, exhibit a very intense peak at about δ = -95 , -89 and -90 ppm for SAPO-11(r), SAPO-31(r), (Figure 4.12) and SAPO-5(r) (Figure 4.13), respectively, with lower intensity signals in the δ = -100 to -110 ppm region indicating that a large amount of the Si is present as Si(4Al) type species in the framework and there is minimal Si island formation in the samples synthesized by rapid crystallization method. Similarily, ^{29}Si MAS-NMR spectra of the samples synthesized from non-aqueous medium (Figure 4.14) reveal a smaller peak at δ = -110 ppm (attributed to the non acidic silica islands) than those of the samples synthesized from the aqueous medium (Figure 4.11) suggesting that the concentration of silica islands (due to substitution of one Al and one P species by two Si atoms) is also less for the samples synthesized from non-aqueous medium (Fig. 4.14). The ^{29}Si MAS-NMR spectrum of SAPO-11 synthesized from non-aqueous medium using TEOS as Si source shows the complete absence of Si islands (Fig. 4.15).

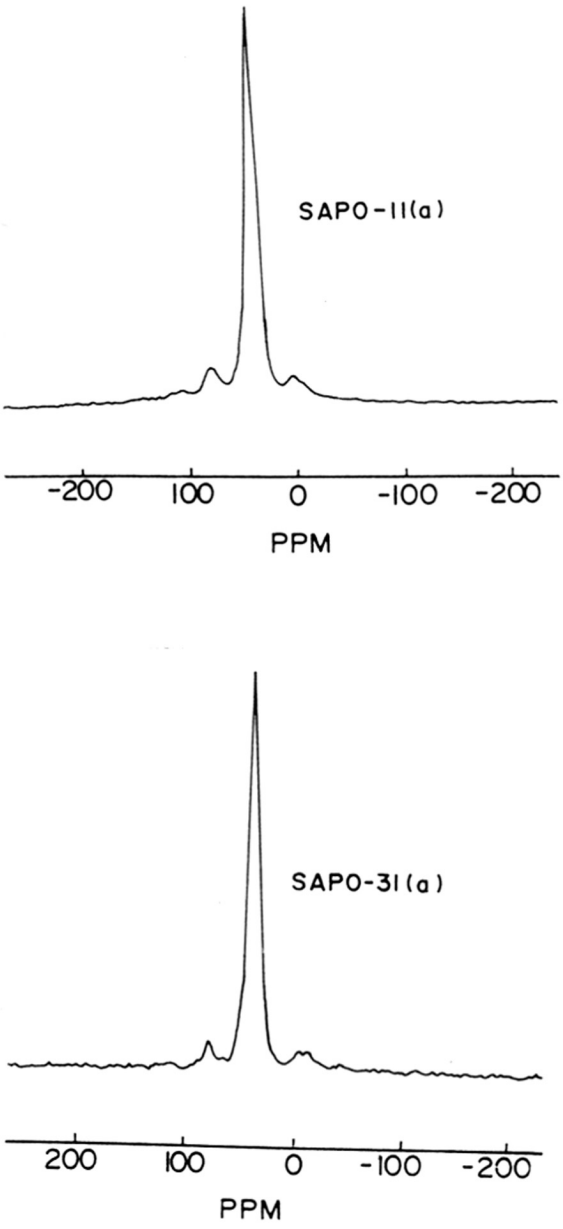

Figure 4.8. ^{27}Al MAS-NMR spectra of SAPO-11(a) and SAPO-31(a).

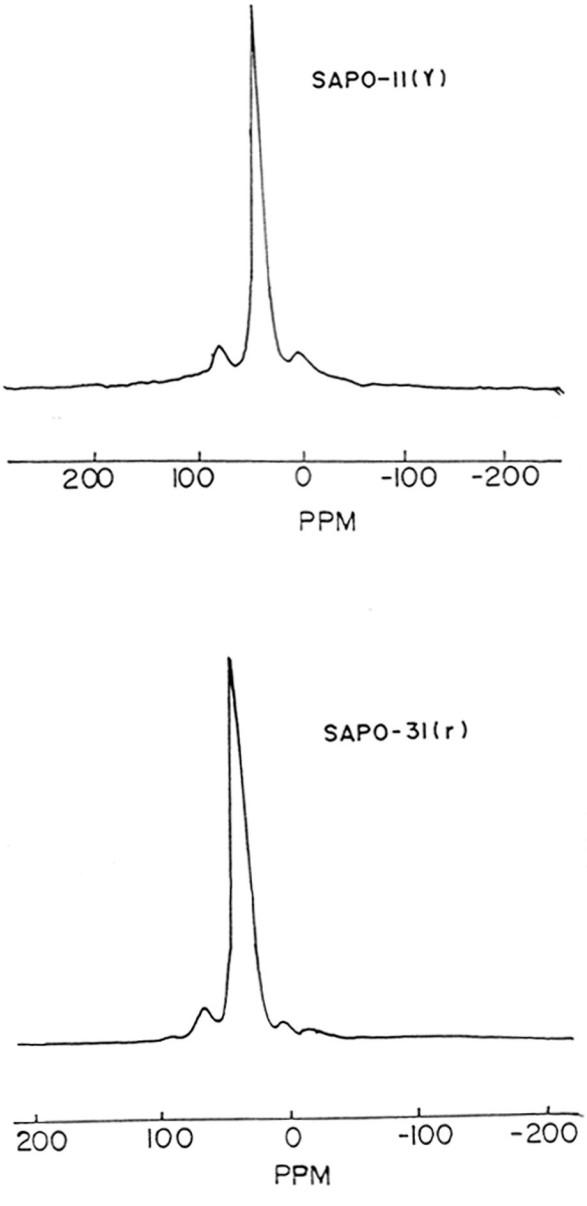

Figure 4.9. ^{27}Al MAS-NMR spectra of SAPO-11(r) and SAPO-31(r).

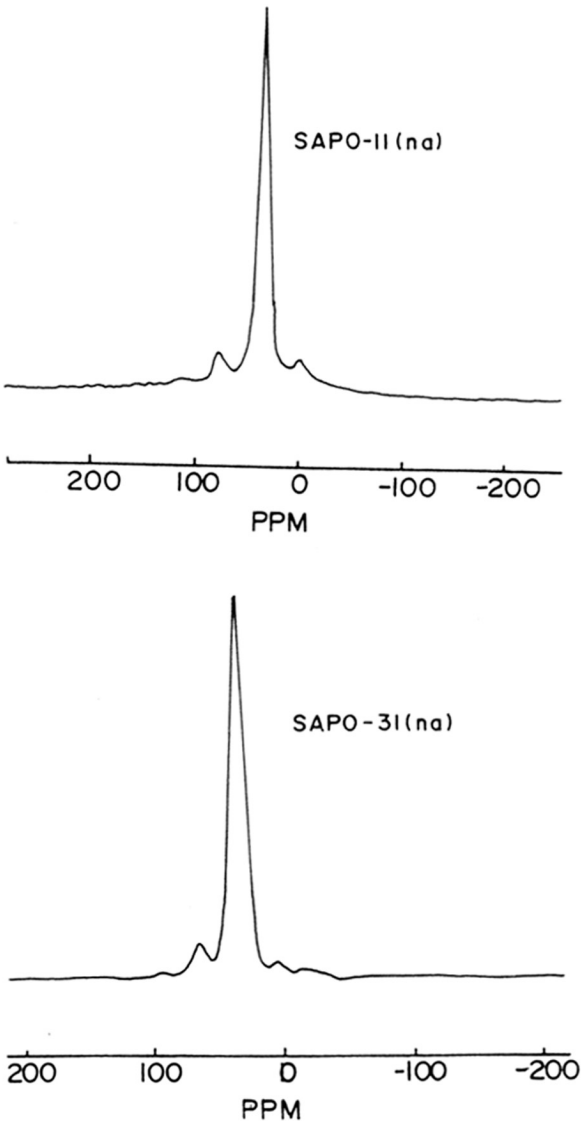

Figure 4.10. ^{27}Al MAS-NMR spectra of SAPO-11(na) and SAPO-31(na).

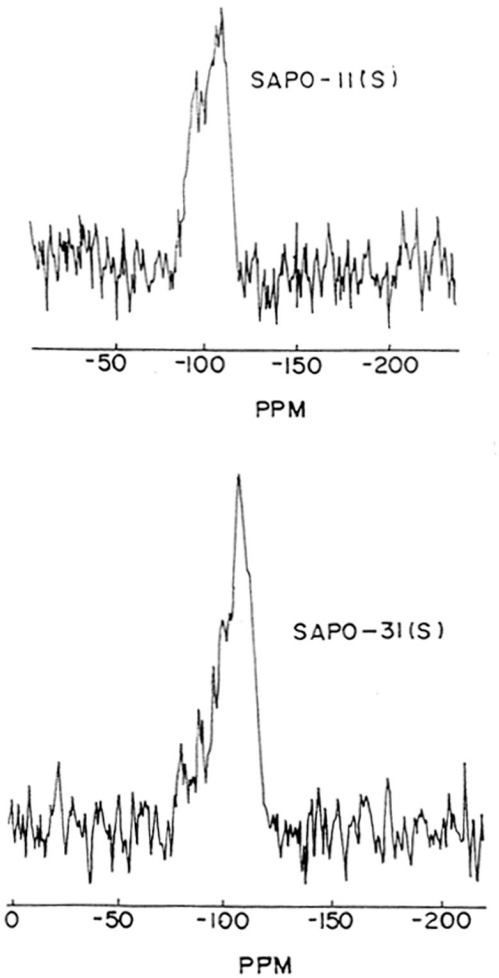

Figure 4.11. ^{29}Si MAS-NMR spectra of SAPO-11(a) and SAPO-31(a).

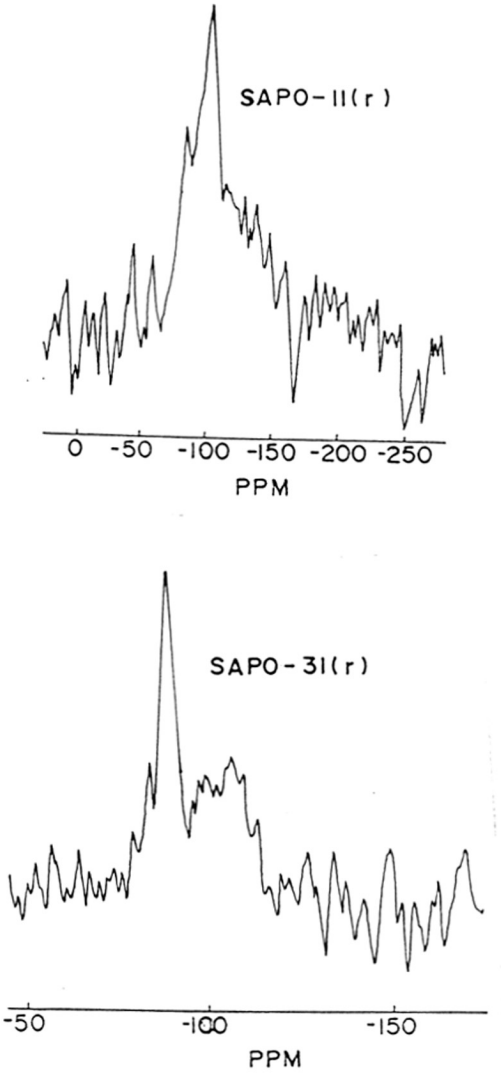

Figure 4.12. ^{29}Si MAS-NMR spectra of SAPO-11(r) and SAPO-31(r).

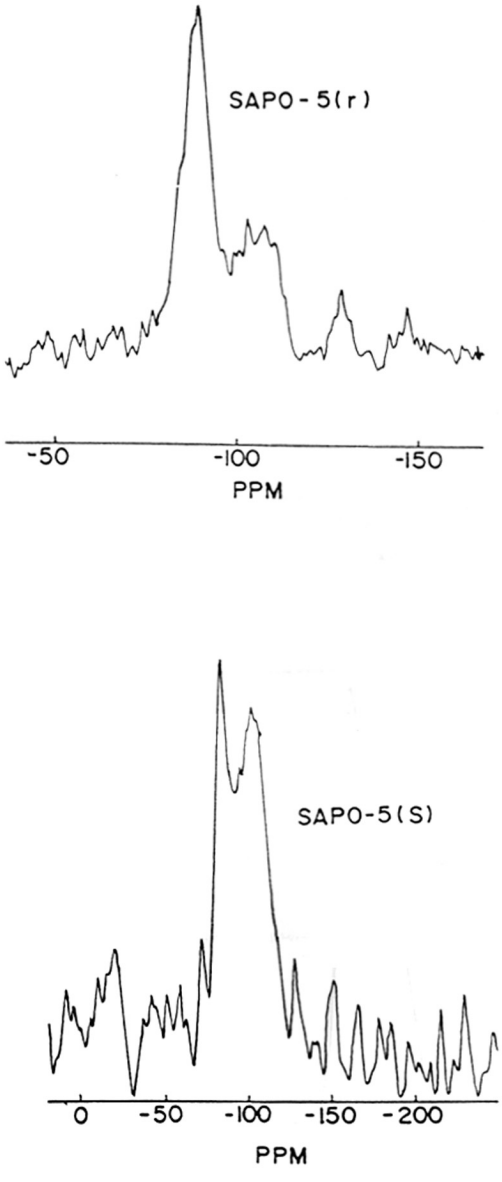

Figure 4.13. ^{29}Si MAS-NMR spectra of SAPO-5(a) and SAPO-5(r).

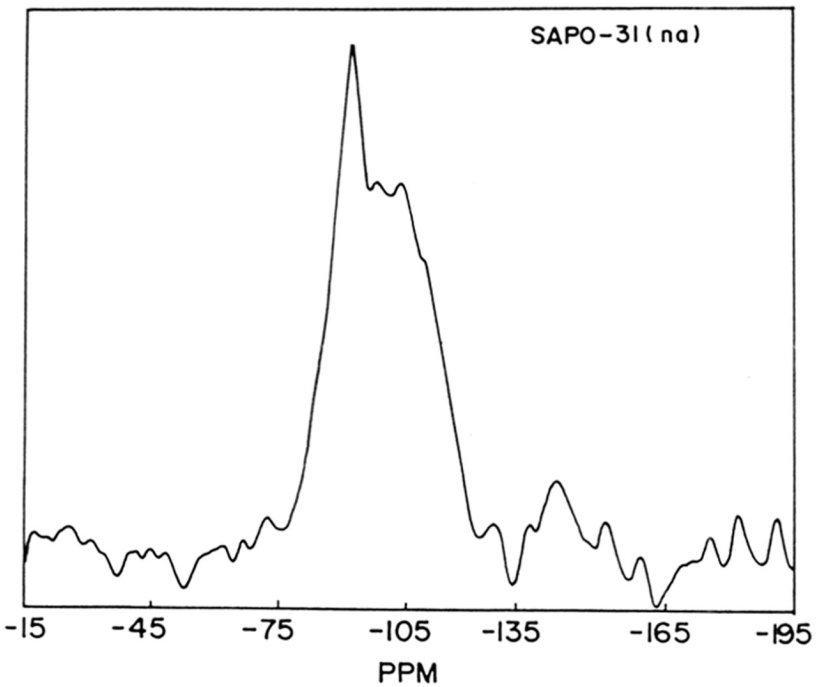

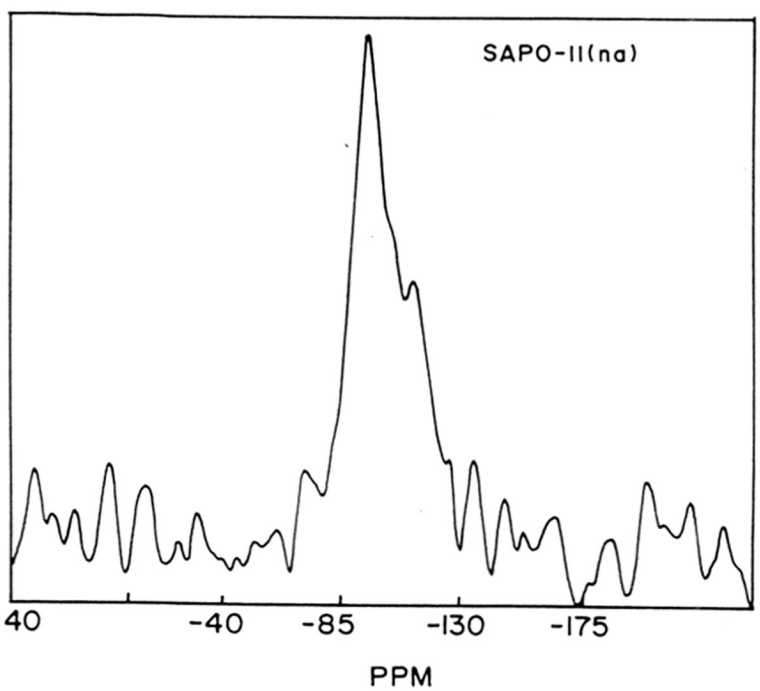

Figure 4.14. ^{29}Si MAS-NMR spectra of SAPO-11(na) and SAPO-31(na).

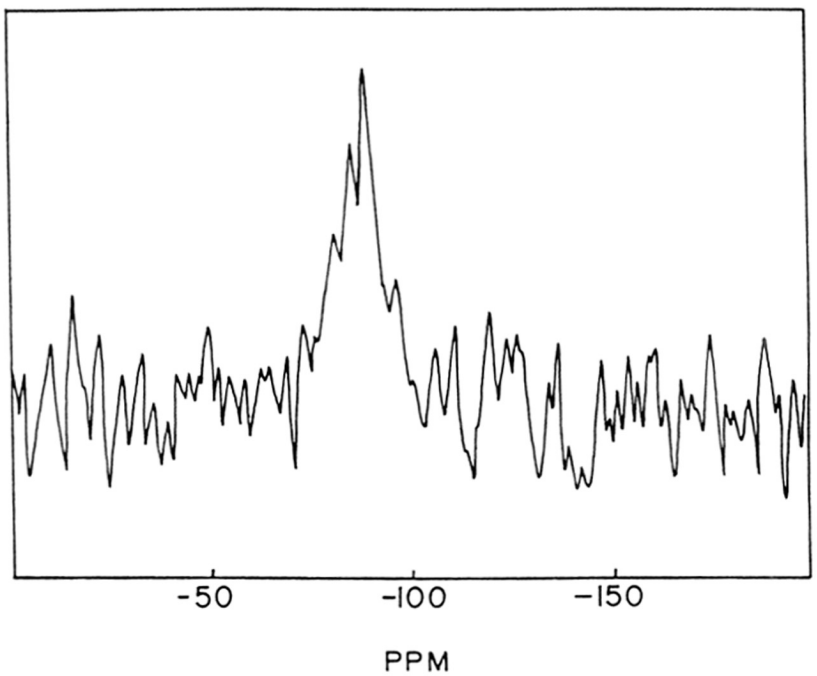

Figure 4.15. ^{29}Si MAS-NMR spectra of SAPO-11(na) synthesized using TEOS as Si source.

4.2.7 TPD of Adsorbed Pyridine

The results of the temperature programmed desorption of adsorbed pyridine are presented in table 4.6 and the corresponding TPD curves are presented in Figure 4.16 (SAPO-11(s), SAPO-11(r) and SAPO-11(na)) and Figure 4.17 (SAPO-31(s), SAPO-31(r) and SAPO-31(na)). The results show that the acidities of the non-aqueous synthesized samples and those of the samples synthesized by rapid crystallization method are higher than those of the conventionally synthesized samples. The decreasing order of acidity in terms of μmol of pyridine desorbed (beyond 573 K) per gram of catalyst is SAPO-31(na) > SAPO-31(r) > SAPO-11(na) > SAPO-11(r) > SAPO-31(a) > SAPO-11(a) while the acidity in terms of mmol of pyridine per mol of Si is in the order SAPO-31(na) > SAPO-31(a) > SAPO-31(r) > SAPO-11(na) > SAPO-11(r) > SAPO-11(a).

4.3 CHARACTERIZATION OF MeAPO-11 AND MeAPSO-11

4.3A Samples synthesized by conventional method (from aqueous medium)

XRD patterns of MeAPO-11 and MeAPSO-11 samples matched well with those of the earlier reported samples [5].

4.3A.1 Elemental Analysis

The elemental composition of various MeAPO-11 and MeAPSO-11 samples (synthesized from aqueous medium) (table 4.6) shows Al/P ratio less than 1 suggesting that metal ions replace Al in the framework. The metal contents (atomic) in the MeAPO-11 samples are similar, being 0.028 ± 0.003. The metal contents are however lower in the MeAPSOs, being only 0.018 ± 0.003 (atom). Similarily, the Si contents in the MeAPSOs are much lower (0.011 ± 0.02 atm) than in SAPO-11 (0.03). The total substituents (Me + Si) are nearly constant (0.03 ± 0.005) in all the samples including SAPO-11. As the metal (Me^{2+}) ions are expected to replace Al^{3+}

Table 4.6 Data for temperature programmed desorption of adsorbed pyridine above 573K.

Sample	Pyridine desorbed	
	μ mol / g	mmol/mol Si
SAPO-11(s)	59.0	71.2
SAPO-31(s)	69.3	140.1
SAPO-11(r)	98.0	84.7
SAPO-31(r)	121.0	122.3
SAPO-11(na)	112.0	95.7
SAPO-31(na)	139.0	210.7

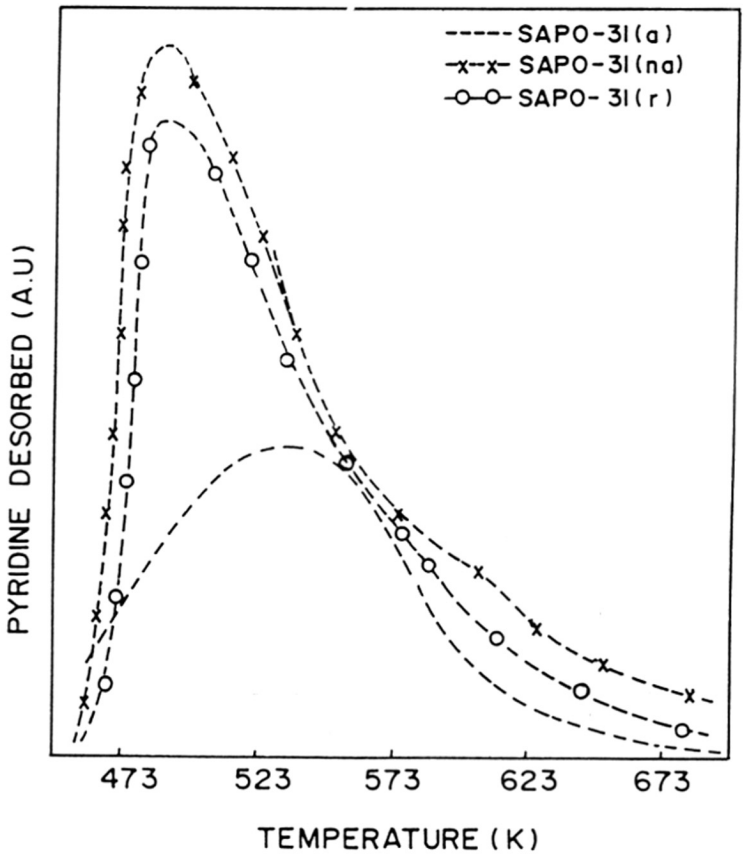

Figure 4.16. Temperature programmed desorption profiles of pyridine over SAPO-11 prepared by different procedures.

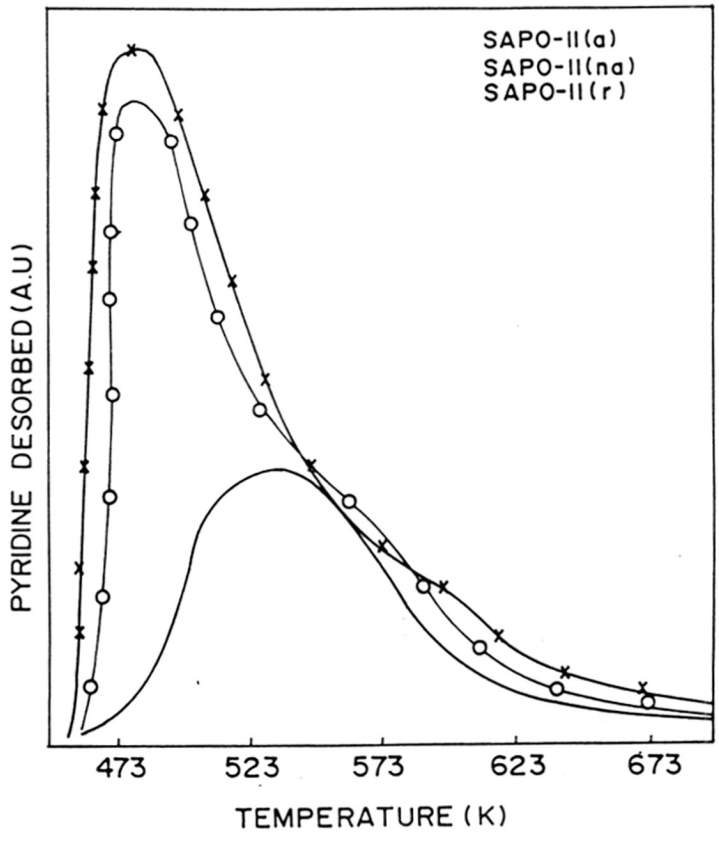

Figure 4.17. Temperature programmed desorption profiles of pyridine over SAPO-31 prepared by different procedures.

ions and, the Si^{4+} ions the P^{5+}, the total number of acid sites should in principle be similar in number in all the samples if the substituents are well dispersed. However, the acid strengths could be different in the samples depending on the substituent metal.

4.3A.2 Surface area measurement

Surface areas of the various MeAPO-11 and MeAPSO-11 samples are tabulated in table 4.7. All the MeAPO-11 and MeAPSO-11 samples had similar surface areas.

4.3B. Comparison of synthesis from aqueous and non aqueous methods:

MnAPO-11

4.3B.1 Elemental Analysis

A comparison of the elemental composition of the MnAPO-11 samples synthesized from aqueous (a) and non-aqueous (na) media (Table 4.7) shows that even though the Mn content in MnAPO-11(na) is slightly less than that in MnAPO-11(a), the lower Al content in the former sample suggests that more of the manganese appears to substitute the Al ions when synthesized in non-aqueous medium.

4.3B.2 Scanning Electron Microscopy

The SEM photographs of the MnAPO-11 samples synthesized from aqueous (a) and non-aqueous (na) media are shown in Fig. 4.18. While the crystals of MnAPO-11(a) are composed of microcrystallites aggregated into irregular shaped (cauliflower like) particles, the crystals of MnAPO-11(na) are well defined spheroids.

4.3B.3 Thermogravimetric Analysis

The TGA/DTA curves of as-synthesized MnAPO-11(a) and MnAPO-11(na) are presented in Fig. 4.19A and B respectively. Four stages of weight loss at ~ 363 K, ~ 513 K, ~753 K and ~ 873 K are observed in the thermograms of the samples. The

Table 4.7. Elemental Composition of MeAPOs and MeAPSOs.

Sample	Elemental composition				
	Me	Al	P	Si	Me+Si
CoAPO-11	0.028	0.461	0.511	-	0.028
MgAPO-11	0.025	0.452	0.523	-	0.025
ZnAPO-11	0.031	0.461	0.508	-	0.031
MgAPSO-11	0.015	0.482	0.492	0.011	0.026
CoAPSO-11	0.018	0.478	0.495	0.009	0.027
ZnAPSO-11	0.021	0.485	0.491	0.013	0.034
MnAPO-11	0.040	0.480	0.480	-	0.040
MnAPSO-11	0.022	0.472	0.494	0.012	0.034
MnAPO-11(na)	0.030	0.40	0.57	-	0.030

Table 4.8: Surface areas of various MeAPO-11 and MeAPSO-11 samples.

Sample	Surface Area (m^2g^{-1})
MgAPO-11	149
MgAPSO-11	169
MnAPO-11	143
MnAPSO-11	159
CoAPO-11	157
CoAPSO-11	164
ZnAPO-11	167
ZnAPSO-11	154

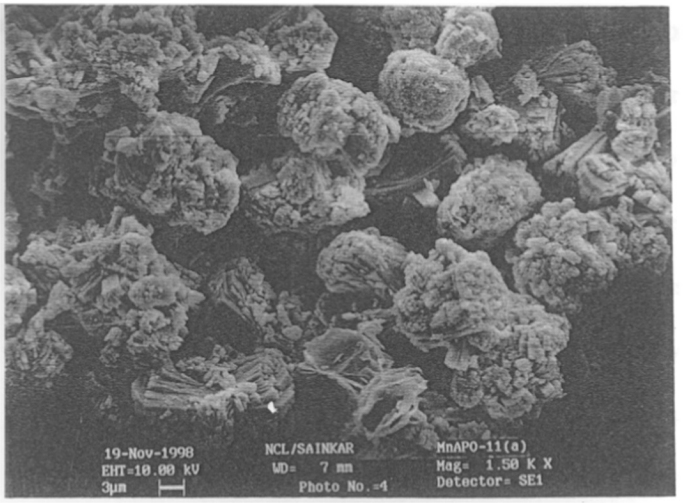

(A)

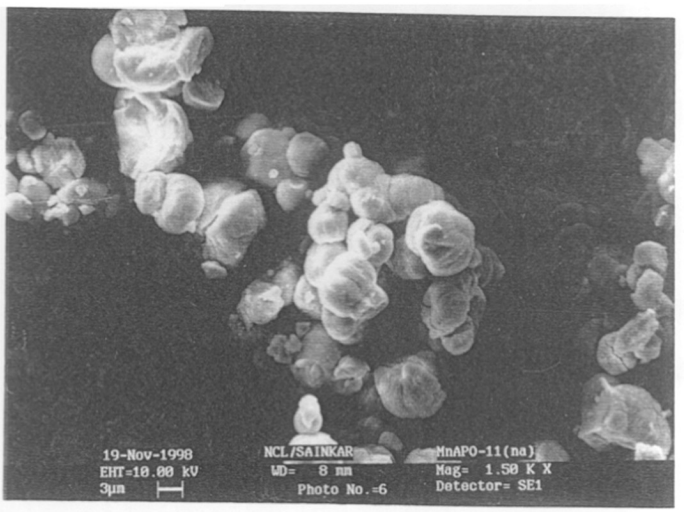

(B)

Figure 4.18. Scanning Electron Micrographs of MnAPO-11(a) (A) and MnAPO-11(na) (B).

first stage of weight loss is due to the desorption of physically adsorbed water. The other weight losses are probably due to the decomposition of the organic templating agent, dipropylamine. While the temperatures of the first and second weight losses are only slightly higher for MnAPO-11(na), the temperatures of the third and fourth losses are much higher for MnAPO-11(na) (by 23 K and 42 K, respectively). The desorption around 513 K is probably due to the physically adsorbed free dipropylamine and the weight loss beyond 673 K are assigned to the decomposition/combustion of protonated dipropylamine. The reason for the higher temperature of desorption/decomposition observed for as-synthesized MnAPO-11(na) compared to that for MnAPO-11(a) is not clear. It is probably due to a larger amount of Mn(II) substitution for Al(III) resulting in a larger charge build up of the framework and stronger adsorption of the organic molecules in MnAPO-11(na). The total amount of the protonated template lost above 673 K is more in MnAPO-11(na) suggesting a larger substitution of Al(III) by Mn(II) in its famework.

4.3B.4 ESR studies

In general, bivalent metal ions such as Mn(II) are expected to substitute the Al(III) in $AlPO_4$ frameworks. The possible locations of Mn(II) in $AlPO_4$ molecular sieves are:

(i) isolated Mn(II) in regular Al sites

(ii) patches containing two or more Mn(II) ions occupying the adjacent or nearby Al positions

(iii) defect (broken framework) sites

(iv) isolated Mn(II) ions in extraframework positions and

(v) bulk MnO_2 in extraframework positions.

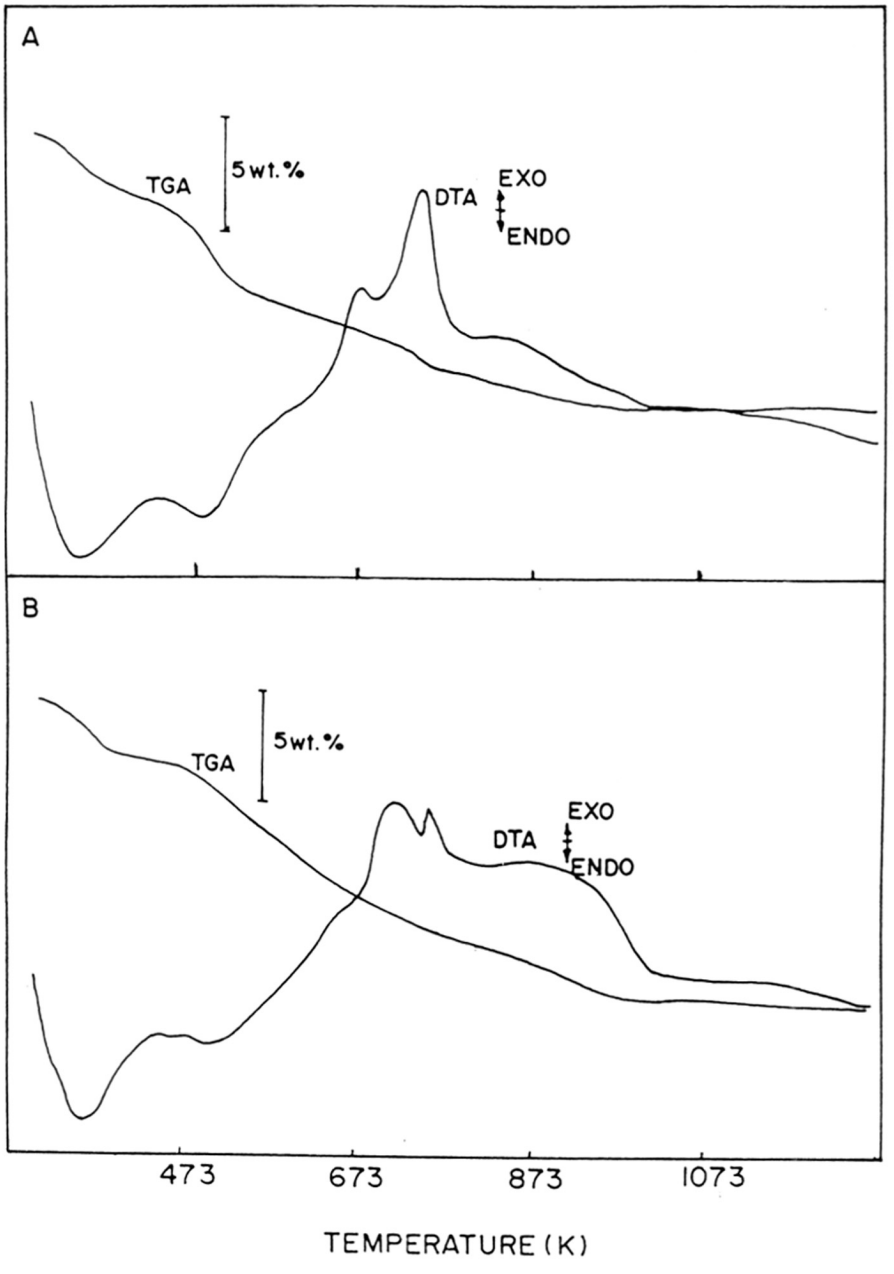

Figure 4.19 TGA/DTA curves of as-synthesized MnAPO-11(a) (A) and MnAPO-11(na) (B).

Mn(II) ions could be present in all these possible sites in MnAPO-11(a) and (na), though the proportions of the various species could be different in the two samples.

The method of preparation (a or na) has a significant effect on the spectra as well as on the nature of Mn sites formed. As-synthesized samples of MnAPO-11(a) and MnAPO-11(na) showed spectra at 298 K consisting of six hyperfine features at g = 2.0039. The separation between the lines is not equal as shown in Fig. 4.20 (a and b) and increases from 72 to 112 G while the line width (ΔHpp) changes from 37.5 to 75.5 G in the direction of increasing field. The average hyperfine coupling constant A_{mn} and ΔH_{pp} are 92 G and 59 G, respectively. The spectra could be attributed to M_s: -1/2 → +1/2 transition of the Mn(II) ion (S = 5/2, I = 5/2) (species I). Although the value of A_{Mn} falls in the range of the values reported for isolated Mn(II), the line width is larger than that reported for MnMCM-41 (12 G) [6] and zeolites X and Y [7]. It appears, therefore, that majority of these ions are probably present in regular framework positions (with O_h coordination) substituting for Al ions in MnAPO-11. O_h coordination of Al-locations in many $AlPO_4$s including $AlPO_4$-11 [8] is known. Measurements at 77 K did not provide any additional information.

Calcined samples of MnAPO-11(a) and MnAPO-11(na) showed at 298 K an intense broad signal (ΔHpp = 500 G for MnAPO-11(a) and 550 G for MnAPO-11(na); Species II) at g = 2.004 and weak signals at g_{eff} = 4.27 and 2.42 (Species III) (Fig.4.20c and d). Moreover, the normalized overall signal intensity of the calcined samples is more (4 times for aqueous and 9 times for non aqueous) than the as-synthesized samples. This could be because the majority of the Mn(II) ions in the as-synthesized samples occupy framework Al position for which the spin lattice relaxation time in the presence of template ions and hydrated water molecules are

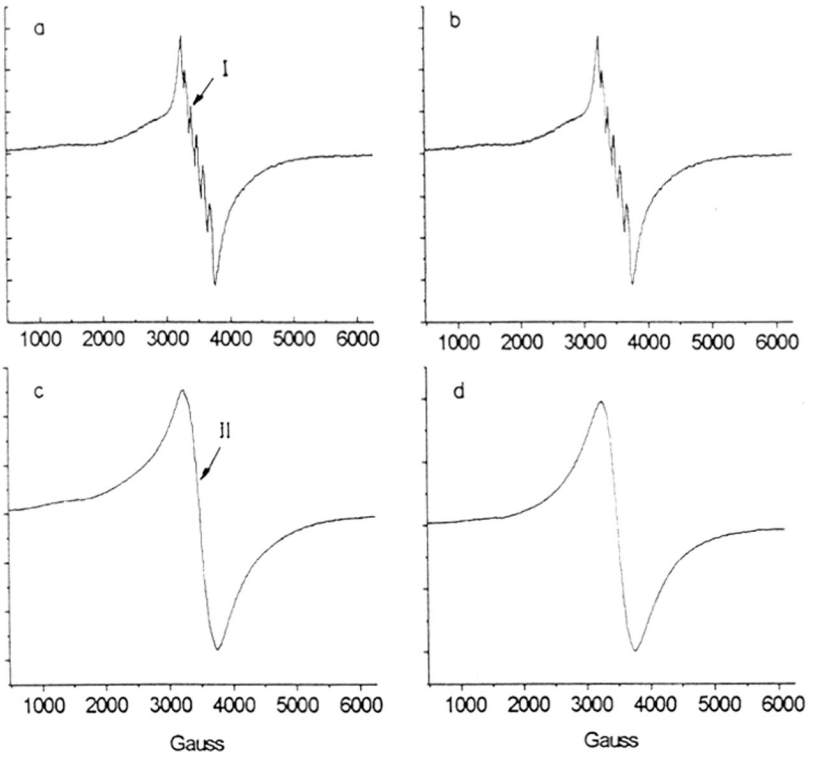

Figure 4.20 X-band ESR spectra of MnAPO-11 samples at 298 K. (a), as-synthesized MnAPO-11(a); (b), as synthesized MnAPO-11(na); (c), calcined MnAPO-11(a); and (d), calcined MnAPO-11(na). Species I due to isolated octahedral Mn(II) and species II due to spin-spin coupled Mn(II) are indicated.

very short and the spectra could not be detected. The line due to Species II is broad due to spin-spin interactions from the nearest neighbours. Similar broad signals were reported also for Mn containing MCM-41 [6], MnAPO-5 [9] and MnAPSO-44 [10]. The additional broad signals at g ~ 4.27 and 2.42 are attributed to isolated distorted tetrahedral (framework) sites (Species III). Weak signals due to species I could also be resolved in the spectra of the calcined samples but these had become broader upon calcination (ΔH_{pp} = 84.5 G) and were masked by the major signal due to species II.

The spectra of the calcined samples did not change much on exchanging with aqueous NaCl and drying at 383 K (MnAPO-11(a)-Na and MnAPO-11(na)-Na) (Fig. 4.21a and b). A major broad signal corresponding to species II and moderately intense signals at g = 4.22, 2.68 and 1.47 corresponding to Species III were the main features of the spectra. The signal due to species III though weakly observed in the calcined samples, becomes more prominent after Na^+ exchange and drying. This is probably due to the removal of extraframework Mn ions causing Mn-Mn interactions and peak broadening in the calcined samples. It is also to be noted that more (7.4 wt. %) Mn was exchanged by Na^+ from MnAPO-11(a) than from MnAPO-11(na) (5.4 wt. %).

Upon exposure to water vapours (ambient atmosphere; relative humidity ~ 80%) the calcined samples exhibited resolved six line pattern corresponding to species I with the average line width of 64 G and A_{Mn} of 96 G (Fig.21 c and d). The 6-line pattern is more intense and better resolved in MnAPO-11(na) than in MnAPO-11(a) probably due to more homogeneous distribution of the isolated Mn(II) sites (species I) in the framework. Additionally MnAPO-11(a) showed a broad signal at g ~ 15 which cannot be attributed to a monomeric Mn(II) ion but can be associated with the exchange coupled Mn(II) hydrated clusters in extraframework position (Fig. 4.21).

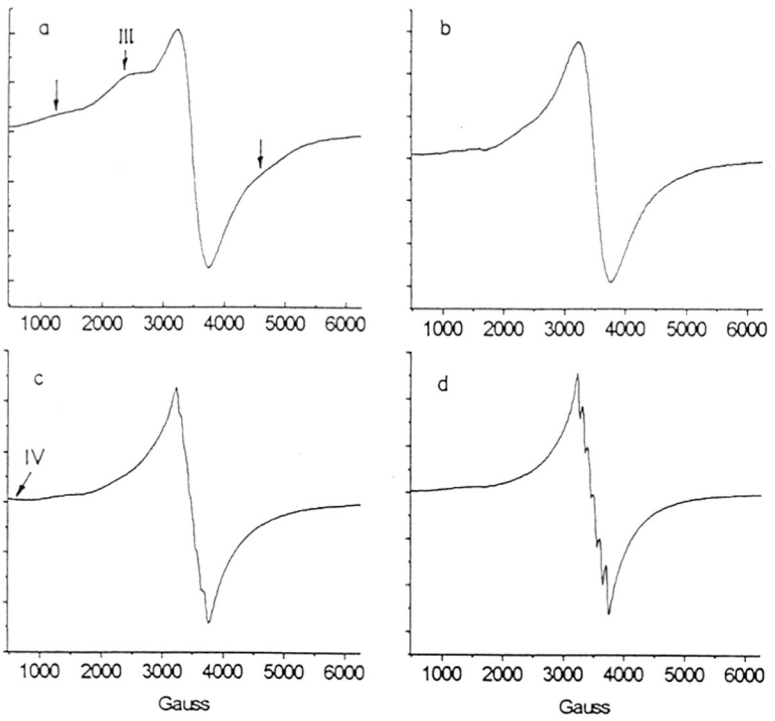

Figure 4.21 X-band ESR spectra of MnAPO-11 samples at 298 K. (a), calcined MnAPO-11(a) after Na exchange (MnAPO-11(a)-Na) and drying at 473 K; (b), calcined MnAPO-11(na) after Na exchange (MnAPO-11(na)-Na) and drying at 473 K; (c), MnAPO-11(a) after hydration and (d), MnAPO-11(na) after hydration. Species III due to distorted tetrahedral Mn(II) and species IV due to extraframework hydrated bulk MnO_x are indicated.

This signal disappeared upon dehydration at 423 K for 16 h suggesting an increase in spin lattice relaxation time of Mn(II) clusters due to removal of hydrated water. This low field signal was not observed in MnAPO-11(na). ESR parameters and the assignments of different Mn(II) species are listed in Table 4.9.

The essential conclusion of esr measurements is that the distribution of Mn is more homogeneous in the sample synthesized from ethylene glycol, with a larger proportion of isolated framework Mn(II) species than in the sample synthesized from aqueous medium. Though extraframework isolated Mn(II) ions could not be observed unequivocally in both the samples, bulk extraframework MnO_2 type species was found to be present in MnAPO-11(a). This was notably absent in MnAPO-11(na). The esr studies confirm the observations made based on the composition and TGA/DTA studies of the samples that Mn(II) incorporation in the framework is more in MnAPO-11(na) than in MnAPO-11(a).

Table 4.9: EPR parameters and assignments for different Mn(II) species.

Species	g	H_{pp} (G)	A_{mn} (G)	Assignment	Location
I	2.0039	59 (60)	91 (95)	Distorted octahedral	Framework
II	2.004	500 (550)	-	Tetrahedral	Framework
III	4.27, 2.42	-	-	Distorted Tetrahedral	Framework
IV	15	-	-	MnO_2	Extraframework

values in parentheses are for non-aqueous samples.

4.4 CHARACTERIZATION OF SAPO-39

4.4.1 X-ray diffraction

The powder XRD pattern of as-synthesized SAPO-39 (Fig. 4.22 C) was identical to that reported earlier for $AlPO_4$-39 and MAPO-39 [11,12].

4.4.2 Elemental Analysis

Comparison of the elemental composition of SAPO-39 $[(Al_{0.49}P_{0.44}Si_{0.07})O_2]$ with that of $AlPO_4$-39 $[(Al_{0.5}P_{0.5})O_2]$ and MAPO-39 $(Al_{0.405}P_{0.504}Mg_{0.096})O_2$ shows that Al/P ratio for $AlPO_4$-39 was 1, but it was greater than 1 for SAPO-39, suggesting the replacement of P^{5+} sites in the aluminophosphate framework by Si^{4+}; on the other hand, the ratio was less than 1 in the case of MAPO-39, suggesting that Mg^{2+} substituted for the Al^{3+} ions.

4.4.3 Scanning Electron Microscopy

SEM photograph of the particles of SAPO-39 (Fig.4.23) shows that the crystals of SAPO-39 are bundles of thin stick-like crystallites; in comparison for MAPO-39 the individual crystallites are bundles varying in size between 5 and 9 μm in diameter and 14 to 19 μm in length.

4.3.4 Thermal Analysis

Fig. 4.24 (A, B) and 4.25 (A, B) present the DTA and TGA curves for the decomposition of DPA-SAPO-39 in nitrogen and air respectively. The DTA and TGA curves for DPA-MAPO-39 and DPA-$AlPO_4$-39 are also given for comparing the influence of variation of substituent in the framework. The DTA and TGA data obtained from the graphs for the three samples are presented in Tables 4.10 and 4.11. From the TGA data it follows that the weight loss from $AlPO_4$-39, MAPO-39 and SAPO-39 containing dipropylamine occurs in three broadly overlapping stages both in inert and oxidizing atmospheres. In inert atmosphere (N_2), the process that occurrs

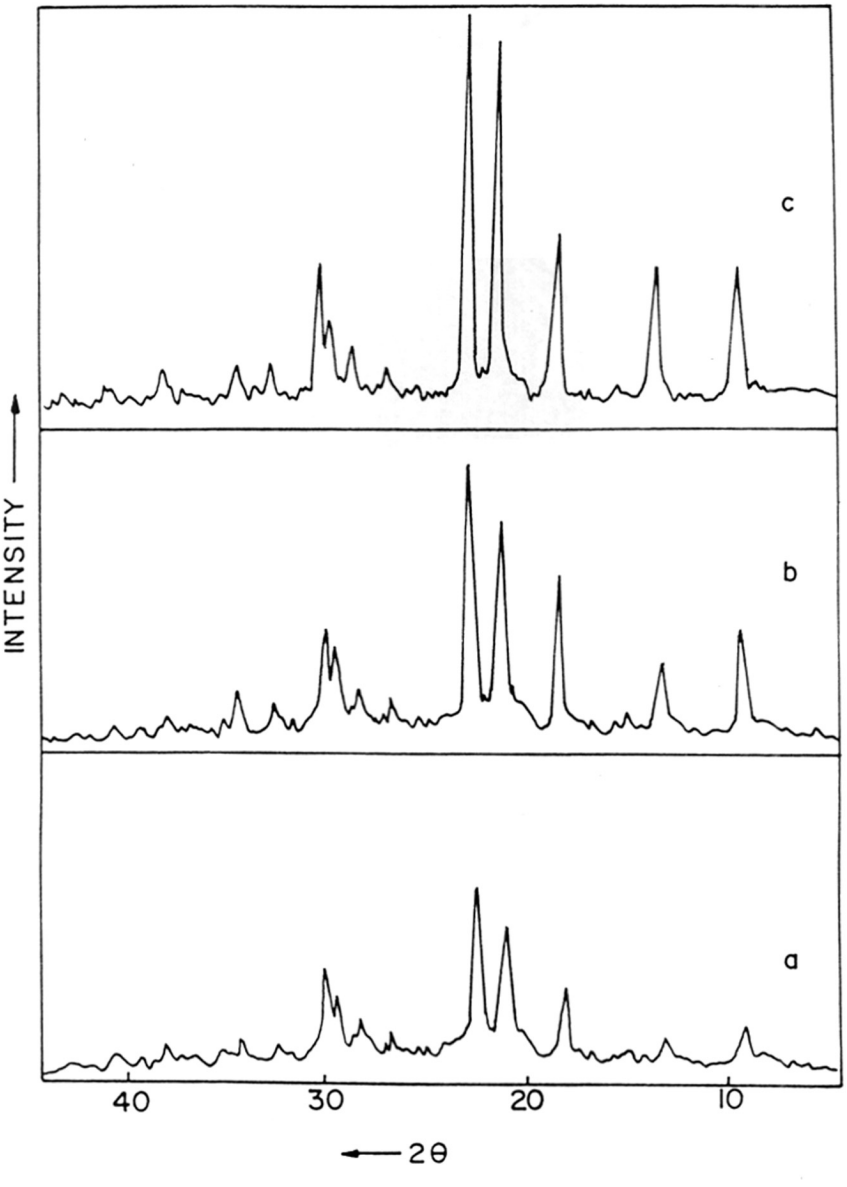

Figure 4.22. XRD patterns of SAPO-39 at various crystallization periods. a) 12 h; b) 24 h; c) 48 h.

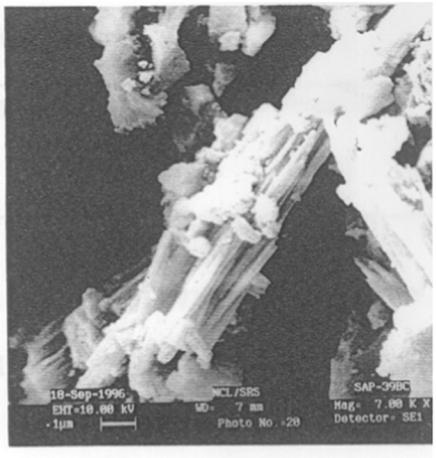

(A)

(B)

Figure 4.23. Scanning Electron Micrographs of SAPO-39 (A) and MAPO-39 (B).

Table 4.10 TGA and DTA data for as-synthesized SAPO-39, MAPO-39 and $AlPO_4$-39 samples (in nitrogen)

Sample	Step	Temperature range (K)	Weight loss (%)	Total weight loss (%)	Peak Temp. (K); DTA
SAPO-39	I	298 - 473	6.4	6.4	377 (endo)
	II	473 - 721	8.5	14.9	533 (endo)
	III	721 - 1123	1.5	16.4	725 (endo)
MAPO-39	I	298 - 473	5.5	5.5	388 (endo)
	II	473 - 831	5.1	7.0	550.8 (endo)
					688 (exo)
	III	832 - 1123	3.0	13.6	791 (exo)
$AlPO_4$-39	I	298 - 473	6.0	6.0	376 (endo)
	II	473 - 747	7.75	13.75	528.5 (endo)
	III	747 - 973	0.5	14.25	444.4 (endo)

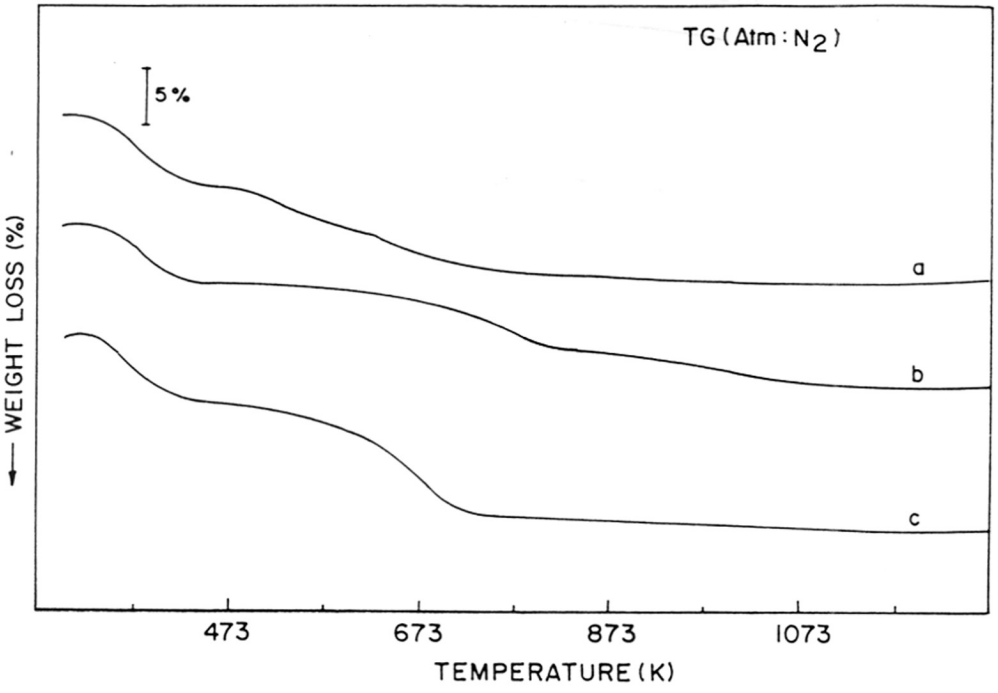

Figure 4.24A. TGA curves of as-synthesized samples in N_2 atmosphere: a) $AlPO_4$-39; b) MAPO-39 and c) SAPO-39.

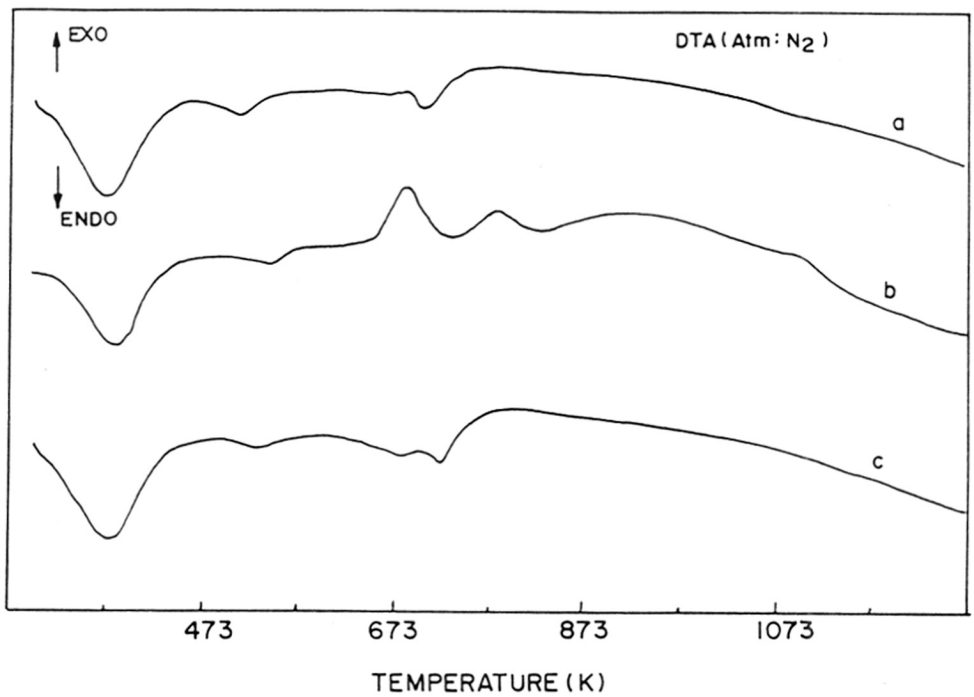

Figure 4.24B. DTA curves of as-synthesized samples in N_2 atmosphere: a) $AlPO_4$-39; b) MAPO-39 and c) SAPO-39.

is the endothermic removal of occluded materials from the different samples. The total weight loss amounts to 16.4 and 13.6 wt% for SAPO-39 and MAPO-39, respectively in inert atmosphere. In the first stage, the weight loss is 6.4 % in the temperature range of 298 to 473 K, which is due to the desorption of physisorbed water and dipropylamine. The major weight loss (8.5 wt%) occurs in the second stage, from 473 to 723 K, which corresponds to the desorption of dipropylamine and possibly to the cracking of the occluded dipropylamine molecule into smaller molecules. This decomposition is consistent with the behaviour of amine-containing ZSM-5 precursors [13] and dipropylamine containing aluminophosphates [14]. In the third stage, the small weight loss of 1.5 wt% occurs in the 722-1123 K range, which is due to the very slow desorption of ammonia and/or dipropylamine adsorbed strongly on the acidic sites in SAPO-39. Also, a fraction of the weight loss (about 1.5 wt%) is exothermic in nature, which is due to the release of the trapped gaseous products with the collapse of the structure [15]. Though the DTA results of the $AlPO_4$ and SAPO samples are similar, two additional exotherms were found for the DTA of MAPO-39. These two exotherms (at 695 and 802 K) are probably due to the decomposition of occluded acetate ions (from the magnesium acetate used as the source of Mg). This was confirmed from the DTA of pure magnesium acetate, wich gave exotherms at 706 and 828 K.

In the oxidizing atmosphere, TG/DTA results indicate that the decomposition occurs in three stages. In the first stage, the desorption of physisorbed water and dipropylamine from DPA-SAPO-39 occurs at lower temperatures (298-473 K) and the weight loss is 6.6 wt%. In the second (473-696.5 K) and the third stages (696.5-873 K), weight losses of 4.9 wt% and 6.0 wt% occur due to the oxidative

Table 4.11 TGA and DTA data for as-synthesized SAPO-39, MAPO-39 and $AlPO_4$-39 samples (in air)

Sample	Step	Temperature range (K)	Weight loss (%)	Total weight loss (%)	Peak Temp. (K); DTA
SAPO-39	I	298 - 473	6.6	6.6	373 (endo)
	II	473 - 696.5	2.25	8.00	651 (exo)
	III	696.5 - 873	6.0	17.5	1023
MAPO-39	I	298 - 473	5.75	5.75	384 (endo)
	II	473 - 696.5	2.25	8.00	695 (exo)
	III	696.5 - 873	8.0	16.00	801 (exo)
$AlPO_4$-39	I	298 - 473	5.25	5.25	369 (endo)
	II	473 - 696.5	5.2	10.45	587 (exo)
	III	696.5 - 873	3.25	13.7	751 (exo)

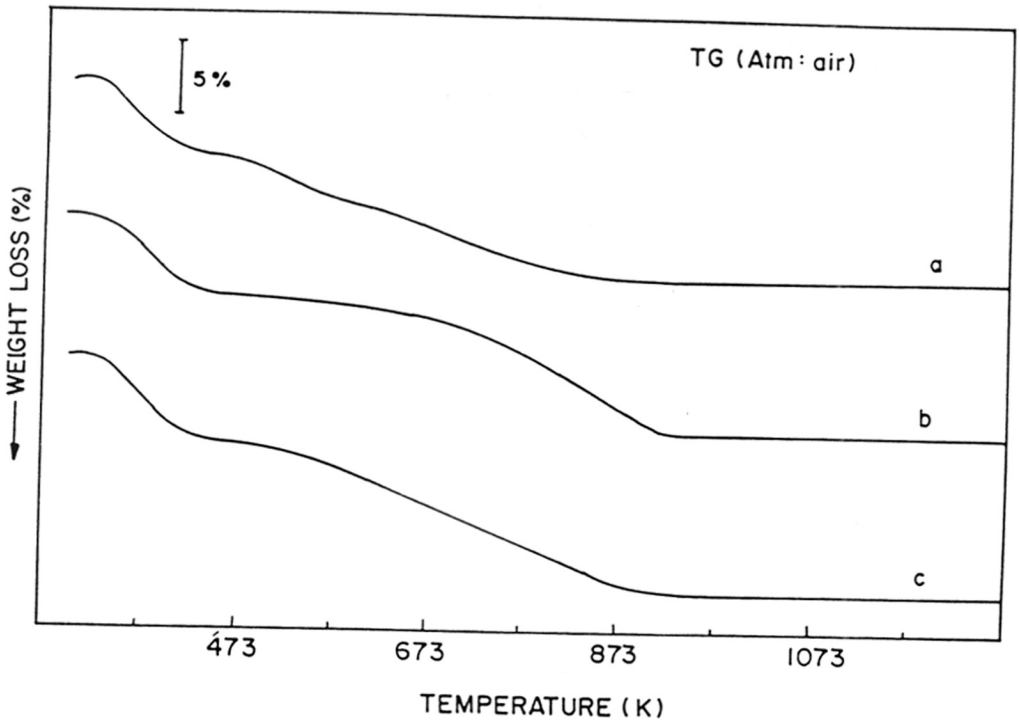

Figure 4.25A. TGA curves of as-synthesized samples in air: a) $AlPO_4$-39; b) MAPO-39 and c) SAPO-39.

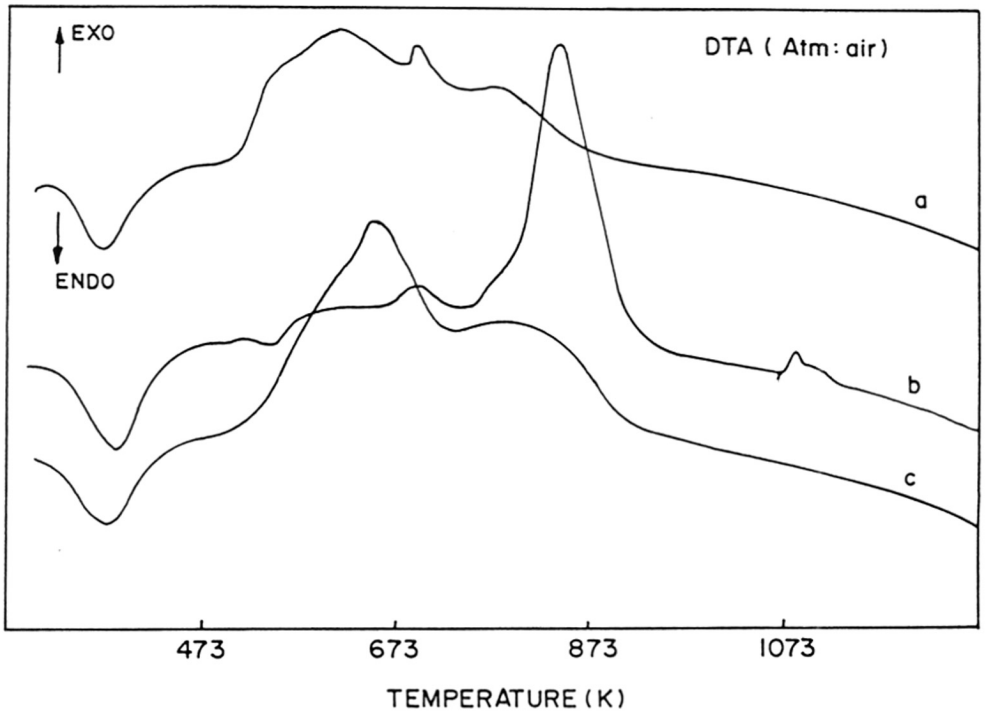

Figure 4.25B. DTA curves of as-synthesized samples: a) $AlPO_4$-39; b) MAPO-39 and c) SAPO-39.

decomposition, which is an exothermic process. The oxidative decomposition is thought to involve the thermal cracking of the occluded dipropylamine, followed by oxidation of the cracked products in the intra- and intercrystalline spaces and also the direct oxidation of dipropylamine within the channels. The DTA of all the samples contain a number of exotherms in the 573 to 873 K range due to the exothermic combustion of the template molecules. In the case of MAPO-39, a sharp and large exotherm is noticed at about 833 K due to the decomposition of occluded acetate ions along with the template molecules.

4.4.5 FTIR - Spectroscopy study of SAPO-39

Figure 4.26, a-c, shows the FTIR spectra of as-synthesized $AlPO_4$-39, MAPO-39 and SAPO-39, respectively. The bands observed around 1,250-1000 cm^{-1}, 800-650 cm^{-1} and 500-400 cm^{-1} are assigned [12, 16] to the asymmetric stretching mode of TO_4 and to the bending mode of T-O-T vibrations. Whereas the nature of the spectra is similar to that reported for MAPO-39 [2], a shift in the peak positions of structure-sensitive bands is clearly seen. For example, the band at 1,133 cm^{-1} in $AlPO_4$-39 due to asymmetric stretching vibration of T-O-T linkage is shifted to around 1,083 cm^{-1} in MAPO-39 and SAPO-39, which indicates the framework substitution of Mg and Si in $AlPO_4$-39.

FTIR spectra of adsorbed NH_3 are presented in Figure 4.27, a-c, and Figure 4.28, a-c, as the difference between the sample with adsorbed NH_3 and the pure sample. In Figure 4.27, a-c, surface hydroxyl groups that are shifted by the adsorption of NH_3 appear as negative bands. They are observed at 3,780, 3,735 and 3,670 cm^{-1} for $AlPO_4$-39; at 3,780, 3,740, 3,670, 3,618, 3,540 cm^{-1}, and a broad band at 3,450 cm^{-1} for SAPO-39; and at 3,780, 3,740, 3,670 and 3,625 cm^{-1} for MAPO-39. For $AlPO_4$-type molecular sieves, bands around 3,780, 3,740 and 3,670 cm^{-1} are assigned

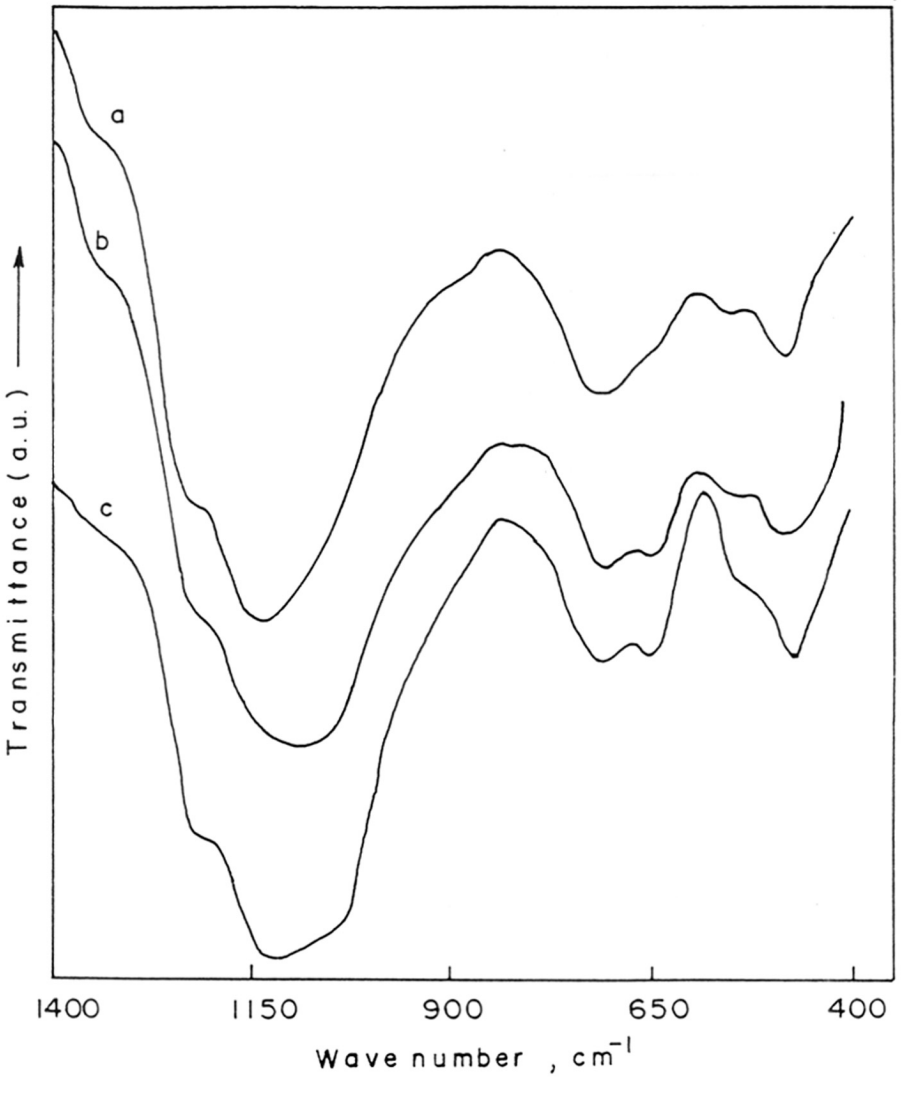

Figure 4.26 Mid-FT i.r. spectra of as-synthesized samples: a) $AlPO_4$-39; b) MAPO-39 and c) SAPO-39.

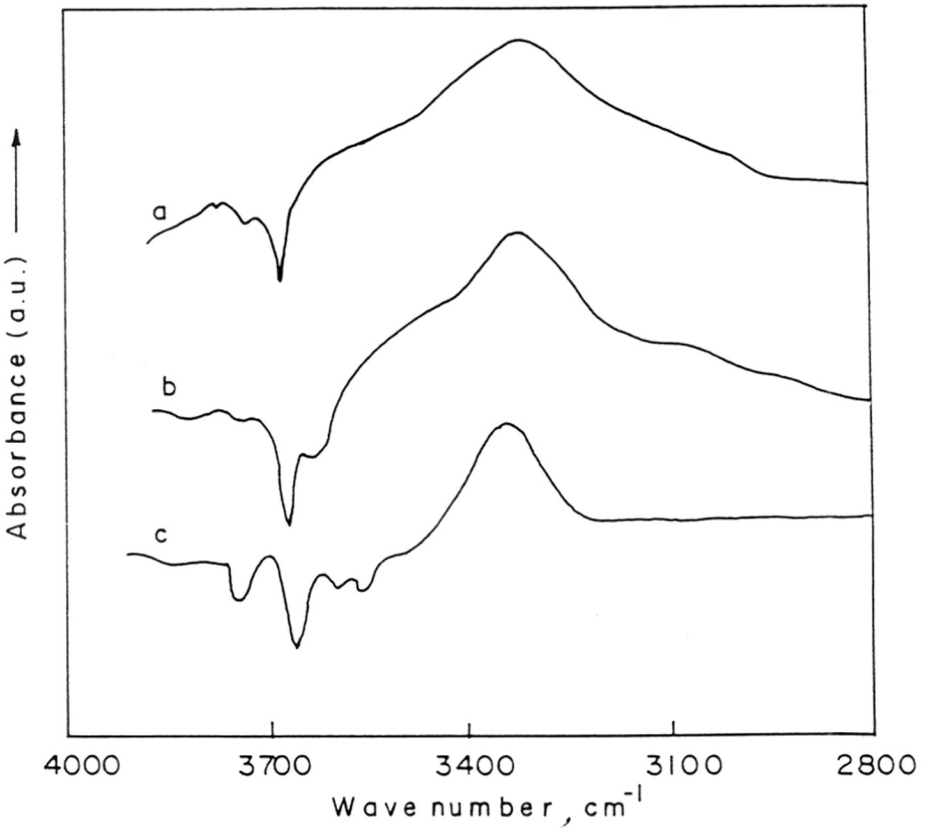

Figure 4.27 Difference FT i.r. spectra (4,000-2,650 cm^{-1}) of adsorbed NH_3 and a pure sample after vacuum activation at 373 K: a) $AlPO_4$-39; b) MAPO-39 and c) SAPO-39.

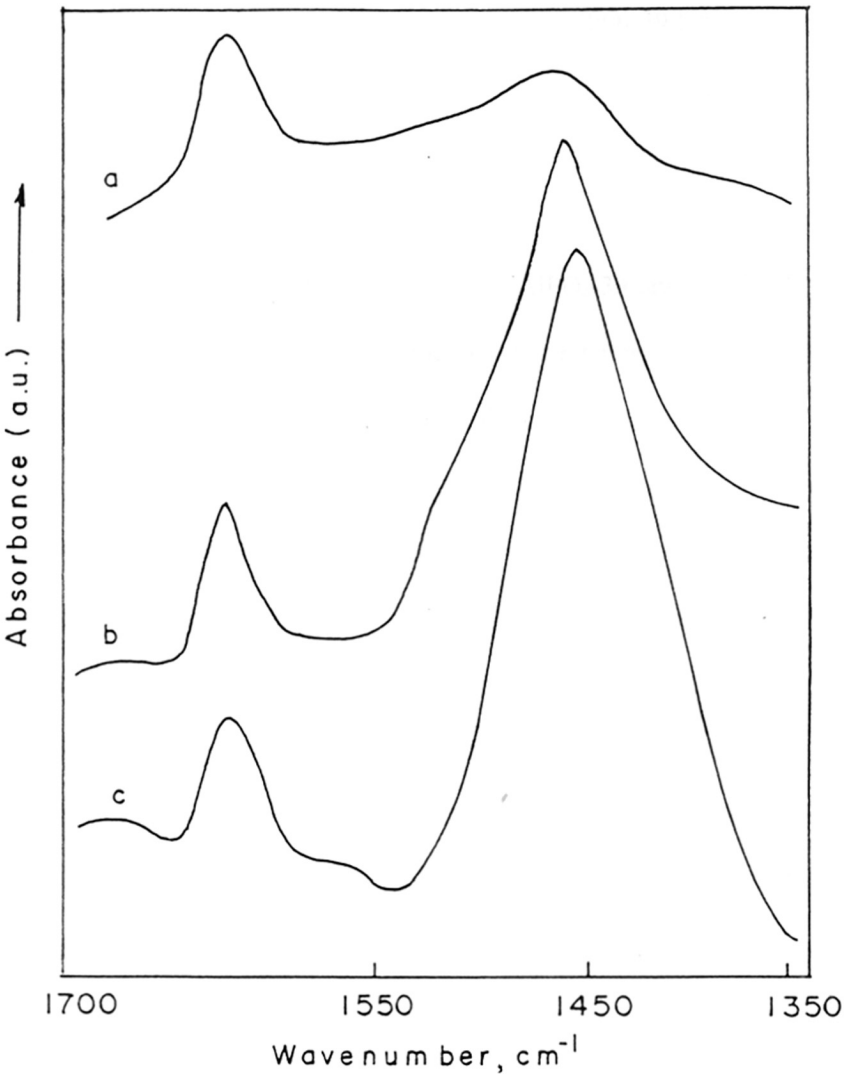

Figure 4.28 Difference FT i.r. spectra (1,800-1,350 cm^{-1}) of adsorbed NH_3 and a pure sample after vacuum activation at 373 K: a) $AlPO_4$-39; b) MAPO-39 and c) SAPO-39.

to Al-OH and P-OH groups, respectively. In the case of MAPO-39, an aditional broad band appears at 3,625 cm^{-1}, which is assigned to Bronsted acidic bridging hydroxyl groups due to Mg^{2+} cation insertion in the $AlPO_4$-39 lattice. Akolekar *et al.* [12] have also observed weak bands in this region, which they attributed to Mg incorporation. For SAPO-39, the peak at 3,740 cm^{-1} is attributed to Si-OH groups and the peaks at 3,618 and 3,540 cm^{-1} to acidic bridging hydroxyl groups, which indicates the lattice incorporation of Si^{4+} in the $AlPO_4$-39 lattice. The broad band at around 3,340 cm^{-1} in all the spectra is due to N-H stretching vibration of chemisorbed NH_3^+. Corresponding deformation vibrational bands are seen in the 1,800-1,350 cm^{-1} region (Figure 4.28, a-c).

Adsorption of NH_3 on Bronsted and Lewis acid sites gives bands at around 1,450 and 1,620 cm^{-1} respectively. For $AlPO_4$-, SAPO- and MAPO-39, we find corresponding bands at 1,452 and 1,620 cm^{-1}, respectively. From Figure 4.28a, it seems that $AlPO_4$-39 has very few Bronsted and Lewis acid sites, whereas MAPO-39 and SAPO-39 show strong bands at 1,452 cm^{-1} due to Bronsted acid sites and a weak band at 1,620 cm^{-1} due to Lewis acid sites. The presence of a high concentration of Bronsted acid sites indicates that in SAPO-39 and MAPO-39, Si^{4+} and Mg^{2+} cations are incorporated in the $AlPO_4$-39 framework replacing, respectively, the P^{5+} and Al^{3+} cations.

REFERENCES

1. Lok, B.M., Messina, C.A., Patton, R.L., Gajek, R.T., Cannan, T.R. and Flanigen, E.M., US Patent 4,440,871 (1984).
2. Jahn, E., Muller, D., Weiker, W. and Richter-Mendau, J., *Zeolites*, **9**, 177 (1989).
3. Jelinek, R., Chemelka, B.F., Wu, Y., Davis, M.E., Ulan, J.G., Gronsky, R. and Pines, A., *Catal. Lett.*, **15**, 65 (1992).
4. Kustanovich, Y. and Goldfarb, D., *J. Am. Chem. Soc.*, , 8818 (1991).
5. Messina, C.A., Lok,B.M., Flanigen, E.M., US Patent,4,544,143 (1985).
6. Xu, J., Luan, Z., Wasowicz, T. and Kevan, L., *Microporous and Mesoporous Mat.*, **22**, 179 (1998).
7. Tikhomirova, N.N. and Nikolaeva, I.V., *Russ. J. Phys. Chem.*, **55**, 2224 (1981).
8. Goepper, M., Guth, F., Delmotte L., Guth, J.L. and Kessler, H. in 'Zeolites: Facts, Figures, Future', (Eds. P.A. Jacobs and R.A. Van Santen), *Studies in Surface Science and Catalysis,* vol. 49 B, Elsevier, Amsterdam, 857 (1989).
9. Levi Z., Raitsimring, A.M. and Goldfarb, D., *J. Phys. Chem.*, **95**, 7830 (1991).
10. Olender (Levi) Z., Goldfarb, D. and Batista, J., *J. Am. Chem. Soc.*, **115**, 1106 (1993).
11. Szostok, R., "Handbook of Molecular Sieves" Van Nostrand Reinhold, p. 50 (1992).
12. Akolekar, D.B. and Kaliaguine, S.K., *Zeolites*, **14**, 620 (1994).
13. Parker, L.M., Bibby, D.M. and Patterson, J.C., *zeolites*, **4**,168 (1984).
14. Chowdhary, V.R. and Sansare, S.D., *J. Thermal. Anal.*, **32**, 777 (1987).
15. Chen, J,, Wright, P.A., Natarajan, S. and Thomas, J.M., Zeolites and Related Microporous Materials: State of the art, 1994, [Eds. Weitkamp, J., Karge, H.G., Pfiefer, H., Holderich, W.) *Stud. Surf. Sci. Catal.*, Vol. 84, Elsevier, Amsterdam,

173 (1994)

16. Flanigen, E.M. in Zeolite Chemistry and Catalysis (Ed. J. A. Rabo) ACS Monograph Ser. 171, Am. Chem. Soc., Washington DC, 1976, p. 80.

CHAPTER V

CATALYTIC ACTIVITIES OF SAPOs, MeAPOs AND MeAPSOs

5.1 INTRODUCTION

The pore dimensions of zeolites and molecular sieves with unkown structures has often been estimated using various catalytic reactions in combination with other techniques [1, 2]. The catalytic tests yield data obtained under realistic conditions, which may include mass-transfer and intrinsic chemical effects [3]. Even though characterization by spectroscopic techniques and adsorption of probe molecules provide general information about pore topology, the picture of pore characteristics given by these techniques is sometimes not complete. Catalytic test reactions often provide additional information on the nature of the pore openings, side pockets and windows [4, 5].

Apart from catalyst test reactions such as m-xylene isomerization, ethylbenzene disproportionation and n-decane cracking, there are a number of other reactions which are either acid or base catalyzed that are industrially important. Now a days, zeolites and molecular sieves are replacing conventional acid catalysts which are hazardous and deleterious to the environment. In contrast, zeolites are eco-friendly, non-hazardous and easy to handle. Zeolites are used in petroleum refining, petrochemical processing and in the synthesis of fine chemicals and drug intermediates. One of the many advantages of zeolites arises from their inherent shape-selective nature and their ability to discriminate molecules by their shapes and sizes which can lead to high selectivities for the desired products.

Medium pore aluminophosphate - based molecular sieves are active and selective catalysts for a variety of important hydrocarbon conversion reactions such as catalytic dewaxing, p-xylene production from C_8 aromatics, olefin isomerization,

conversion of methanol to light olefins, alkylation of aromatics and octane boosting applications, both in FCC and hydrocracking.

The present chapter (Chapter V) discusses the use of the test reaction, isomerization of m-xylene. This chapter also addresses the performance of SAPO-11, SAPO-31, MeAPO-11 and MeAPSO-11 as catalysts in the hydroisomerization of n-alkane and that of the small pore SAPO-39 and MAPO-39 in the transformation of methanol to hydrocarbons.

5.2 EXPERIMENTAL

The methods of preparation of SAPO-11, SAPO-31, SAPO-39, MeAPO-11 and MeAPSO-11 samples and their modifications are described in chapter III.

The catalysts used for all the acid catalyzed reactions were in the protonic form except in the case of hydroisomerization reactions, where Pt impregnated H-forms were used. The catalyst powder was pressed into a pellet, crushed and sieved into 12-18 mesh size particles. Generally, 2-3 g of sample was used in the catalytic studies. The experimental set up used in the studies and the methodology for product analysis have been reported in chapter II.

5.3 RESULTS AND DISCUSSIONS

5.3.1 Isomerization of m-xylene

m-Xylene and ethylbenzene are the major constituents of the feed for a commercial xylene isomerization unit. The m-xylene is converted into an equilibrium mixture of xylene isomers and ethylbenzene is eliminated from the feedstock through isomerization into xylenes and dealkylation. An important cosideration of the process is that minimal xylene loss (through disproportionation/ transalkylation reactions) should occur.

Mechanism

m-Xylene undergoes two types of reactions in the presence of an acid catalyst, namely,

(I) isomerization to ortho- and para- xylenes and

(II) disproportionation or transalkylation to trimethyl benzene and toluenes. The reaction network is depicted in Fig. 5.1.

The isomerization of m-xylene mainly gauges the largest cavity and not the window size. Csicsery [6] has proposed two types of mechanisms and concluded that intramolecular 1,2-alkyl shift was favoured at higher temperatures and intermolecular shifts are favoured below 473 K. Later Corma *et al.* proposed a bimolecular mechanism for the isomerization of m-xylenes [7]. Gnep *et al.* were the first to use m-xylene isomerization as a test reaction to gauge the pore dimensions of zeolites [8].

The zeolites could be ranked as 10 MR or 12 MR pore types depending on the distribution of trimethyl benzene (TMBs) isomers formed during m-xylene isomerization [9]. Three possible pathways are believed to account for the formation of TMBs. The reaction pathways are presented in Fig. 5.1 (scheme II).

Martens *et al.* proposed the formation of diphenyl methane type intermediates during the isomerization of m-xylene [9] (see Fig. 5.1 (VI A-C)). Each intermediate leads to a particular TMB isomer (Figure 5.1 (V A-C)). 1, 3, 5- Trimethyl benzene (VA) is bulkier than the other isomers (VI B and C). The formation of the above isomer will be sterically hindered in the case of medium pore zeolites, but in the case of large pore zeolites they will be formed with relative ease due to the availability of space inside the pores / cages.

The presence of any specific TMB in the product is determined mainly by the extent of steric hindrance inside the zeolite cavity [7, 9]. Thus the differences in the

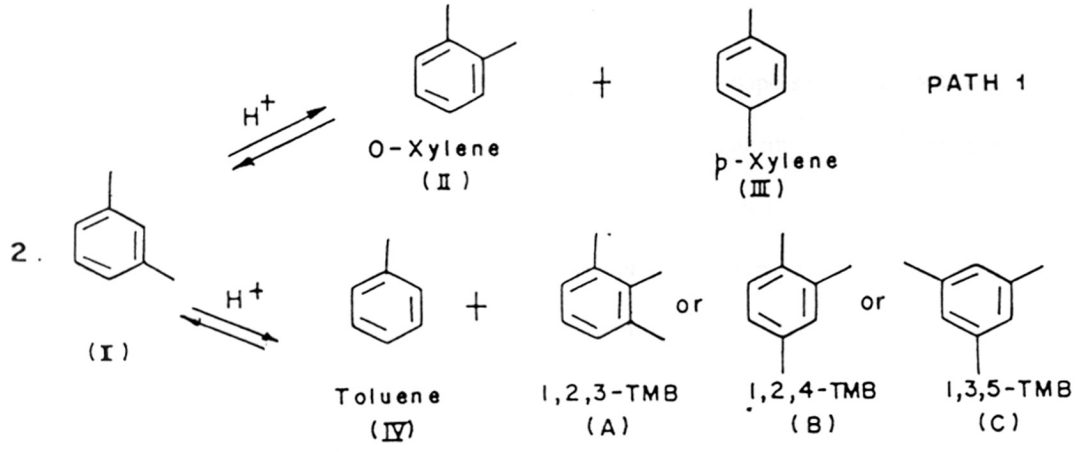

SCHEME – I

Reactions during the isomerization of m-xylene

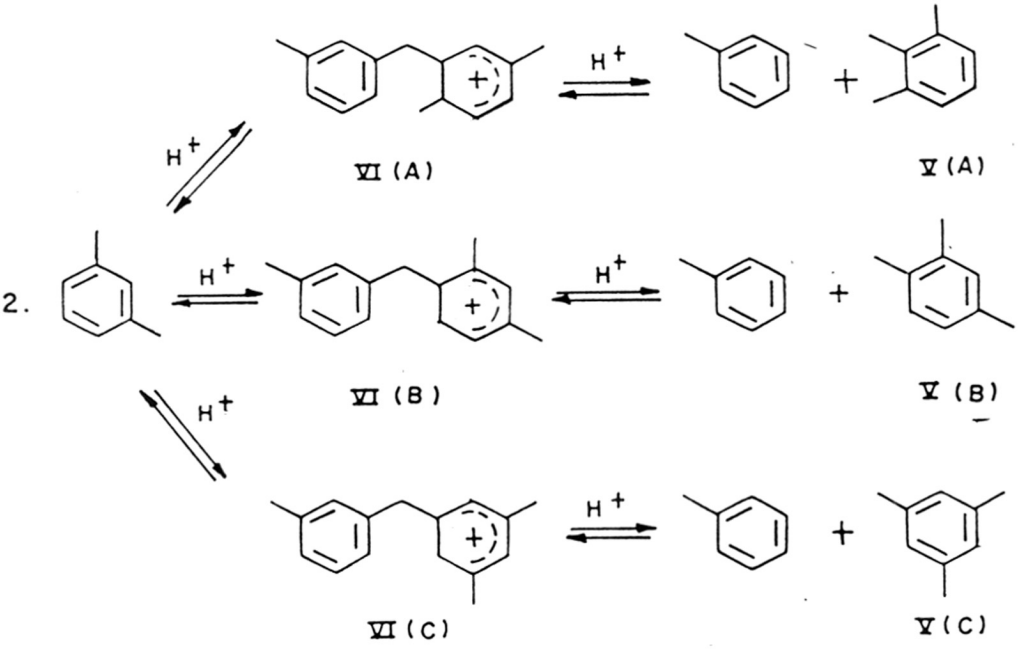

SCHEME - II

Probable transition states during the disproportionation of m-xylene

Figure 5.1. Reactions and transition states during the transformation of m-xylene.

diffusion of TMB isomers through the channels (product shape selectivity, PSS) is believed to be less important than the steric effects on the transition states (restricted transition state shape selectivity, RTSS). Medium pore molecular sieves offer more steric hindrance leading to more isomerized products than the trans alkylated products. Thus, the ratio of isomerization/disproportionation (I/D) ratio is larger over medium pore molecular sieves.

Results and Discussions

Isomerization

Isomerization reactions were carried out over SAPO-11(s), SAPO-11(r), SAPO-31(s), SAPO-31(r) and different MeAPO-11 and MeAPSO-11 samples.

The p-xylene/o-xylene (p-/o-) ratio in the product at various reaction temperatures are presented for various catalysts in table 5.1 to 5.7. It has been shown by earlier workers that when diffusion is absent, the probabilities of producing para and ortho-isomers from m-xylene are nearly equal and p-/o- xylene ratio did not depend on the acid strength of the zeolite [9]. The important parameter that affected the p-/o- xylene ratio was diffusion selectivity. Dewing [10] reported that the diffusivity ratios of p-xylene to o-xylene (D_{para}/D_{ortho}) were 12.82 and 1.73, respectively in the case of ZSM-5 (medium pore; 0.55 nm) and mordenite (large pore, 0.67 nm) at 673 K.

It is found that the p-/o- xylene ratio of SAPO-11, SAPO-31, MeAPO-11 and MeAPSO-11 is well above the thermodynamic equilibrium value of 1.1. In these medium pore molecular sieves, the "diffusion controlled product shape selectivity" (PSS) [9, 11] is believed to be responsible for enhanced para selectivity i.e. more para xylene in the product stream. In the large pore zeolites, an equilibrium distribution of both ortho and para isomers were found suggesting that there is no diffusion

controlled product shape selectivity, as the pores are large enogh to permit rapid diffusion of the xylene isomers. SAPO-31 was found to have a p-/o- xylene ratio of 1.4 to 1.7 (Table 5.7) which is well above the equilibrium value. Thus, SAPO-31 was found to behave as a medium pore molecular sieve, even though structural studies have shown the existance of 12 MR channels normally associated with large pore molecular sieves.

The p-/o- ratio over MeAPO-11 and MeAPSO-11 molecular sieves (Table 5.2 - 5.5) was higher than that over SAPO-11 which could be due to the presence of some extraframework metal ions on the surface partially blocking the pores thereby restricting the diffusion of o-xylene.

Disproportionation

The isomerization of m-xylene is invariably accompanied by disproportionation over acid catalysts. m-Xylene disproportionates into toluene and trimethylbenzenes [9]. (see Fig. 5.1, Scheme II).

During the isomerization of m-xylene, the product pattern is believed to be controlled by PSS, while RTSS is believed to determine the selectivities in disproportionation reactions. The facility or the ability of the transition state to be formed inside the void of a particular molecular sieve governs the formation of a particular type of TMB isomer. Thus, in medium pore molecular sieves, 1,3,5-TMB formation is sterically hindered and is, therefore, present in negligible amounts in the products, while the least bulky isomer, 1, 2, 4-TMB is formed in relatively large quantities. In fact, 1,2,4 -TMB is the only trimethyl benzene observed over all the catalysts under the present study (Tables 5.2- 5.7). The results of temperature variation on the distribution of products (Tables 5.2 - 5.7) shows that as the temperature is increased, the overall conversion as well as disproportionation

Table 5.1 Product distribution in m-xylene isomerization over CoAPO-11 and CoAPSO-11.

	CoAPO-11			CoAPSO-11		
	598 K	623 K	648 K	598 K	623 K	648 K
Conv. (wt%)	11.0	12.7	15.9	11.5	14.5	18.6
Product Distribution (wt %)						
Benzene	-	-	-	-	-	0.1
Toluene	0.2	0.3	0.5	0.3	0.4	0.6
p-xylene	7.8	8.8	10.7	8.2	10.1	12.8
o-xylene	2.8	3.3	4.3	2.7	3.5	4.4
TMB[1]	0.2	0.3	0.4	0.3	0.5	0.7
I/D[2]	26.5	20.2	16.7	18.2	15.1	12.3
p/o[3]	2.8	2.7	2.5	3.0	2.9	2.9

[1]TMB = Trimethyl Benzene; [2]I/D = isomerization / disproportionation ratio;

[3]p/o = p-xylene/o-xylene

Table 5.2 Product distribution in m-xylene isomerization over MgAPO-11 and MgAPSO-11.

	MgAPO-11			MgAPSO-11		
	598 K	623 K	648 K	598 K	623 K	648 K
Conv. (wt%)	12.1	15.5	19.1	12.5	15.9	21.0
Product Distribution (wt %)						
Benzene	-	-	-	-	-	0.2
Toluene	0.3	0.6	0.7	0.4	0.5	0.8
p-xylene	8.2	10.1	12.3	8.6	10.7	13.7
o-xylene	3.3	4.2	5.3	3.1	4.0	5.5
TMB[1]	0.3	0-.6	0.8	0.4	0.7	0.8
I/D[2]	19.2	11.9	11.7	14.6	12.3	10.7
p/o[3]	2.5	2.4	2.3	2.8	2.7	2.5

[1]TMB = Trimethyl Benzene; [2]I/D = isomerization / disproportionation ratio;

[3]p/o = p-xylene/o-xylene

Table 5.3 Product distribution in m-xylene isomerization over ZnAPO-11 and ZnAPSO-11.

	ZnAPO-11			ZnAPSO-11		
	598 K	623 K	648 K	598 K	623 K	648 K
Conv. (wt%)	12.2	13.9	17.1	13.6	15.8	17.6
Product Distribution (wt %)						
Benzene	-	-	-	-	-	-
Toluene	0.2	0.4	0.6	0.3	0.4	0.5
p-xylene	8.9	9.8	11.9	9.7	11.1	12.2
o-xylene	2.9	3.3	4.0	3.3	3.8	4.4
TMB[1]	0.2	0.4	0.6	0.3	0.5	0.5
I/D[2]	29.5	16.4	13.3	21.7	16.6	16.6
p/o[3]	3.1	3.0	3.0	2.9	2.9	2.8

[1]TMB = Trimethyl Benzene; [2]I/D = isomerization / disproportionation ratio;

[3]p/o = p-xylene / o-xylene

Table 5.4 Product distribution in m-xylene isomerization over MnAPO-11 and MnAPSO-11.

	MnAPO-11			MnAPSO-11		
	598 K	623 K	648 K	598 K	623 K	648 K
Conv. (wt%)	9.2	11.8	14.4	10.4	13.3	15.5
Pdt. Distribution (wt %)						
Benzene	-	-	-	-	-	-
Toluene	0.1	0.2	0.3	0.2	0.3	0.4
p-xylene	6.5	8.2	9.8	7.3	9.2	10.7
o-xylene	2.5	3.2	3.9	2.7	3.5	4.1
TMB[1]	0.1	0.2	0.4	0.2	0.3	0.4
I/D[2]	45.0	28.5	19.6	25.0	21.2	18.5
p/o[3]	2.6	2.6	2.5	2.7	2.6	2.6

[1]TMB = Trimethyl Benzene; [2]I/D = isomerization / disproportionation ratio;

[3]p/o = p-xylene/o-xylene

Table 5.5 Product distribution in m-xylene isomerization over SAPO-11(r) and SAPO-11(s).

	SAPO-11(r)			SAPO-11(s)		
	598 K	623 K	648 K	598 K	623 K	648 K
Conv. (wt%)	11.1	14.7	19.9	7.5	9.4	13.3
Product Distribution (wt %)						
Benzene	-	-	0.1	-	-	-
Toluene	0.1	0.2	0.4	0.2	0.4	0.7
p-xylene	7.6	9.4	12.6	4.8	6.0	8.2
o-xylene	3.2	4.7	6.3	2.3	2.7	4.3
TMB[1]	0.2	0.3	0.5	0.2	0.4	0.6
I/D[2]	36	29.5	18.9	17.8	11.8	9.6
p/o[3]	2.4	2.2	2.0	2.1	2.0	1.9

[1]TMB = Trimethyl Benzene; [2]I/D = isomerization / disproportionation ratio;

[3]p/o = p-xylene/o-xylene

Table 5.6 Product distribution in m-xylene isomerization over SAPO-31(r) and SAPO-31(s).

	SAPO-31(r)			SAPO-31(s)		
	598 K	623 K	648 K	598 K	623 K	648 K
Conv. (wt%)	9.2	13.2	16.5	5.7	7.8	10.4
Product Distribution (wt %)						
Benzene	-	-	-	-	-	-
Toluene	0.3	0.5	0.6	0.4	0.6	0.9
p-xylene	5.3	7.1	8.9	3.1	4.0	5.2
o-xylene	3.3	5.1	6.4	1.8	2.6	3.5
TMB[1]	0.3	0.5	0.6	0.4	0.6	0.8
I/D[2]	14.3	12.6	12.8	6.1	5.2	5.1
p/o[3]	1.6	1.4	1.4	1.7	1.5	1.5

[1]TMB = Trimethyl Benzene; [2]I/D = isomerization / disproportionation ratio; [3]p/o = p-xylene/o-xylene

increased. The rate of formation of the transalkylated products is higher at higher temperatures and a slight decrease in p/o ratio has also been noticed. Among all the catalysts, though the overall conversions were not very different, MgAPSO-11 showed highest conversion at all temperatures. At similar conversion levels (~10%) MnAPO-11 exhibited the highest I/D ratio (45) while SAPO-31(s) showed the least I/D ratio (Table 5.8). The maximum p/o xylene ratio (3.1) was found over ZnAPO-11 at an I/D ratio of 29.5 and at a similar conversion level (~10%) (Table 5.8).

Table 5.7 I/D ratios and p/o xylene ratios for different catalysts at ~ 10 % conversion

	SAPO-11(s)	SAPO-11(r)	SAPO-31(s)	SAPO-31(r)	MgAPO-11	MgAPSO-11
I/D[a]	11.8	36.0	5.1	14.3	19.2	14.6
p/o[b]	2.0	2.4	1.5	1.6	2.5	2.8
temp. (°C)	350	325	350	325	325	325

	MnAPO-11	MnAPSO-11	ZnAPO-11	ZnAPSO-11	CoAPO-11	CoAPSO-11
I/D[a]	45.0	25.0	29.5	21.7	26.5	18.2
p/o[b]	2.6	2.7	3.1	2.9	2.8	3.0
temp. (°C)	325	325	325	325	325	325

[a]I/D = isomerization / disproportionation ratio; [b]p/o = p-xylene/o-xylene

5.3.2 Transformation of methanol to hydrocarbons

Introduction

Light olefins, the key components of petrochemical intermediates, are often obtained by the thermal cracking of petroleum gases and naphtha. The transformation of methanol into compounds with higher carbon number could be of industrial importance in the production of light olefins and fuels. The process could become globally important especially when the present efforts to convert methane directly to methanol are successful.

Label and Greene made the first report of the transformation of methanol in 1880 [12]. The conversion was carried out over molten $ZnCl_2$. Hexamethylbenzene was observed as the major product in addition to traces of methane. The mechanism proposed by Label and Greene [12] involved the dehydration of methanol to form "CH_2" (active methylene/carbene) which cyclized to benzene and exhaustive ring alkylation by methyl chloride generated *in situ* (Friedel Craft alkylation) which produced hexamethyl benzenes (HMBs). Later, other researchers examined a variety of catalysts such as P_2O_5 [13], $ZnCl_2$ [14], Al_2O_3 [15], silica gel, Al_2O_3 and silica alumina [16], activated alumina [17] and metal-molybdate catalysts for the transformation of methanol to hydrocarbons [18].

A major technological breakthrough was achieved by Mobil Oil Corporation by successfully converting methanol into gasoline in a catalytic process called the Mobil MTG process [19, 20]. The catalyst used was the shape selective, medium pore zeolite, ZSM-5, with a high silica to alumina ratio [21]. Till today, ZSM-5 has proven to be the best catalyst for the conversion of methanol with good selectivities for aromatics. The major hydrocarbons produced from the transformation of methanol over ZSM-5 are C_1-C_4 alkanes, C_2-C_4 alkenes and C_6-C_{10} aromatics. No

higher aromatics were found in the product stream of the shape selective pentasil zeolite [22].

Apart from ZSM-5 [23], ZSM-8 [24], small pore zeolite Nu-1 [25, 26] and the large pore zeolite offretite [27] have also been used in the conversion of methanol. Cormerais *et al.* [28] have investigated the influence of acidity of zeolite Y on this reaction. Later Sulikowski and Popierlaz have reported the selective formation of HMBs over ultra stable zeolite Y [29].

More recent studies have shown that non-zeolitic molecular sieves like SAPO-34 can produce ethylene and propylene at high selectivity and still remain active (coke free) over a long period of time [30 -33].

Mechanism

The mechanism of the conversion of methanol to hydrocarbons over an acid catalyst comprises of three key steps:

(I) Formation of the ether.

(II) The first C-C bond formation leading to reactive olefins.

(III) Cyclization and aromatization with H-transfer.

Ether formation occurs via adjacent surface methoxyls. Since, methanol does not possess any parent olefin, the formation of ether and the subsequent formation of C-C bond appears to be the important route. Many researchers have reported ethene as the primary intermediate during methanol transformation [23, 24]. Nováková *et al.* [34] have suggested that the reaction of gaseous methanol resulted in a very reactive surface C_1 species which further led to the formation of the first C-C bond. Hydrocarbon formation was considered to occur by condensation of methoxy groups accompanied by dehydration and hydride transfer as proposed by Topchieva *et al.*

[16]. Salvador *et al.* [35] have proposed the α-elimination mechanism. Chang *et al.* [23] have proposed an intermediate of carbenoid type during the α-elimination mechanism. Van-der Berg *et al.* have proposed oxonium ylide type of intermediate to explain the formation of the C-C bond, which also involved a Stevens type rearrangement [36].

Many reaction mechanisms have been proposed for cyclization and aromatization. Dejaifve *et al.* [37] have proposed a carbenium ion mechanism and have accounted for the formation of higher aliphatics and aromatics.

Results and Discussions

The catalytic activities of SAPO-39 in the transformation of methanol are given in Table 5.8. The activities of MAPO-39 and $AlPO_4$-39 are also presented for comparison. Because SAPO based catalysts are found to deactivate relatively fast when used in methanol conversion, the methanol conversion studies were carried out for a short time-on-stream (60 min.). Both the degree of conversion and the selectivity for light olefins are relatively low when compared to SAPO-34 [38] which could be due to differences in acidity and pore characteristics. $AlPO_4$-39 catalyzes methanol conversion mainly to dimethyl ether as it has very little Bronsted acidity. SAPO-39 and MAPO-39 convert methanol to hydrocarbons at elevated temperatures. However, the activity, selectivity and the life of the samples vary significantly (Fig. 5.2 and 5.3). The maximum conversion to hydrocarbons is about 92 % for SAPO-39 at 723 K, whereas for MAPO-39

Table 5.8 Methanol conversion on $AlPO_4$-39, SAPO-39 and MAPO-39 at WHSV = 1.5 h^{-1}.

	SAPO-39				MAPO-39				$AlPO_4$-39	
Temperature (K)	623	673	723	773	623	673	723	773	673	723
Methanol Conversion (%)	90.2	71.9	98.6	91.1	89.3	53.3	63.8	87.4	62.4	56.5
Hydrocarbon Formation (%)	10.1	57.1	92.4	83.0	5.4	17.4	38.3	52.7	Traces	Traces
Dimethyl Ether (%)	89.9	42.9	7.6	17.0	94.6	82.6	61.7	47.3	99.9	99.9

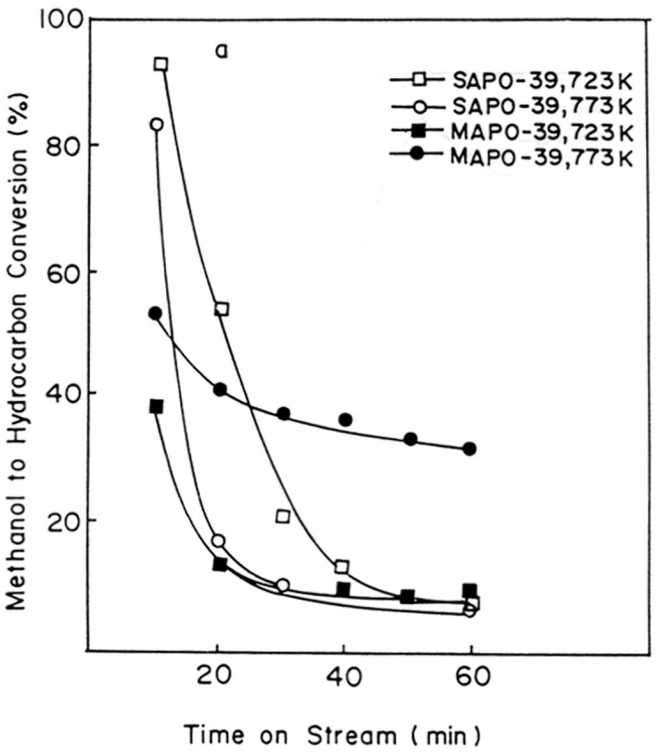

Figure 5.2. Methanol conversion to hydrocarbons (wt. %) versus time on stream (min.) for SAPO-39 and MAPO-39.

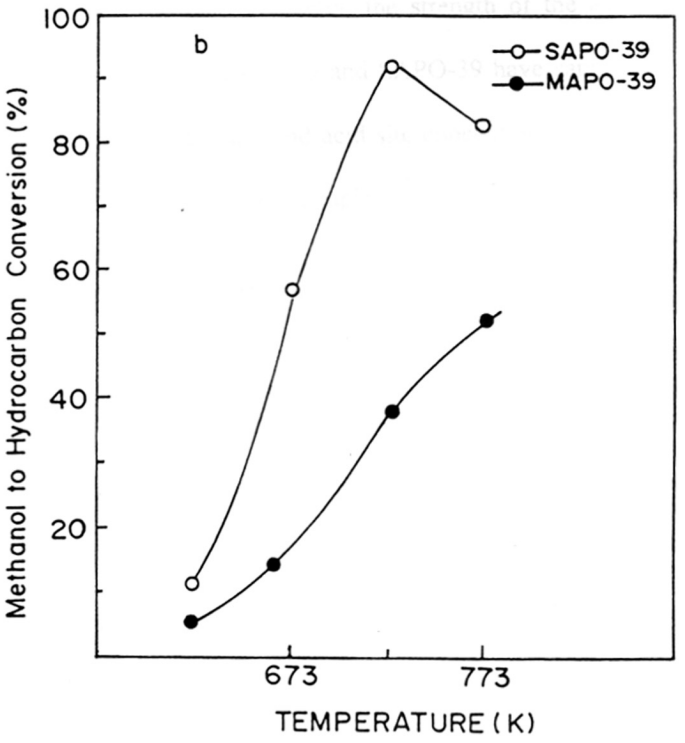

Figure 5.3. Variation of methanol conversion to hydrocarbons (wt. %) with temperature for SAPO-39 and MAPO-39 (time on stream = 20 min.).

the maximum conversion is only 50% at a temperature of 773 K. SAPO-39 is more active than MAPO-39 at all test temperatures.

At 773 K, SAPO-39 deactivates very rapidly, and within an hour the activity drops to 6% but the corresponding deactivation under the same conditions for MAPO-39 is less (only 31%). The deactivation rate of a microporous material in a catalytic reaction depends upon the pore geometry, the strength of the acid sites and their concentration. Because both MAPO-39 and SAPO-39 have same pore geometry, it seems that the higher acid strength and acid site concentration in SAPO-39 (than in MAPO-39) are responsible for the more rapid deactivation of SAPO-39.

5.3.3 Hydroisomerization of n-alkanes

Introduction

The hydroisomerization of light naphtha (C_5-C_6 fractions) is an industrially important process and is used in the production of high octane gasoline blend stocks [39, 40]. The process involves the transformation (with minimal cracking) of the low octane normal (and less branched) paraffin components into high octane isomers with greater branching of the carbon chain. For example, n-hexane has a blending research octane number of 19 [41] which on isomerization yields an equilibrium mixture of n- and i-hexanes, the overall RON of the mixture (at 503 K) being 74.9. The dimethyl butanes (2,2-dimethyl butane; RON = 92.3 and 2, 3-dimethyl butane; RON = 103.5) have larger RON values than the monomethyl pentanes (2-methyl pentane; RON = 73.4 and 3-methyl pentane; RON = 74.5) and constitute a larger proportion of the equilibrium mixtures at lower temperatures.

Hydroisomerization reactions are generally carried out over bifunctional catalysts, containing often, platinum. The metal component aids in increasing the rate

of isomerization besides lowering catalyst deactivation. The reactivity of the n-alkane increases as the carbon number increases but the selectivity towards isomerization decreases [42]. The monobranched isomers are formed predominantly as they are the primary products. These undergo consecutive reactions to yield multiple branched isomers. The chain length has a marked influence on the reaction rate and over the formation of the multiple branched isomers, which increases with increasing the chain length [42].

The hydroisomerization of n-hexane has already been studied over Pt-loaded zeolites such as Pt-Y [43], Pt-beta [44] and Pt-mordenite [45]. There is a general consensus on the mechanism of alkane hydroisomerization. n-Alkane molecules are adsorbed at dehydrogenation/ hydrogenation sites where n-alkenes are formed. These migrate and interact with acid sites and secondary carbenium ions are generated, which further rearrange to more stable tertiary carbenium ions. Finally, the tertiary carbenium ions are hydrogenated at the metallic sites yielding isoalkanes [46, 47].

The isomerization of n-hexane over Pt supported on acidic zeolites is supposed to proceed by a bifunctional mechanism [43, 44]. The metal atoms act as dehydrogenation sites and generate reactive olefinic intermediates. The olefinic intermediates isomerize via carbocations over Bronsted acid sites. The iso-olefins transform into iso-paraffins over the metal atoms by hydrogenation.

During the isomerization of n-paraffins, shape selective molecular sieves suppress multibranched isomer formation [48] which are more susceptible to hydrocracking thereby leading to higher isomerization selectivities [49]. In general, methyl branching increases with decreasing pore width of the zeolite while ethyl and propyl branched isomers are obtained from wide pore openings and large cavities. In the isomerization of n-decane, bifunctional ten-membered ring zeolites (ZSM-5 and

ZSM-22) produce very little di- and tri-branched isomers. Besides, the rate of formation of 4-methyl nonane and 5-methyl nonane were low when compared to that of the 2-methyl isomer [50, 51]. Also, the isomerization of n-heptadecane over ZSM-22 resulted in the preferential formation of certain dimethyl isomers [52]. These results have been explained on the basis of pore mouth catalysis mechanism operative when the reactant is a long chain n-alkane. Again, Pt-ZSM-22 (0.45 x 0.55 nm) showed a preferential central hydrocracking of n-decane different from that over the medium pore Pt-ZSM-5 (0.52 x 0.54 and 0.51 x 0.55 nm) [53].

Results and Discussions

I. Studies on SAPOs

n-hexane isomerization

Catalytic hydroconversion of n-hexane involves the initial dehydrogenation of n-hexane to n-hexene on metallic sites, the subsequent isomerization of n-hexenes to isohexenes on acidic sites and their final migration to metallic sites and hydrogenation to isohexanes. In addition, the isohexenes formed may undergo isomerization among themselves or cracking on the acid sites.

i) Influence of Pt content on n-hexane isomerization

In all the experiments described, the catalysts generally deactivated slightly with duration of run (time on stream, TOS), the deactivation being more rapid during the first few minutes. The influence of TOS on conversion and selectivity to isomerization (expressed as the isomerization/cracking ratio, I/C) is presented in Fig. 5.4 for different samples. The deactivation noted is presumably due to the loss of the very strong acid centres and the overactive Pt sites. It is also noticed that the I/C ratio increases with TOS due to reduced cracking and hydrogenolysis activities which were

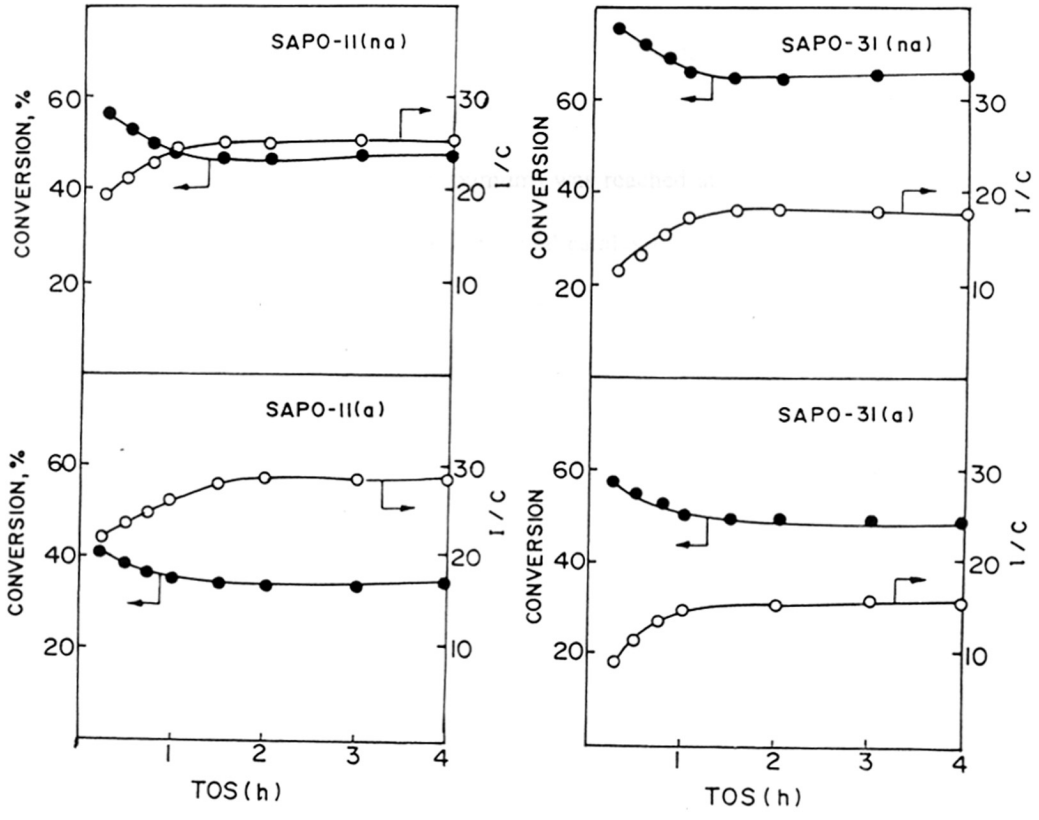

Figure 5.4. Influence of time on stream on conversion (•) and I/C ratio (o).

more prominent at short TOS. Since the activity became nearly stable after about 45 min., the data collected at a TOS of 1 h are reported. The influence of Pt content on conversion and selectivity to isomerization (expressed as the isomerization/cracking ratio, I/C) was investigated using SAPO-11(a) and SAPO-31(a). The results obtained at 573 K (WHSV = $1h^{-1}$ and H_2 / n-hexane (mole) = 5) after a TOS (time on stream) of 1h are presented in Fig. 5.5. Increasing the Pt content increased both the conversion and I/C ratio until a plateau (or a maximum) was reached at about 0.5 wt% Pt (Fig. 5.5). This behaviour is typical of bifunctional catalysis [54-56]. The reason for the initial increase in the I/C ratios with increasing Pt content was the greater availability of Pt sites in the vicinity of acid sites enabling rapid hydrogenation of the carbenium ions (and olefins) which desorbed as alkanes before they underwent cracking reactions.

ii) Influence of temperature

The conversion of n-hexane increased with temperature over all the four catalysts (Fig. 5.6a). The increase in conversion is less rapid at higher temperatures. This is probably due to diffusion effects at high conversions, besides being also due to more rapid initial deactivation at higher temperatures as the data were collected at a TOS of 1 h. As expected from their higher acidities, SAPOs synthesized from non-aqueous media showed higher conversions. SAPO-31 was more active than SAPO-11 due to the larger number of acid sites in the former (Table 4.6). Hydroconversion activity decreased as: Pt-SAPO-31(na) > Pt-SAPO-31(a) > Pt-SAPO-11(na) > Pt-SAPO-11(a). Over the SAPO catalysts studied, the yields of the cyclized products (and aromatics) were always small (less than 2% at the highest conversion). Small amounts of olefins were also found in the products. The major products were isohexanes (methyl pentanes and dimethylbutanes) and cracked gases (C_1 - C_5) (Fig.

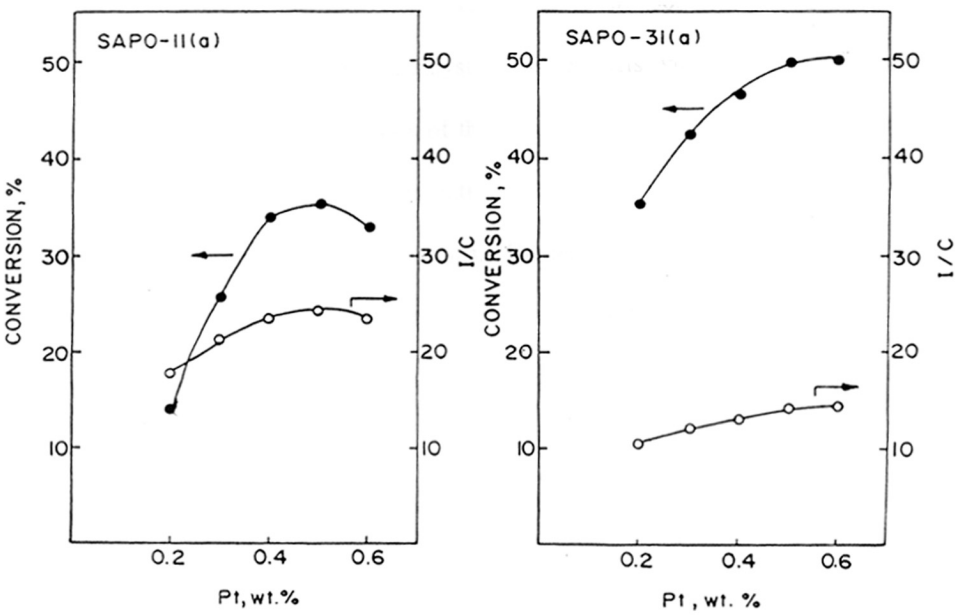

Figure 5.5. Influence of Pt content on n-hexane isomerization.

(Temp. = 573 K; WHSV (h^{-1}) = 1; H_2/n-hexane (mole) = 5; TOS = 1 h)

5.6 b). It can be assumed that the major production of C_1 and C_2 resulted from n-hexane hydrogenolysis along with equimolar amounts of C_4 and C_5. Acid catalyzed cracking of 3-methylpentane could have also yielded ethane and butane. Propane was the major cracking product.

A good measure of the performance of the samples as hydroisomerization catalysts can be arrived at from the weight ratios of the isomerized products to the cracked products (I/C); the better catalyst yields products with higher I/C ratios at a specified conversion. The I/C ratios of the products obtained over the four catalysts are presented in Fig. 5.6c and d. The ratios pass through maxima (at ~ 573 K) with increasing temperature for all the samples. The reason for the maximum is not clear though a possible explanation is that at the intermediate temperature (573 K), the desorption and hydrogenation of the intermediate iso-olefins into isoparaffins is maximum. At lower temperatures, the desorption of the iso-olefin may be slower resulting in greater cracking of the adsorbed species, while at higher temperatures, the hydrogenolysis activity of the metal may be more. In general, the samples (na) prepared from non-aqueous media possessed greater isomerization selectivities. The isomerization products obtained were predominantly monobranched over both Pt/SAPO-31 and Pt/SAPO-11 due to diffusional limitations in the one dimensional medium size pores. Only at higher temperatures (high conversions) dimethyl butane formation was substantial. There was a continuous increase in the yields of the isomers, the increase in the dimethylbutanes becoming more rapid at higher temperatures. The breakdown of the components in the isohexane fraction showed that the monobranched isomers decreased while the dibranched isomers increased with increasing temperature suggesting the transformation of the former into the latter compounds. The 2-methyl pentane/3-methyl pentane ratios were in the range of 1.7

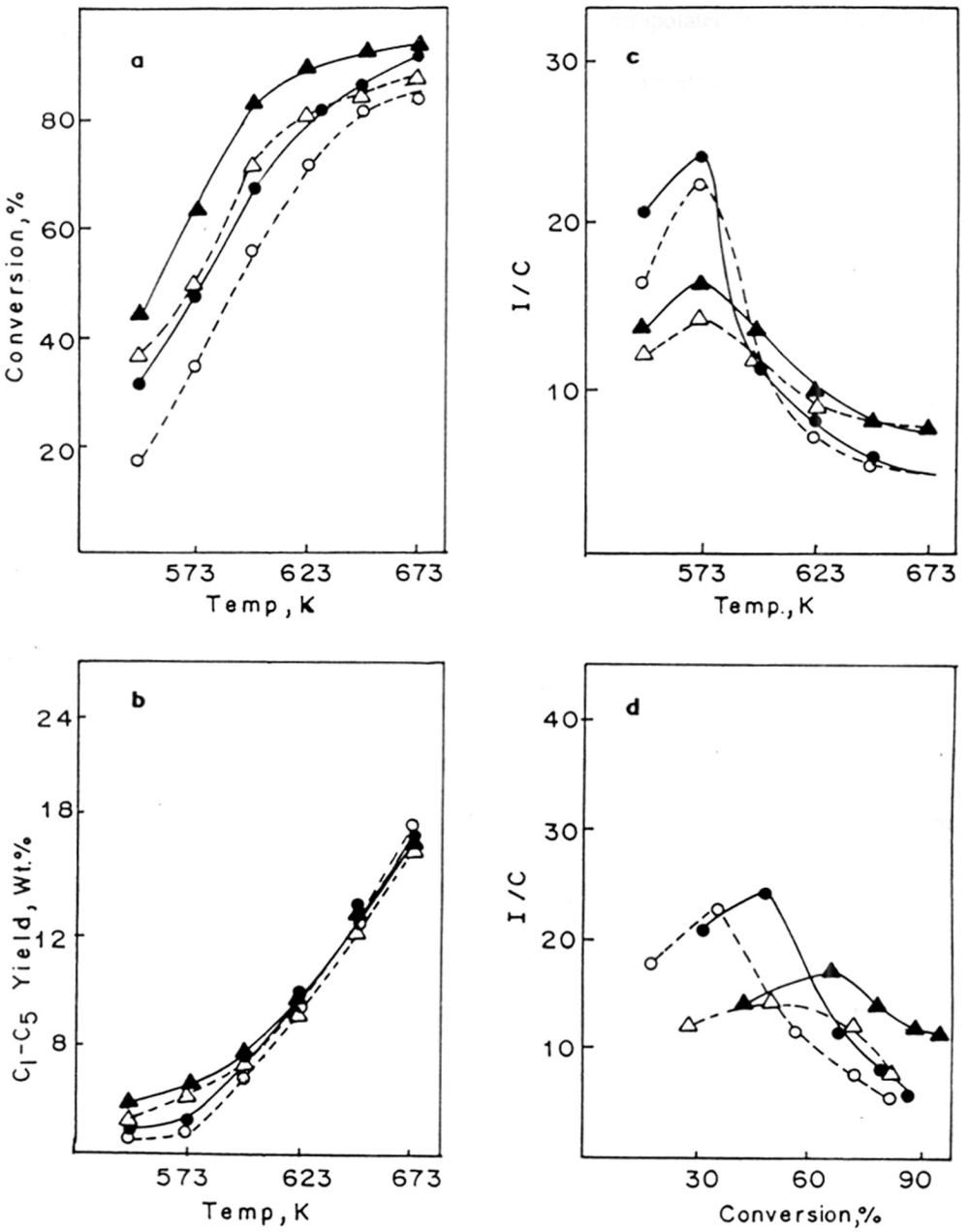

Figure 5.6. Influence of temperatue on n-hexane isomerization.

(WHSV (h^{-1}) = 1; H_2/n-hexane (mole) = 5; TOS = 1 h)

(O) Pt-SAPO-11(a); (●) Pt-SAPO-11(na); (Δ) Pt-SAPO-31(a);

(▲) Pt-SAPO- 31(na).

to 1.45 in the temperature range studied, being very close to the thermodynamic equilibrium values (1.65 at 523 K to 1.45 at 673 K; extrapolated from [56]) over all the catalysts (Fig. 5.7). However the methylpentanes / dimethylbutanes (MP/DMB) ratios were far from the equilibrium values (Fig. 5.7). Similarily, the 2,3- dimethyl butane / 2,2-dimethyl butane ratios were also far from the equilibrium values. The MP/DMB ratios were farther away from equilibrium values in the case of SAPO-31 than SAPO-11 eventhough the former was more acidic suggesting that the pore dimensions play an important role.

iii) Influence of space velocity

An increase in conversion and a decrease in I/C ratio was found with increasing contact time (Fig. 5.8a, b). The decrease in the I/C ratio is due to an increase in cracking, which being slower than the isomerization reaction is favoured at longer residence times. Besides, under these conditions, higher concentrations of the isomerized products (secondary and tertiary carbocations) can lead to dominance of cracking. Plots of yields of individual isohexanes as a function of conversion in the case of SAPO-11 and SAPO- 31 are presented in Fig. 5.8c and 5.8d, respectively. The plots for 2-methyl and 3-methyl pentanes pass through the origin on extrapolation suggesting these to be the primary products of the isomerization reaction. The dimethyl butanes are formed through the subsequent isomerization of the methyl pentanes [56, 57]. The yields of dimethyl butanes were higher over Pt-SAPO-11 than over Pt-SAPO-31 (Fig. 5.8c, d). This may be attributed to the elliptical nature of the pores and the slightly larger pore diameter in SAPO-11 (0.64 Å major diameter) enabling the dimethyl butanes (5.6 to 7.0 Å diameter) to diffuse out of the channels.

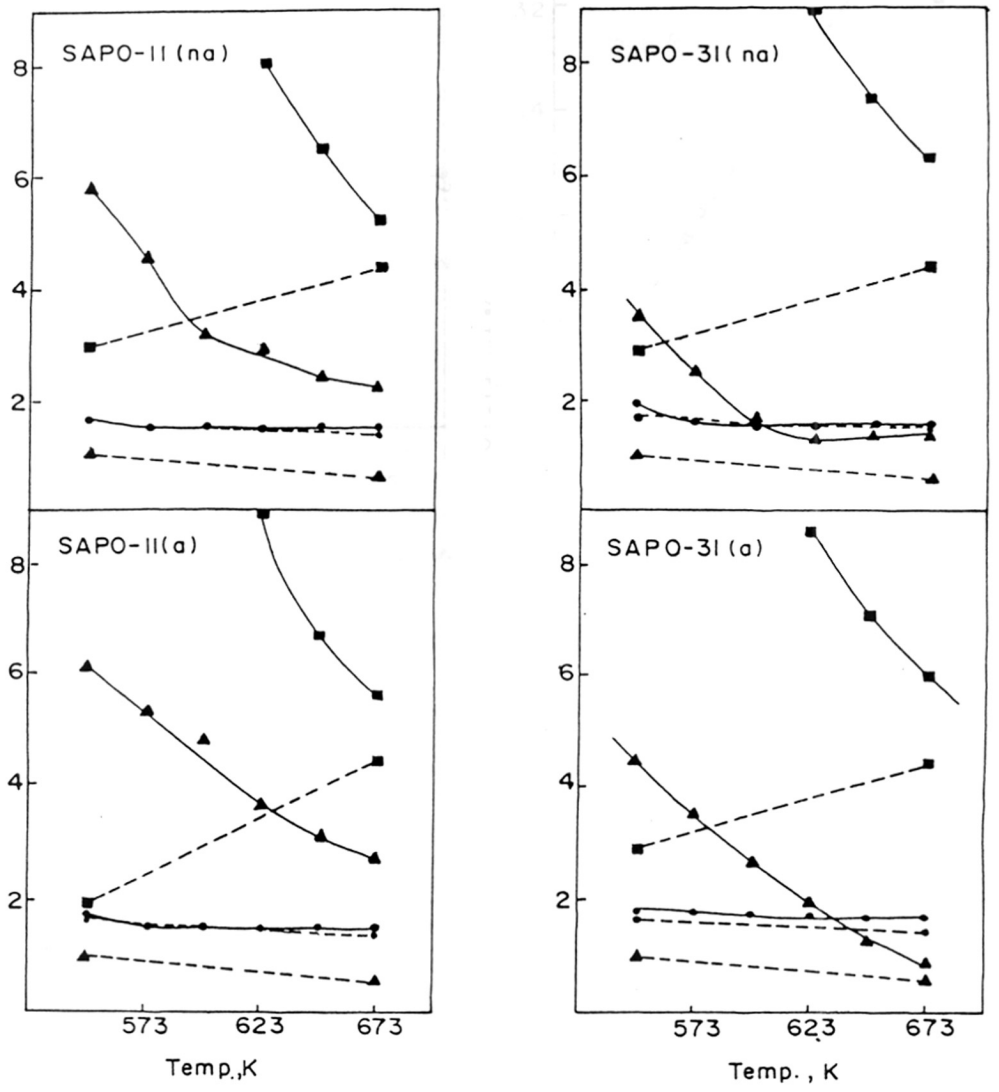

Figure 5.7. Influence of temperature on ratios of isomeric hexanes.

(WHSV (h^{-1}) = 1; H_2/n-hexane (mole) = 5; TOS = 1 h)

(●) 2 methyl pentane/ 3 methyl pentane; (▲) 2,3 dimethyl butane/ 2,2 dimethyl butane; (■) methyl pentanes/ dimethyl butanes; (—) experimental; (---) thermodynamic (adapted from Ref. 56)

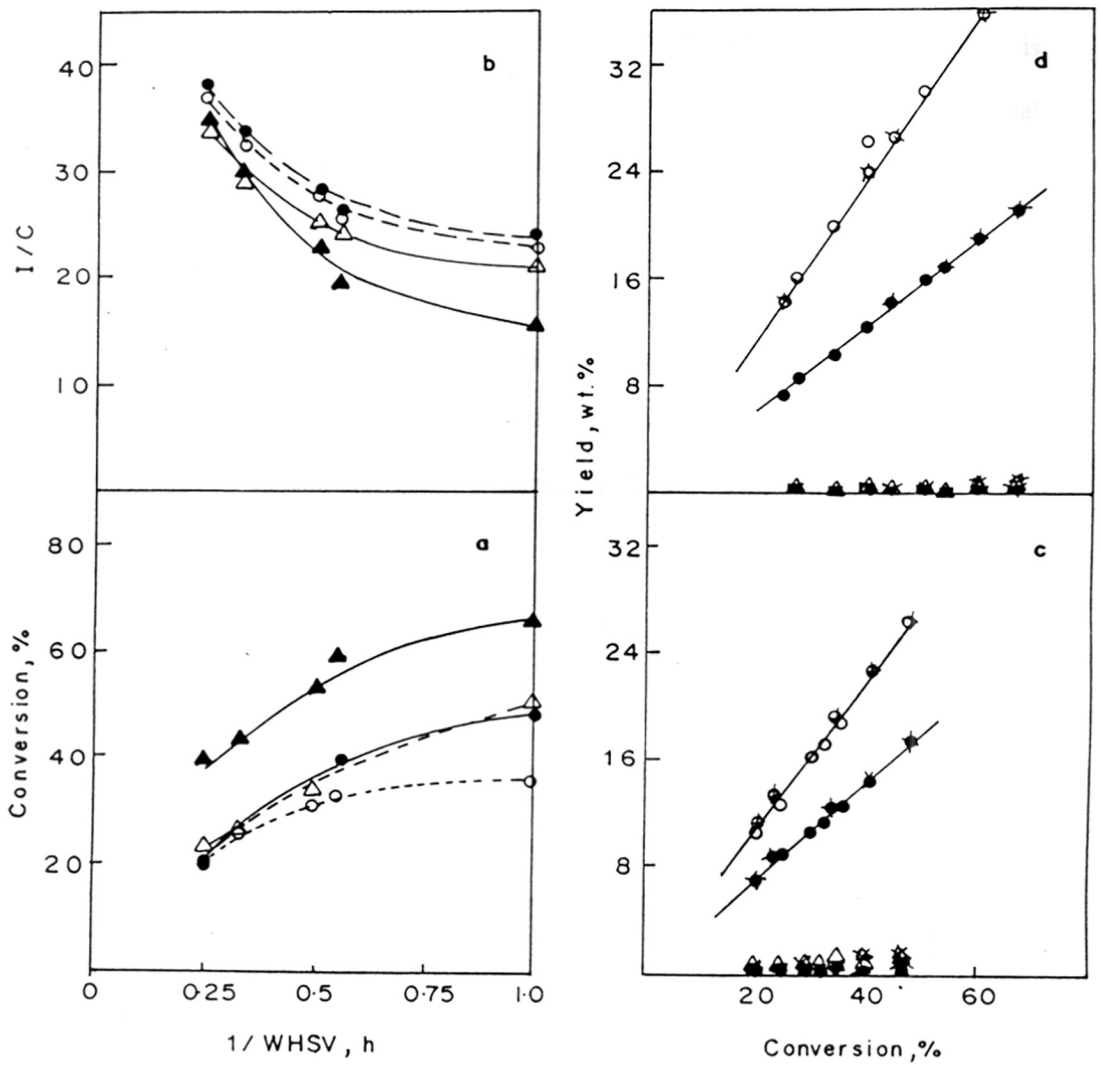

Figure 5.8. Influence of space velocity (and conversion) on n-hexane isomerization.
(Temp. = 573 K; H_2/n-hexane (mole) = 5; TOS = 1 h)
a, b: (O) Pt-SAPO-11(a); (●) Pt-SAPO-11(na); (Δ) Pt-SAPO-31(a);
(▲) Pt-SAPO31(na).
c, d : (O) 2 Me-Pentane; (●) 3 Me-Pentane; (Δ) 2,3 dime-butane;
(■) 2, 2 dime-butane; (X) for samples from non-aqueous medium.

iv) Influence of H_2/n-C_6 mole ratio

The influence of H_2/n-C_6 (mole) ratio on the conversion and I/C ratio is presented in Fig. 5.9. Increasing the H_2/n-C_6 (mole) ratio from 5 to 20 (H_2 partial pressure from 0.83 to 0.95 atm.) led to decreased conversion and increased I/C ratios. As the studies were conducted at a constant feed rate of n-hexane (WHSV (h^{-1}) = 1), the decrease in conversion was probably more due to an increase in the overall (n-C_6 + H_2) space velocity than due to a negative order w.r.t. H_2 (as reported by earlier workers [58] especially as the H_2 partial pressures were changed only to a small extent from 0.83 to 0.95 atm. The increase in the I/C ratios is mainly due to lower conversions as the more easily crackable isoalkanes were present in smaller amounts.

v) Influence of chain length of alkane

The hydroconversion of alkanes with different chain lengths (n-hexane, n-octane and n-hexadecane) was carried out over SAPO-11 and SAPO-31 samples. The conversion of all the alkanes (n-hexane, n-octane and n-hexadecane) increased with temperature over all the four Pt-SAPO catalysts (Fig. 5.10). As expected from their higher acidity, SAPOs synthesized fron non-aqueous media showed higher conversions [59]. SAPO-31 was slightly more active than SAPO-11 probably due to the larger number of acid sites (on weight basis) in the former (Table 4.6). Hydroconversion activity decreased in the order: Pt-SAPO-31 (na)> Pt-SAPO-31 (a) > Pt-SAPO-11(na) > Pt-SAPO-11(a). Among the three n-alkanes, n-hexane as expected was the least reactive and n-hexadecane was the most reactive. Plots of isomer and cracked product over the four catalysts as a function of conversion are presented in figures 5.11 and 5.12. The yields of the mono- and di (multi) - branched isomers are plotted separately in these figures. Even though the data were collected at

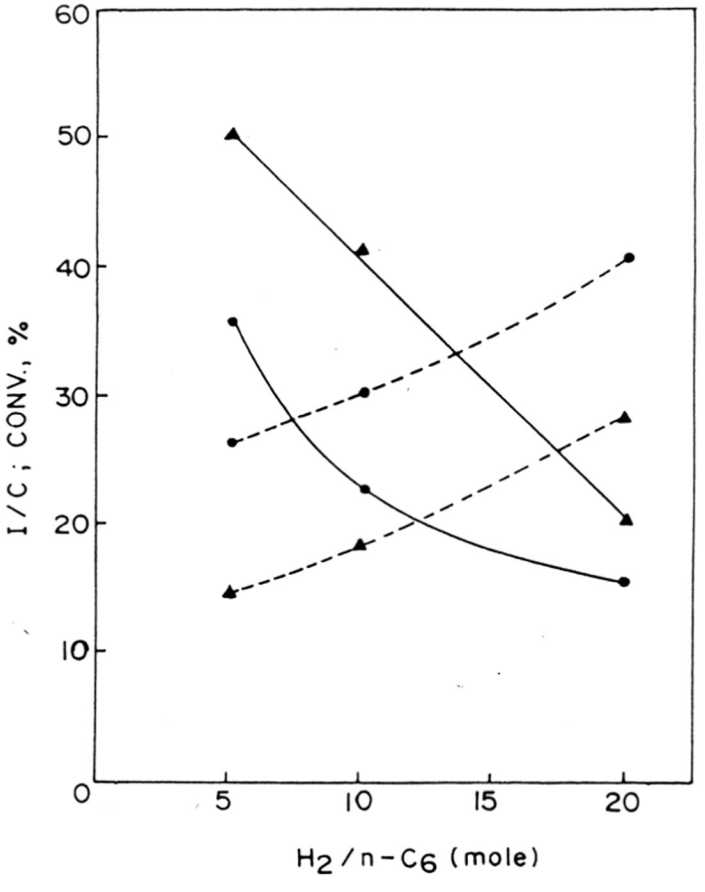

Figure 5.9. Influence of H_2/n-C_6 (mole) ratio (at constant feed ratio of n-hexane) on conversion and I/C ratios. (Temp. = 573 K; WHSV (h^{-1}) = 1; TOS = 1 h) (●) Pt-SAPO-11(a); (▲) Pt-SAPO-31(a); (—) conversion; (---) I/ C

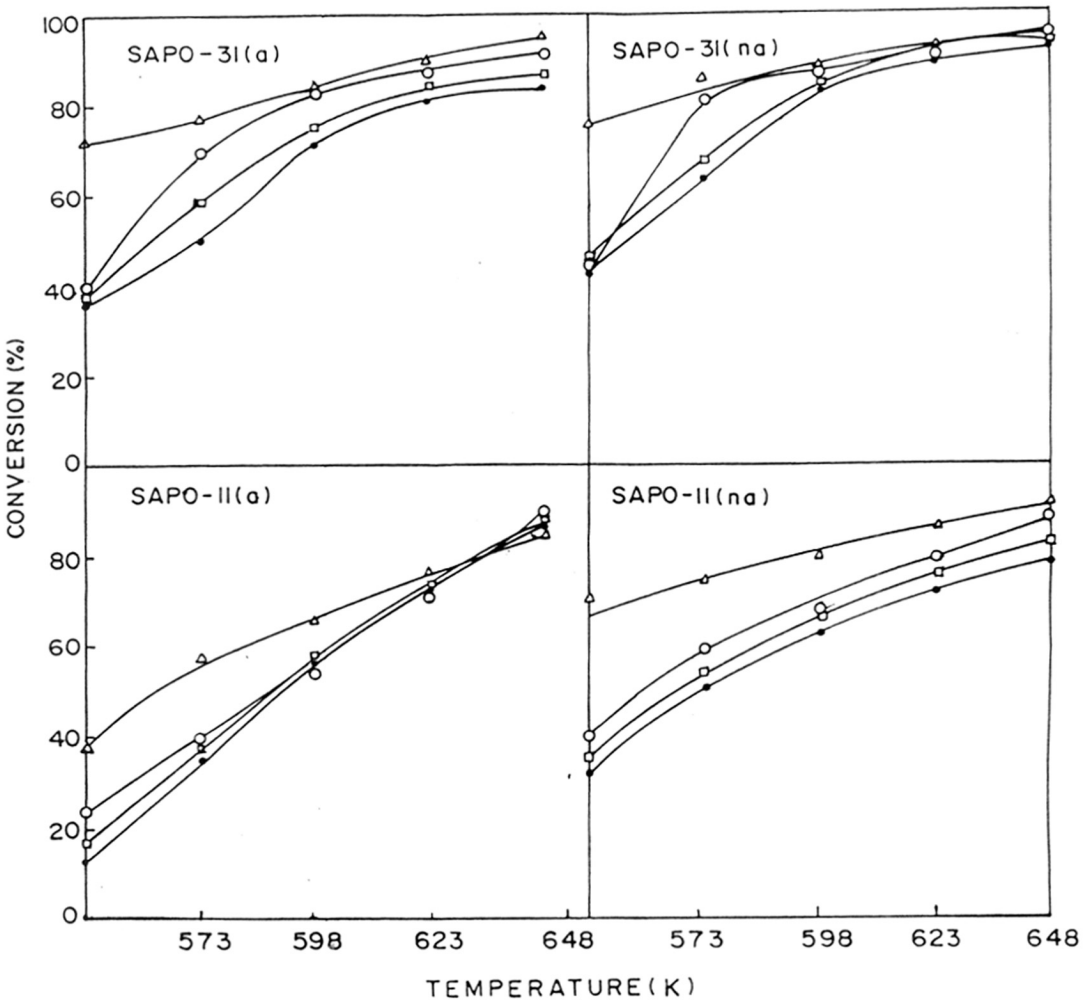

Figure 5.10. Influence of temperature on conversion.

(WHSV (h^{-1}) = 1; H_2/ n-hexane (mole) = 5; TOS = 1 h)

(●) n-hexane; (□) n-heptane; (O) n-octane and (Δ) n-hexadecane.

fairly high conversions, it is apparent (clearly seen in the case of n-hexane and n-octane) that the yield of the monobranched isomer becomes zero only at zero conversion on extrapolation. This result suggests that (as reported earlier by Weitkamp et al. [53]) the monobranched isomers are the primary products of the isomerization reaction. The yields of the monobranched isomer go through a maxima (clearly seen in the case of the heavier alkanes), suggesting that (1) the monobranched isomers further transform into more branched products at higher conversions and (2) isomerization into di- and multibranched products occurs more rapidly with increasing carbon number of the alkane. The yields of the di- (and multi-) branched isomers also go through maxima (Fig. 5.11 and 5.12), though at higher conversion levels. There is little cracking at lower conversions, but the yields of the cracked products increase with conversion, the increase being rapid beyond conversions at which monobranched isomers are converted further into di- and multi- branched analogues. As expected from classical carbenium ion chemistry, the latter are cracked more easily. The sequence of reactions is: n-paraffins → mono-branched isomers → di- (multi-) branched isomers → cracked products. Isomerization (relative to hydrogenolysis, cyclization and cracking) was more predominant over Pt-SAPO-31 than over Pt-SAPO-11 (Figures 5.11 and 5.12).

For all the alkanes, the yields of the cyclized products (and aromatics) were always small (< 2% at the highest conversion in the case of n-hexane and n-octane). Small amounts of olefins (< 5%) were also present in many cases (as estimated by the Bromine index of the products). The olefinic compounds could not be estimated accurately by GC because of the large number of close boiling isomeric alkenes for each alkane isomer. The isomeric alkane and the corresponding alkenes generally eluted together. The I/C ratios of the products obtained over the four catalysts are

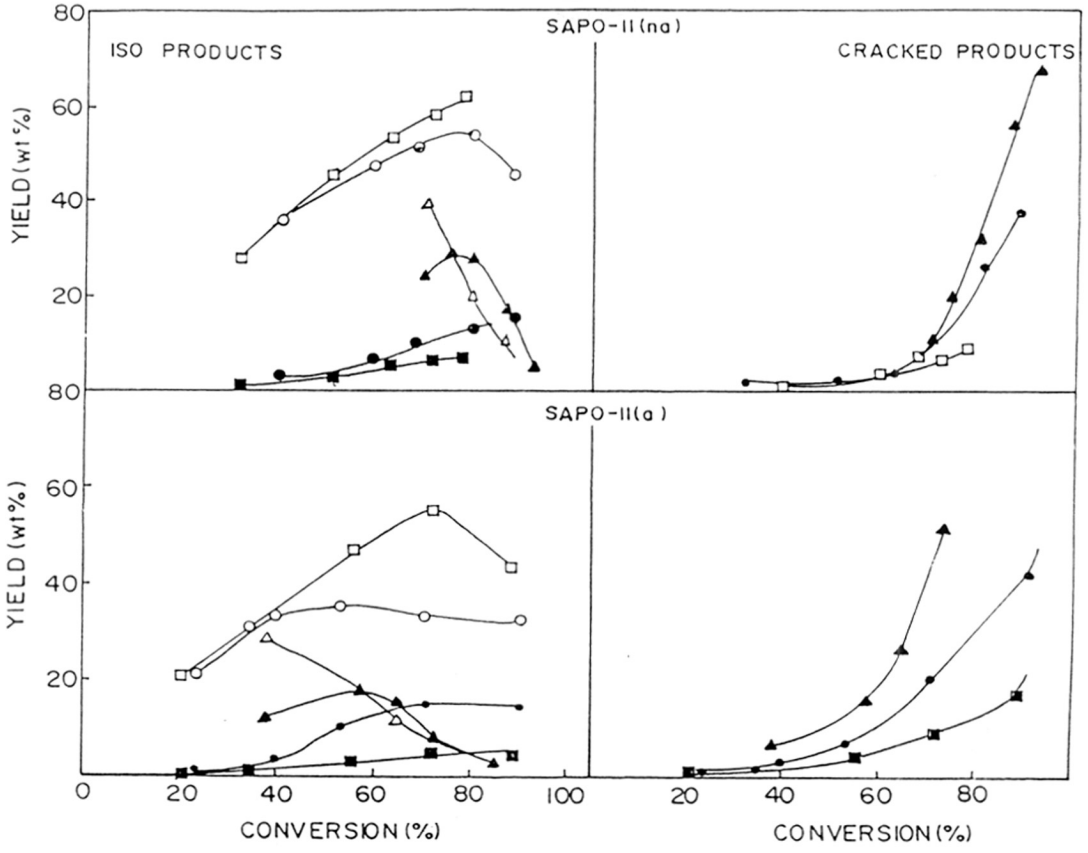

Figure 5.11. Isomer and cracking yields as a function of conversion.

(□) n-hexane; (o) n-octane; and (Δ) n-hexadecane; open points, monomethyl isomers; filled points, di (multi)- methyl isomers and cracked products.

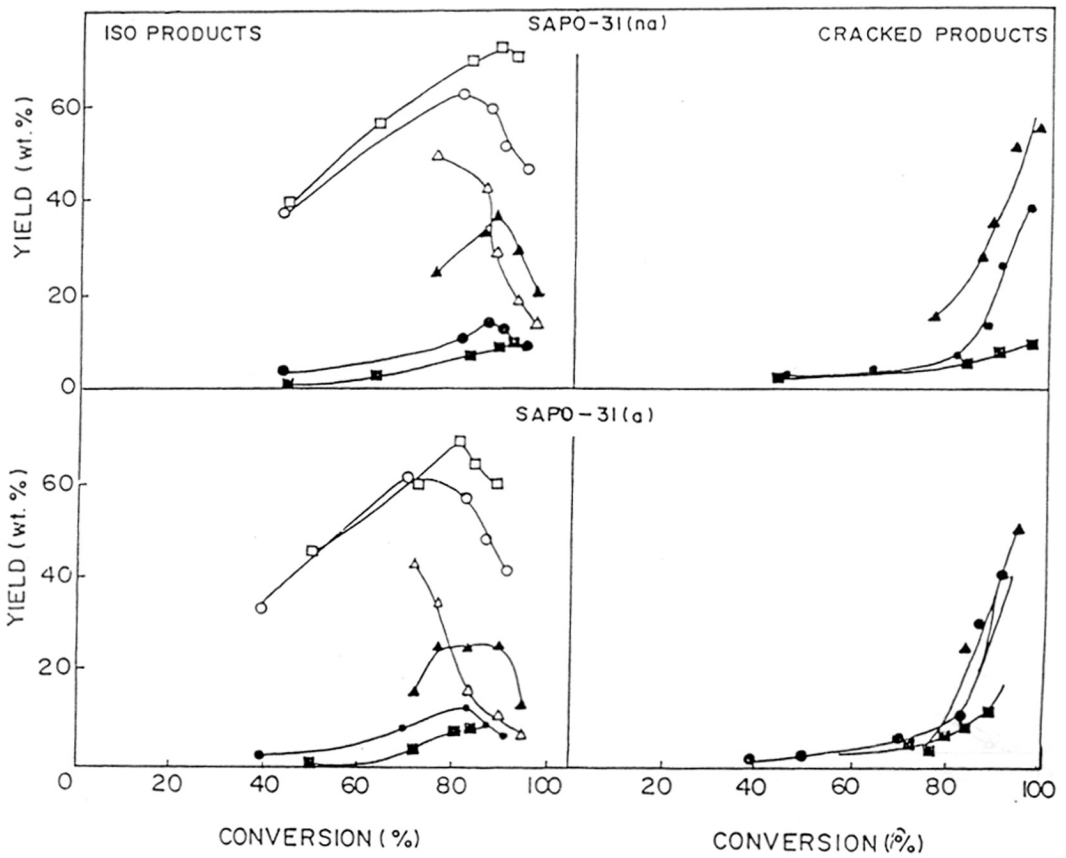

Figure 5.12. Isomer and cracking yields as a function of conversion.

(□) n-hexane; (o) n-octane; and (Δ) n-hexadecane; open points, monomethyl isomers; filled points, di (multi)- methyl isomers and cracked products.

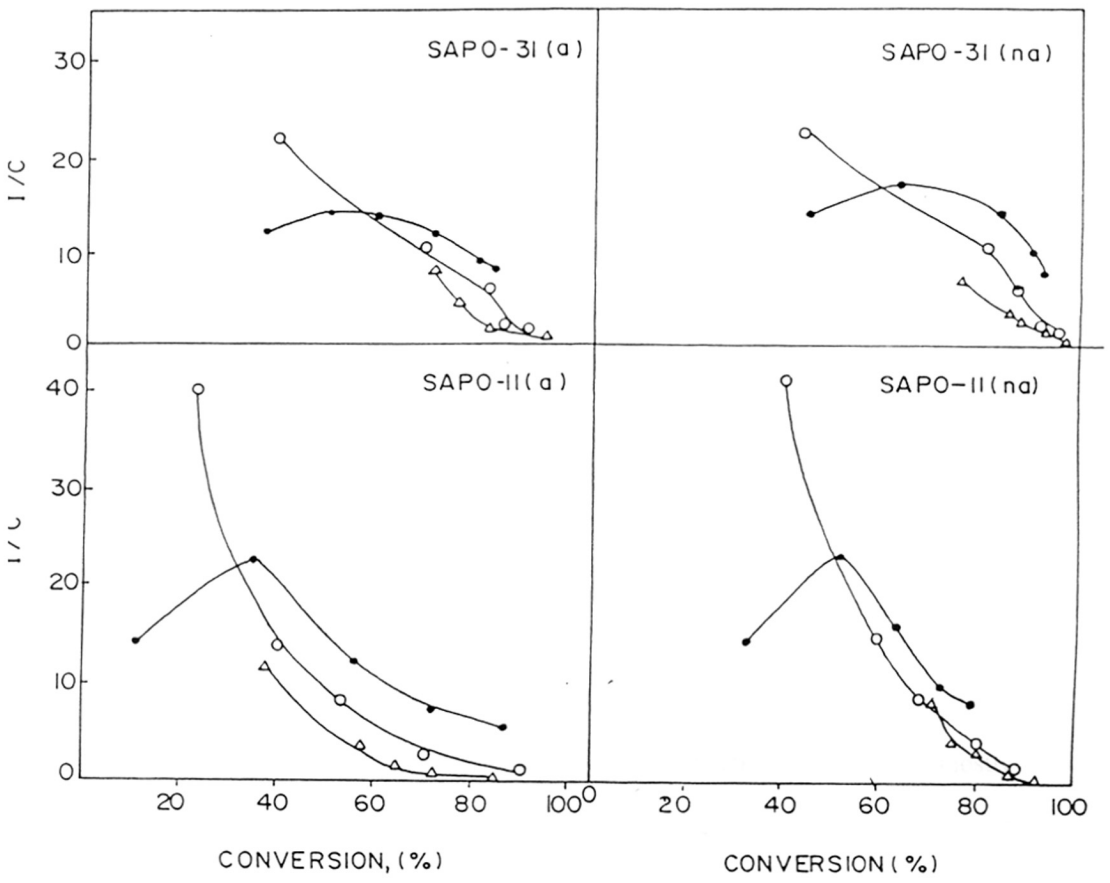

Figure 5.13. Ratio of isomerization/cracking yield (I/C) as a function of conversion.

(●) n-hexane; (o) n-octane; (Δ) n-hexadecane.

presented in Figure 5.13. The I/C ratio for n-hexane hydroconversion passed through a maximum with conversion, whereas the I/C ratio for n-octane and n-hexadecane decreased monotonically (Figure 5.13). It is possible that in the latter case, the maximum I/C ratio lies at lower conversion levels (Figure 5.13). In general, the samples (na) prepared from non aqueous media possessed greater isomerization selectivity. At lower conversion levels, the I/C ratios for n-octane conversion were higher than those for n-hexane conversion. As the conversion level increased, the I/C ratio for n-octane dropped below that for n-hexane. The probable reason is the greater propensity of the dibranched isomers formed more easily from n-octane at higher conversion levels to cracking.

The product pattern from n-hexadecane cracking at ~ 75% conversion over the four catalysts has been presented in Figure 5.14. Distinct yield maxima are observed at 4, 8 and 12 carbons. Similarily, the ratios of the multibranched isomers to the monobranched isomers is maximum at these carbon numbers at 75% conversion (Figure 5.15) especially in the case of SAPO-11. As cracked products are mostly obtained from branched hydrocarbons, the observed cracking pattern might suggest methyl branching of the chain occurring at locations separated by 4 or 5 carbons. Similar results were observed by Martens and Jacobs [52] for the isomerization of n-heptadecane over ZSM-22. They attributed their results to the isomerization of the 2-methyl isomer at the pore mouths on the external surface [52].

In the case of SAPO-11, the channels (pore) are lined with troughs of depth 0.28 nm (separated by 0.31 nm), thereby increasing the effective diameter of the channels (Figure 5.16) [60]. As a result, a significant amount of multibranched isomers can be produced even inside the channels. These (di-) multi-branched isomers can also diffuse out more easily in the case of SAPO-11 through its elliptical

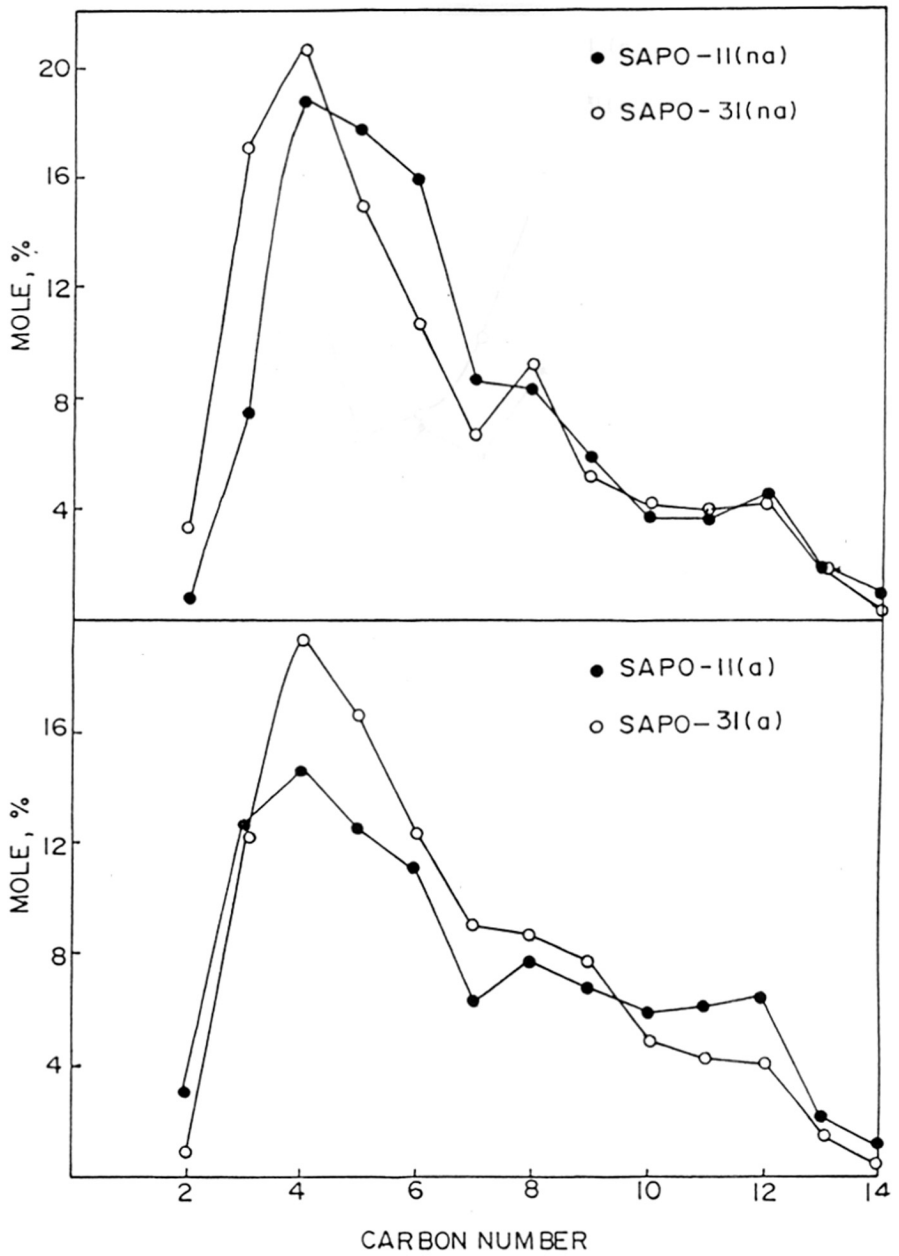

Figure 5.14. Distribution of cracked products as a function of carbon number during n-hexadecane conversion.

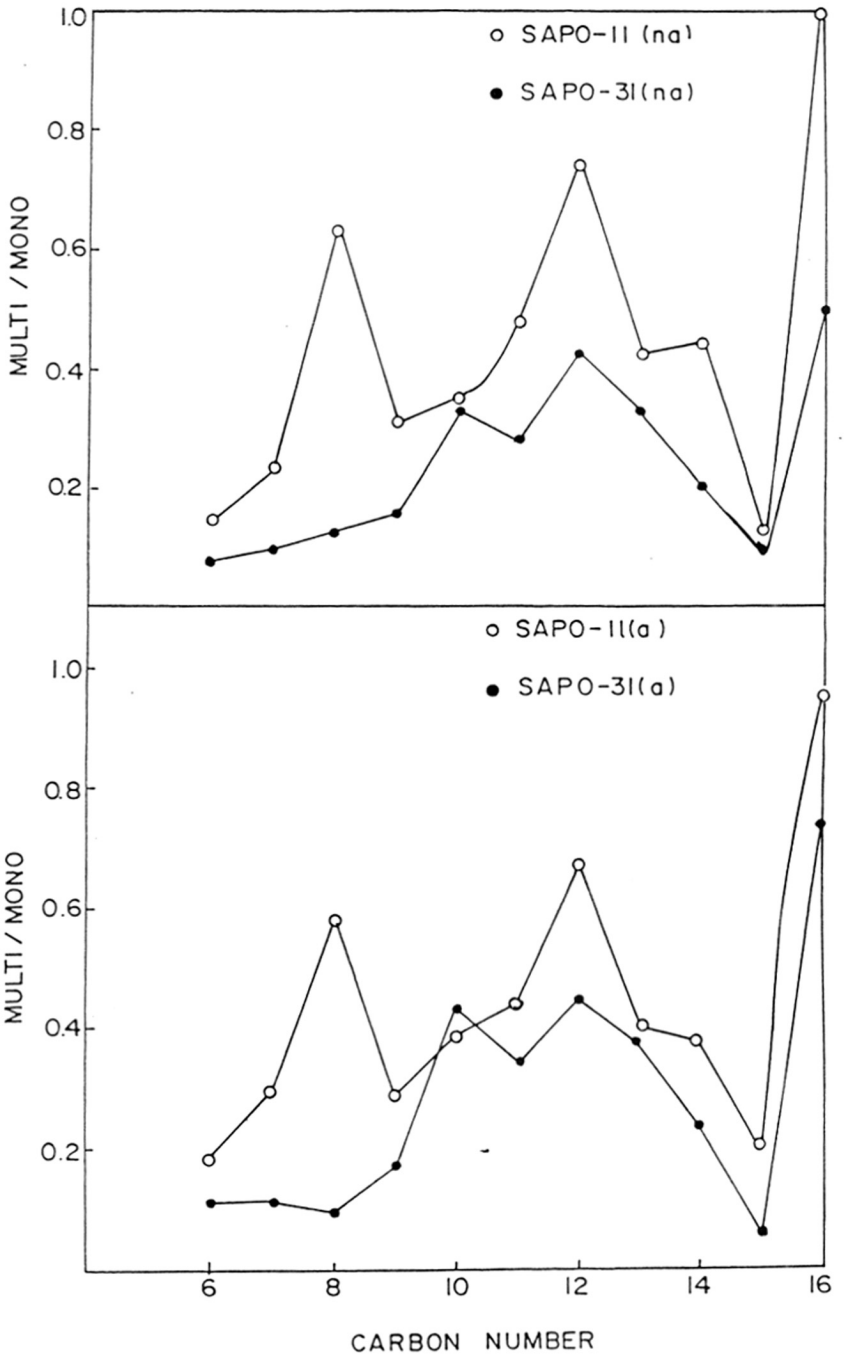

Figure 5.15. Ratio of multi-methyl/monomethyl isomers as a function of carbon number during n-hexadecane conversion.

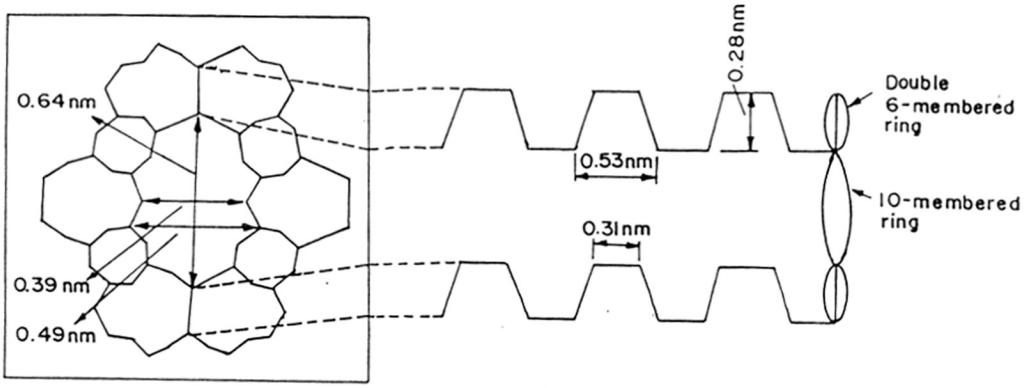

Figure 5.16. Dimensions of the pore channels in SAPO-11.

pore openings with sufficiently large long-diameter (0.64 nm). Hence one can expect the formation of more multi-branched isomers over SAPO-11. This result is clearly noticed in Figure5.15. The differences in the "ratio-patterns" for SAPO-11 and SAPO-31 noticed in Figure 5.15 also suggest differences in the relative contributions of the internal and external surfaces to the reaction in the two SAPOs, the reaction at the pore mouth probably being more important in the case of SAPO-31.

The distribution of monomethyl isomers in the product during n-hexadecane isomerization (at ~ 75 % conversion) is presented in Figure 5.17. The distribution is nearly identical over all the catalysts and no preference for any one isomer is found. This distribution is similar to that reported by Miller [61] over Pt-SAPO-11. However, it is significantly different from the greater selectivity for the 2-methyl isomer observed by Martens and Jacobs [52] for the isomerization of n-heptadecane over ZSM-22. The main reason for the difference is that the distribution reported in this study (Figure 5.17) and Miller [61] were obtained at conversion levels (72 - 96 %) higher than that of Martens and Jacobs (15%) [52].

II. Studies on MeAPOs and MeAPSOs

n-hexane isomerization

Product distribution for the isomerization of n-hexane at different temperatures over ZnAPO-11, ZnAPSO-11, MgAPO-11, MgAPSO-11, CoAPO-11 and CoAPSO-11 samples are given in Tables 5.9-5.15. A comparison of the activities of the MeAPOs and MeAPSOs in n-hexane transformation is made with SAPO-11 in Fig. 5.18a and 5.18b. The n-hexane conversions of the MeAPOs are very similar to that of SAPO-11, though SAPO-11 is slightly more active at higher temperatures. In the case of the MeAPSO catalysts, the Mg containing sample shows higher activity

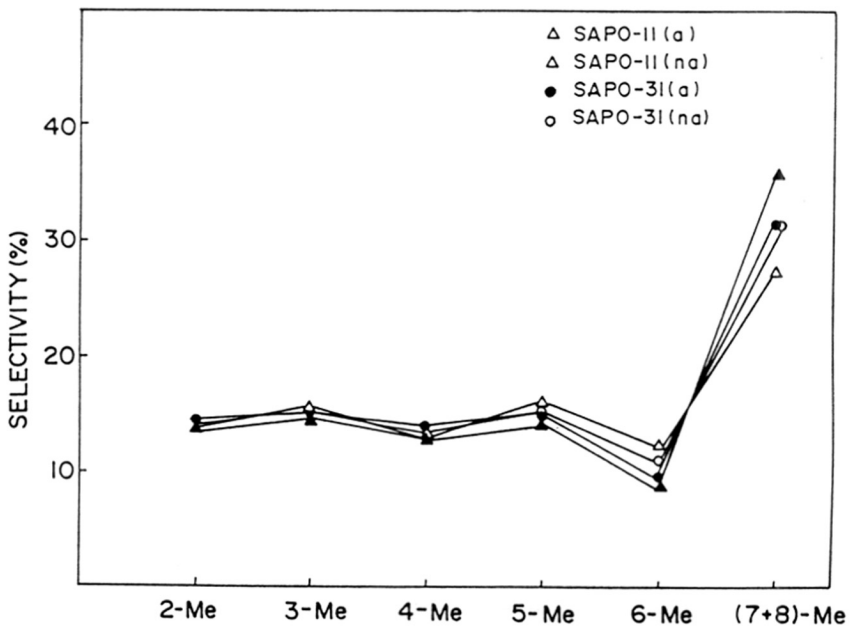

Figure 5.17. Distribution of monomethyl pentadecanes during n-hexadecane isomerization.

than SAPO-11 upto 573 K but shows less activity above 573 K. One explanation could be that even though the MgAPSO possesses intrinsically higher acidity, diffusional constraints may be playing a role at higher temperatures.

The relative isomerization selectivities of the catalysts can be evaluated by comparing the ratios of the isomerization to cracked products (I/C) at similar conversion levels. Plots of I/C vs. conversion for the MeAPOs and MeAPSOs are presented in Fig. 5.19 a and b. Among the MeAPOs, CoAPO-11 is the most selective for isomerization and the samples can be arranged in decreasing order of selectivity as follows: CoAPO-11 > ZnAPO-11 > SAPO-11 > MgAPO-11. Among MeAPSOs, the order is less easy to discern, though it appears that SAPO-11 is the best. Interestingly, the I/C ratio for SAPO-11 goes through a maximum at about 35% conversion whereas it decreases monotonously with conversion for all the other samples. The complete product distribution obtained over the MeAPOs, MeAPSOs and SAPO-11 at various temperatures are presented in Tables 5.9 - 5.15. It is seen that the major isomers are methyl pentanes and only traces of the dimethyl butanes are formed.

The isomerization of n-hexane proceeds sequentially as shown below [56, 57].

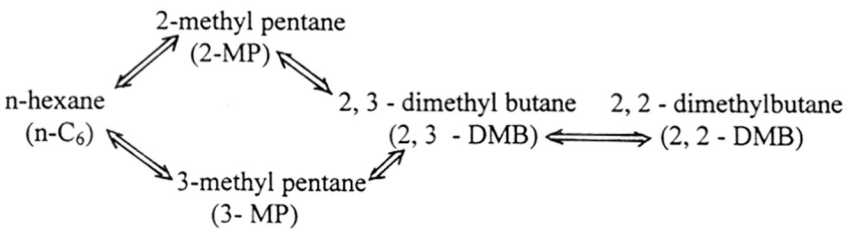

The relative rates of isomerization decrease from left to right in the above sequence of reactions [56, 57], the formation of dimethyl butanes being more difficult than the methyl pentanes. Hence an examination of the ratios of the different products, in general should give a good picture of the performance of the catalyst. However, in the case of shape selective catalysts like SAPOs with pore sizes too

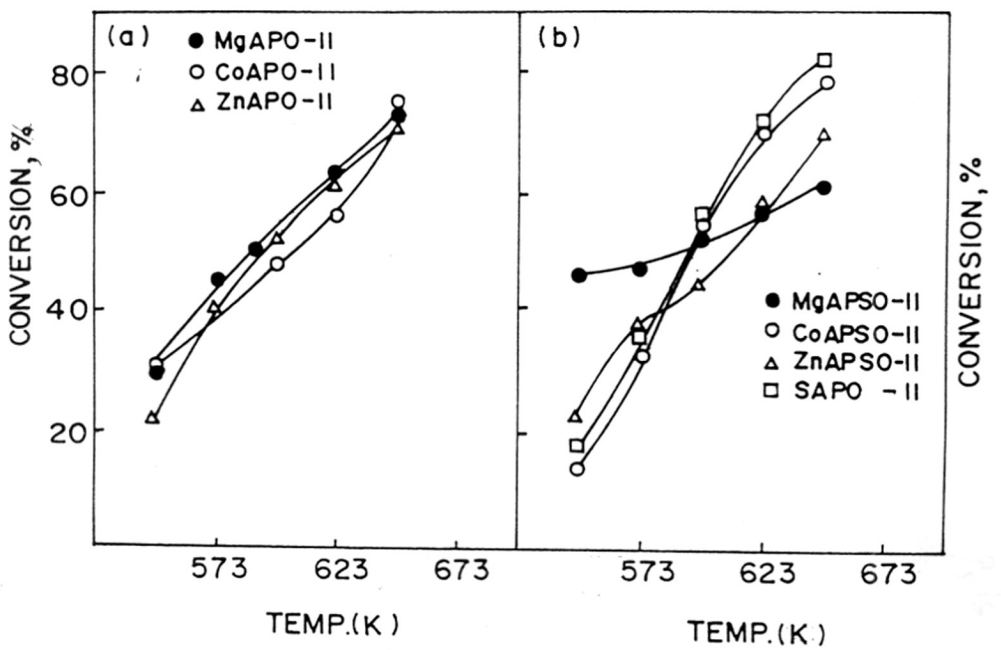

Figure 5.18. Influence of temperature on conversion of n-hexane.

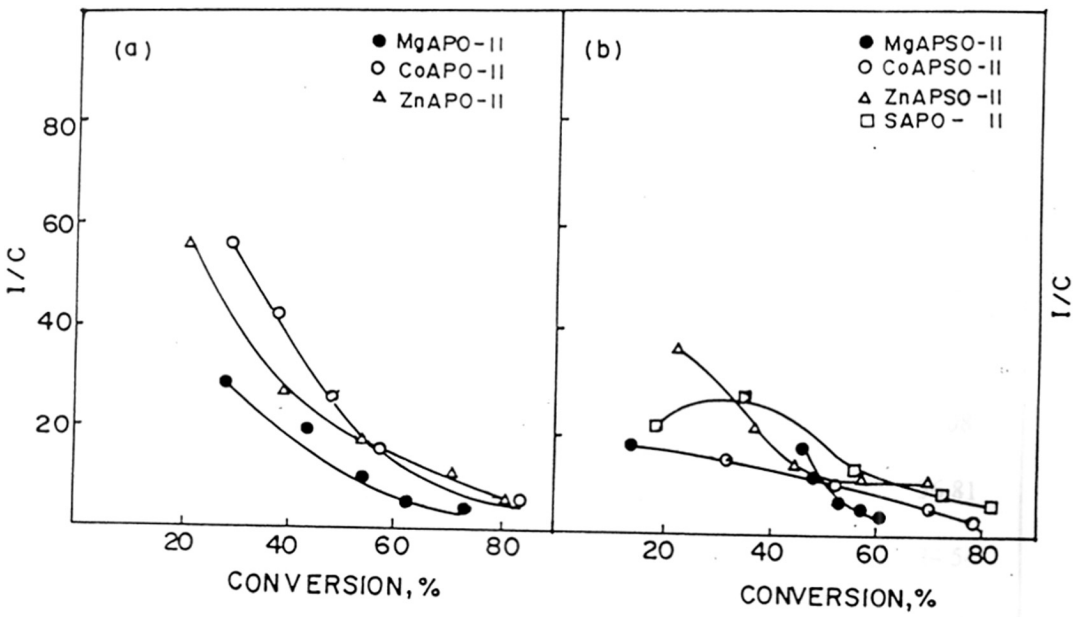

Figure 5.19. Isomerization selectivities (I/C) of the samples.

Table5.9 Product distribution in the isomerization of n-hexane over ZnAPSO-11

Temp.(K)	548	573	598	623	648
Product Distribution (wt%)					
C_1	0.04	0.09	0.14	0.16	0.19
C_2	0.08	0.19	0.35	0.45	0.56
C_3	0.20	1.09	1.58	2.20	3.8
i-C_4	0.04	0.05	0.11	0.14	0.18
n-C_4	0.09	0.27	0.53	0.66	0.75
i-C_5	0.05	0.07	0.15	0.20	0.31
n-C_5	0.10	0.14	0.28	0.29	0.42
2,2-DMC_4	0.05	0.10	0.15	0.22	0.36
2,3-DMC_4	0.31	0.37	0.66	0.75	1.08
2-MP	13.83	21.94	25.50	31.64	36.81
3-MP	6.99	12.84	14.49	19.31	24.54
MCP	0.03	0.04	0.23	0.43	0.56
benzene	0.39	0.38	0.39	0.52	0.63
conversion	22.29	38.07	44.18	57.07	70.19
I/C ratio	35.3	19.3	12.8	12.7	10.2
2,3-/2,2-DMB	6.2	4.7	4.4	3.4	3.0
2-MP/3-MP	1.98	1.85	1.75	1.63	1.50
MP/DMB	57.8	59.2	49.4	52.5	42.6

Table 5.10 Product distribution in the isomerization of n-hexane over ZnAPO-11

Temp.(K)	548	573	598	623	648
Product Distribution (wt%)					
C_1	0.02	0.08	0.15	0.23	0.32
C_2	0.03	0.14	0.27	0.45	0.82
C_3	0.15	0.64	1.26	2.38	6.73
i-C_4	0.01	0.05	0.10	0.19	0.35
n-C_4	0.06	0.22	0.41	0.65	1.11
i-C_5	0.02	0.09	0.19	0.33	0.42
n-C_5	0.09	0.20	0.30	0.38	0.40
2,2-DMC_4	0.01	0.04	0.09	0.16	0.59
2,3-DMC_4	0.18	0.41	0.66	1.06	2.53
2-MP	12.59	22.41	29.93	31.09	33.44
3-MP	7.36	13.84	19.0	20.72	21.23
MCP	0.48	0.74	1.23	1.81	2.12
benzene	0.04	0.12	0.34	0.75	1.86
conversion	20.92	39.17	53.73	61.19	71.55
I/C ratio	56.1	26.37	19.00	11.95	5.87
2,3-/2,2-DMB	1.71	1.62	1.58	1.5	1.51
2-MP/3-MP	18.0	10.25	7.33	6.63	4.31
MP/DMB	105.0	80.56	65.24	42.47	17.52

Table 5.11 Product distribution in the isomerization of n-hexane over MgAPO-11

Temp.(K)	548	573	598	623	648
Product Distribution (wt%)					
C_1	0.08	0.09	0.22	0.57	0.67
C_2	0.25	0.27	0.61	1.27	2.34
C_3	0.64	1.82	2.20	3.54	5.72
i-C_4	0.06	0.07	0.24	0.79	1.01
n-C_4	0.38	0.45	0.95	1.98	2.15
i-C_5	0.08	0.12	0.35	1.09	1.55
n-C_5	0.23	0.32	0.51	1.02	1.76
2,2-DMC_4	0.01	0.02	0.03	0.09	0.12
2,3-DMC_4	0.12	0,22	0.28	0.56	0.77
2-MP	15.88	24.04	28.18	30.10	32.62
3-MP	9.74	15.16	17.25	18.26	19.78
MCP	0.79	1.28	1.56	2.69	3.05
benzene	0.20	0.38	0.59	1.35	1.52
conversion	28.45	44.21	52.96	63.30	73.06
I/C ratio	31.12	19.02	9.30	5.04	3.70
2,3-/2,2-DMB	1.63	1.59	1.63	1.65	1.65
2-MP/3-MP	12.0	11.0	9.33	6.22	6.40
MP/DMB	197.0	163.3	146.5	74.4	58.9

Table 5.12 Product distribution in the isomerization of n-hexane over MgAPSO-11

Temp.(K)	548	573	598	623	648
Product Distribution (wt%)					
C_1	0.01	0.20	0.24	0.31	0.51
C_2	0.25	0.42	0.54	0.62	0.72
C_3	1.45	1.66	4.79	5.71	6.19
i-C_4	0.13	0.21	0.39	0.57	0.70
n-C_4	0.34	0.64	0.80	1.10	1.61
i-C_5	0.19	0.27	0.42	0.61	0.73
n-C_5	0.29	0.44	0.45	0.67	0.80
2,2-DMC_4	0.05	0.06	0.09	0.12	0.16
2,3-DMC_4	0.16	0.17	0.26	0.37	0.48
2-MP	26.21	26.66	26.65	27.72	28.95
3-MP	15.11	15.15	15.91	16.55	17.28
MCP	1.17	1.38	1.49	1.72	2.01
benzene	0.24	0.30	0.43	0.61	0.75
conversion	46.16	47.09	52.44	56.69	60.89
I/C ratio	16.31	11.23	5.83	5.15	4.34
2,3-/2,2-DMB	3.2	2.8	2.9	3.08	3.0
2-MP/3-MP	1.73	1.76	1.68	1.67	1.68
MP/DMB	196.8	181.8	121.6	90.35	72.23

Table 5.13 Product distribution in the isomerization of n-hexane over CoAPO-11

Temp.(K)	548	573	598	623	648
Product Distribution (wt%)					
C_1	0.02	0.04	0.09	0.16	0.70
C_2	0.05	0.09	0.17	0.37	1.01
C_3	0.25	0.41	0.76	1.64	4.19
i-C_4	0.01	0.02	0.05	0.12	0.52
n-C_4	0.09	0.15	0.30	0.43	1.52
i-C_5	0.03	0.05	0.14	0.32	1.36
n-C_5	0.09	0.14	0.26	0.40	1.06
2,2-DMC_4	0.01	0.02	0.03	0.11	0.24
2,3-DMC_4	0.16	0.30	0.44	1.56	2.58
2-MP	17.61	22.17	27.05	28.21	30.83
3-MP	10.96	13.98	17.45	19.21	21.10
MCP	0.43	0.51	0.92	1.21	3.79
benzene	0.07	0.08	0.21	2.11	4.39
conversion	29.74	37.8	47.71	55.85	74.53
I/C ratio	55.2	41.2	25.84	14.65	5.66
2,3-/2,2-DMB	1.61	1.59	1.55	1.46	1.46
2-MP/3-MP	16.0	15.0	14.7	14.2	10.75
MP/DMB	168.06	112.97	94.68	28.4	18.4

Table 5.14 Product distribution in the isomerization of n-hexane over CoAPSO-11

Temp.(K)	548	573	598	623	648
Product Distribution (wt%)					
C_1	0.03	0.06	0.22	0.54	0.63
C_2	0.10	0.18	0.51	1.19	1.67
C_3	0.42	1.07	2.58	5.67	9.21
i-C_4	0.01	0.04	0.16	0.49	0.74
n-C_4	0.08	0.33	0.86	1.85	2.60
i-C_5	0.02	0.08	0.35	1.09	1.43
n-C_5	0.06	0.28	0.62	1.05	1.10
2,2-DMC_4	0.01	0.03	0.09	0.33	0.40
2,3-DMC_4	0.11	0.31	0.56	1.08	1.24
2-MP	7.43	18.34	28.36	33.22	32.78
3-MP	4.43	10.70	16.94	20.41	20.49
MCP	0.57	0.77	1.46	2.01	2.61
benzene	0.05	0.16	0.36	0.75	2.05
conversion	17.5	32.09	52.6	69.77	77.88
I/C ratio	11.3	14.9	8.9	4.81	3.30
2,3-/2,2-DMB	11.0	10.3	6.2	3.27	3.1
2-MP/3-MP	1.68	1.71	1.67	1.63	1.60
MP/DMB	98.8	85.4	69.7	38.04	32.48

Table 5.15 Product distribution in the isomerization of n-hexane over SAPO-11

Temp.(K)	548	573	598	623	648
Product Distribution (wt%)					
C_1	0.03	0.05	0.10	0.28	0.57
C_2	0.07	0.11	0.41	0.90	1.46
C_3	0.41	0.58	1.70	3.60	4.95
i-C_4	0.02	0.05	0.15	0.41	0.82
n-C_4	0.17	0.22	0.92	1.63	3.03
i-C_5	0.02	0.07	0.28	0.71	0.74
n-C_5	0.10	0.18	0.61	1.03	2.00
2,2-DMC_4	0.03	0.16	0.50	1.34	2.75
2,3-DMC_4	0.20	0.85	2.41	4.78	6.05
2-MP	9.47	18.94	28.72	34.52	36.64
3-MP	5.42	12.35	18.21	21.13	22.19
MCP	0.48	0.96	0.91	0.80	0.96
benzene	0.05	0.25	0.32	0.39	0.41
conversion	17.56	35.38	56.18	71.92	81.75
I/C ratio	19.18	26.40	12.17	7.31	5.06
2,3-/2,2-DMB	6.7	5.3	4.8	3.6	2.2
2-MP/3-MP	1.75	1.5	1.58	1.6	1.65
MP/DMB	64.7	30.98	16.13	9.09	6.7

small to permit the diffusion of the dimethyl isomers, comparisons of product distribution becomes less meanigful, though such comparisons can be used to examine the shape selective characteristics of the catalysts. The ratios of the different products (2-methyl pentane/3-methyl pentane, 2 MP/3 MP and methyl pentanes/dimethyl butanes, MP/DMB) from the samples are presented in Fig. 5.20 a-d. The 2 MP/3 MP ratios for most catalysts are close to the equilibrium values of 1.65 (at 548 K) and 1.5 (at 648 K) [56] suggesting that the acidities of the samples are sufficient to cause the equilibrium distribution of the methyl pentanes. Besides, the pore openings are sufficiently large to permit the diffusion of the methyl pentanes. However, equilibrium distribution of the methylpentanes does not take place at lower temperatures over ZnAPSO suggesting that it possesses relatively weaker acidity. While examining the MP/DMB ratios, we find that the ratios (10-200) are far from the equilibrium values of 2.9 (at 548 K) and 3.8 (at 648 K). The values deviate the most for MgAPO and MgAPSO which may be a result of pore size diminution in these samples. The above data reveal very high shape selectivities for the MeAPOs and MeAPSOs. Earlier [19] it was suggested that a significant proportion of reaction occurs at the external surface of SAPO-11. Since, steric effects are not expected at the external surface, the very high MP/DMB ratios observed suggest that the reaction occurs mainly inside the pores. Therefore, it appears that the high MP selectivities are due to both steric constraints and weak acidities in the samples. A plot of temperature vs. conversion shows that conversion increases rapidly with increasing temperature for all the samples. The conversion curves for different samples overlap so that there is no clear difference between their catalytic activities. The I/C ratio of diferent samples is found to decrease monotonously with increasing temperature while that for SAPO-11 is found to pass through a maximum. The increasing order of

I/C ratio being CoAPO-11>ZnAPO-11>MgAPO-11 for MeAPO-11 samples and ZnAPSO-11>CoAPSO-11>MgAPSO-11 for MeAPSO-11 samples. Plot of conversion vs. I/C shows that the order of I/C ratio at different conversion levels is CoAPO-11>ZnAPO-11>MgAPO-11 for MeAPO-11 samples and ZnAPSO-11>CoAPSO-11>MgAPSO-11 for MeAPSO-11 samples. The 2,3-dimethylbutane to 2,2-dimethylbutane ratios observed at different temperatures (Table 5.9 to 5.15) are in the order CoAPO-11>MgAPO-11~ ZnAPO-11>SAPO-11 and CoAPSO-11>SAPO-11>ZnAPSO-11>MgAPSO-11. The methylpentane to dimethylbutane ratios plotted at different temperatures shows (Fig. 5.20) that the values are much higher than the thermodynamic equilibrium value and they are in the order MgAPO-11>CoAPO-11>ZnAPO-11 and MgAPSO-11>CoAPSO-11>ZnAPSO-11. Formation of dimethyl butane requires higher acidity and larger pore dimensions. Since the pore size of all the MeAPO-11 and MeAPSO-11 samples is nearly the same, it is probably the acidity of the samples which is responsible for the difference in dimethylbutane selectivity. The order of methylpentane to dimethyl butane ratio suggests that the acidity of the samples is likely to be in the order ZnAPO-11>CoAPO-11>MgAPO-11 and ZnAPSO-11>CoAPSO-11>MgAPSO-11. This is supported by the content of the different metals in the various samples (Table 4.7; chapter 4) which is also in the same order as the order of the acidity.

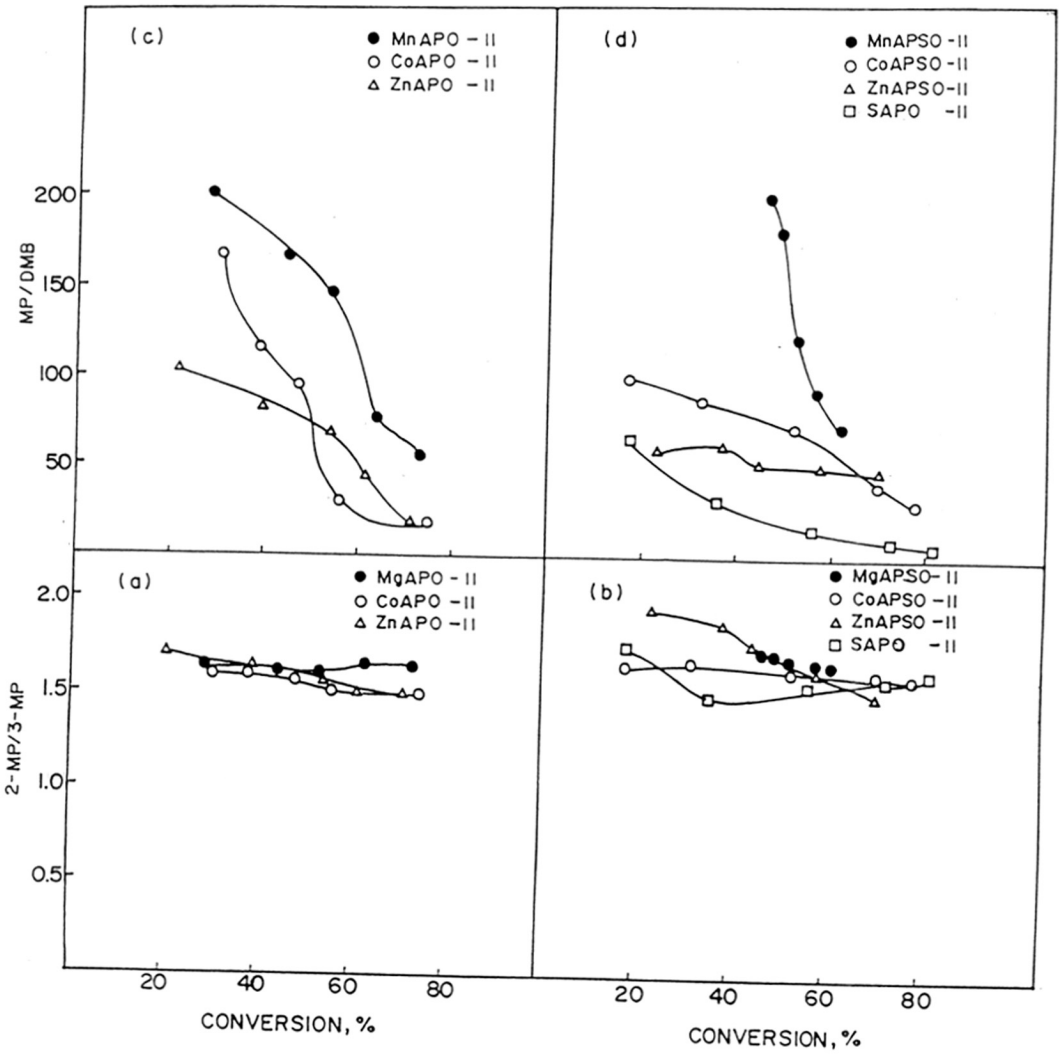

Figure 5.20. The ratios of the products for the different samples.

(a, b), 2-MP/3-MP and (c, d), MP/DMB.

REFERENCES

1. Jacobs, P.A., and Martens, J.A., *Stud. Surf. Sc. Catal.*, **28**, 23 (1988).
2. Weitkamp, J., and Ernst, S., *Stud. Surf. Sc. Catal.*, **38,** 367 (1988).
3. Csicsery, S.M., *Zeolites,* **4,** 202 (1984).
4. Weitkamp, J., and Ernst, S., *Catal. Today,* **19,** 107 (1994).
5. Martens, J.A., Tielen, M., Jacobs, P.A., and Weitkamp, J., *Zeolites,* **4,** 98 (1984).
6. Csicery, S.M., *J. Org. Chem.*, **34,** 3338 (1969).
7. Corma, A., and Sastre, E., *J. Catal.* **129,** 177 (1991)
8. Gnep, N.S., Tejada, J. and Guisnet, M., *Bull. Soc. Chem. Fr.*, **I,** 5 (1982)
9. Martens, J.A., Péréz - parienté, J., Sastre, E., Corma, A., and Jacobs, P.A., *Appl. Catal.*, **45,** 85 (1988).
10. Dewing, J., *J. Mol. Catal.*, **27,** 25 (1984).
11. Kumar, R., Rao, G.N., and Ratnasamy, P., *Stud. Surf. Sci. catal.*, **49 (9),** 1141 (1989).
12. LaBel, J.A., and Greene, W.H., *Am. Chem. J.*, **2,** 20 (1980).
13. Sernagiotto, E., *Gazz. Chim. Ital.*, **44(1),** 587 (1914).
14. Grosse, A.V., and Snyder, J.C., US Patent No. 2,492,984 (1950).
15. Adkins, H., and Perkins, P.D., *J. Phys. Chem.* **32,** 223 (1928).
16. Topchieva, K.V., and Ballod, A.U., *Doki. Akad. Nauk. SSSR,* **75,** 247 (1950).
17. Cullinane, N.M., Chart, S.J., and Meatyard, R., *J. Soc. Chem. Ind.*, **67,** 142 (1948).
18. Fawcett, P.S., and Howk, B.W., US Patent No. 2,744,151 (1956).
19. Meisel, S.L., McCollough, J.P., Lechtlhaler, C.H., and Weisz, P.B., *Chem. Tech.*,**2,** 86 (1976).
20. Chang, C.D., Silvestri, A.J., and Smith, R.L., US Patent Nos. 3,894,103 and

3,928,483 (1975).

21. Chang, C.D., and Silvestri, A.J., *J. Catal.*, **47,** 249 (1977).

22. Lee, W., Mazio, J., Weekmann, V.W., and Yurchak, S., in Froment, G.R., (Ed.), "Large Chemical Plants", Elsevier, Amsterdam, (1974) p.171.

23. Chang, C.D., *Catal. Rev. Sci. Eng.*, **25 (1),** 1 (1983).

24. Khadziev, S.N., Levinbuk, M.I., Shumovskii, Yu, V., and Topchieva, K.V., *Kinet. Katal.*,**20 (6),** 347 (1979).

25. Chang, C.D., Lang, W.H. and Silvestri, A.J., US Patent No. 4,062,905 (1977).

26. Spencer, M.S., and Whittam, T.V., *Acta. Phys. Chem.*, **29,** 347 (1978).

27. Ceckiewicz, S., *J. Chem. Soc. Faraday Trans. I,* **80,** 2989 (1989).

28. Cormerais, F.X., Clen, Y.S., Kern, M., Gnep, N.S., Perot, G., and Guisnet, M., *J. Chem. Res.*, **5**, 290 (1981).

29. Sulikowskii, B., and Popierlaz, A., *Appl. Catal.*, **42,** 195 (1988).

30. Inui, T., Matsuda, H., Okaniwa, H., and Miyamoto, A., *Appl. Catal.*, **58,** 155 (1990).

31. Liang, J., Li, H., Zhao, S., Guo, W., Wang, R., and Ying, M., *Appl. Catal.*, **64,** 31 (1990).

32. Inui, T., Phatanasri, S., and Matsuda, H., *J. Chem. Soc., Chem. Commun.*, 205 (1990).

33. Thomas, J.M., Xu, Y., Catlow, C.R.A., and Cooves, J.W., *Chem. Mater.* **3,** 667 (1991).

34. Nováková, J., Kubelková, L., and Dolejsck, Z., *J. Catal.* **108,** 208 (1987).

35. Salvador, P., and Kladnig, W., *J. Chem. Soc. Faraday Trans.* **1**, 1153 (1977).

36. Vanden Berg, J.P., Wolthnizen, J.P., and Van Hoff, J.H.C., Proc. V Conf. Zeolites, Naples, Italy (1980), p. 649.

37. Dejaifve, P., Vendrine, J.C., Bolis, V., and Derouane, E.G., *J. Catal.*, **63,** 331

(1980).

38. Kaiser, St., W. US Pat. 4,667, 242 (1987)

39. Cusher, N.A., Greenouch, P., Rolfe, J.R.K., and Weiszman, J.A., in Chap. 5, Handbookb of Petroleum Refining.

40. Refining Handbook, '92, *Hydrocarbon Processing*, **71,** 195 (1992).

41. Ciapetta, F.G., Dobres, R.M., and Baker, R.N., *Catalysis*, Vol. IV (Emmett, P.H., Ed.), Rheinhold Pub. Corpn., New York, P.495 (1958).

42. Farmeth, W.E., and Gorte, R.J., *Chem. Rev.* **95,** 615 (1995).

43. Giannetto, G.E., Perot, G.R., and Guisnet M., *Ind. Eng. Prod. Res. Dev.* **25,** 481 (1986).

44. Leu, L.J., Hou, L-Y., Kang, B-D., Li, C., Wu, S-T., and Wu, J-C., *Appl. Catal.* **69**, 49 (1991).

45. Guisnet, M., Fouche, V., Belloum, M., Bourneville, J.P., and Travers, C., *Appl. Catal.*, **71,** 283 (1991).

46. Chen, J.K., Martin, A.M., Kim, Y.G., and John, V.T., *Ind. Eng. Chem. Res.* **27,** 401 (1988).

47. Guisnet, M., Fouche, V., Belloum, M., Bourneville, J.P., and Travers, C., *Appl. Catal.*, **71,** 295 (1991).

48. Ernst, S., Weitkamp, J., Martens, J.A., and Jacobs, P.A., *Appl. Catal. A: Gen.*, **48**, 137 (1989).

49. Martens, J.A., Jacobs, P.A., Weitkamp, J., *Appl. Catal. A:Gen.*, **20,** 239 (1986).

50. Martens, J.A.; Tielen M., Jacobs, P.A., Weitkamp, J., *Zeolites*, **4**, 98 (1984).

51. Jacobs, P.A., Martens, J.A., Weitkamp, J., Beyer, H.K., *Faraday Discuss. Chem. Soc.*, **72,** 353 (1982).

52. Martens, J.A., Jacobs, P.A., *Angew Chem. Int. Ed. Engl.*, **34,** No. 22, 2528 (1995).

53. Weitkamp, J., Jacobs, P.A., and Martens, J.A., *Appl. Catal. A: Gen.*, **8,** 123 (1983).

54. Leu, L.J., Hou, L-Y., Kang, B-D., Li, C., Wu, S-T., Wu, J-C, *Appl. Catal.* **69**, 49(1991).

55. Weisz, P.B., Adv. Catal. **13,** 137 (1962).

56. Chen, J-K., Martin, A.M., Kim, Y.G., and John, V.T., *Ind. Eng. Chem. Res.* **27,** 401 (1988).

57. Marin, G.B., and Froment, G.F., *Chem. Eng. Sci.* **37 (5),** 759 (1982).

58. Guisnet, M., Fouche, V. M., Bournonville, J.P. and Travers, C., *Appl. Catal.* **71**, 295 (1991).

59. Barthomeuf, D., Zeolites, **14**, 394 (1994).

60. Prasad, S., Vetrivel, R., J. Phys. Chem., **93**, 3411, (1997).

61. Miller, S.J., Microporous Materials, **2**, 439 (1994).

62. Sinha, A.K., Sivasanker, S. and Ratnasamy, P., Ind. Eng. Chem.Res., **37**, 2208 (1998).

CHAPTER VI

SUMMARY AND CONCLUSIONS

6.1 SYNTHESIS

SAPO-39 could be crystallized as a completely pure phase by varying the synthesis conditions used for the synthesis of SAPO-11. SAPO-11 could be synthesized using ethylene glycol (na) medium instead of aqueous (a) medium but it required longer crystallization time (144 h) than that required for conventional synthesis (24 h). Similarily complete crystallization of SAPO-31 using ethylene glycol medium required longer crystallization time (72 h) than that required for the conventional synthesis (24 h).

Synthesis of SAPO-11(r) by a slow programmed heating of the gel resulted in rapid crystallization of the material (in 2 h, after the attainment of crystallization temperature). The use of a gel composition similar to that used in the synthesis of SAPO-11(r) but with high Si contents (Si molar ratio > 0.4) resulted in the crystallization of pure SAPO-5 material. Complete crystallization of SAPO-5 occurred just after the attainment of the crystallization temperature. Taking the same gel composition as for SAPO-11(r) but using silica sol instead of fumed silica in the synthesis gel resulted in the crystallization of SAPO-31 material 4 h after the attainment of the crystallization temperature.

6.2 CHARACTERIZATION

X-ray powder diffraction analysis of the various samples showed that (1) SAPO-39 could be obtained as a pure phase, (2) X-ray crystallinities of the SAPO-11 and SAPO-31 samples synthesized from ethylene glycol medium were higher than those of the samples synthesized from aqueous (conventional) medium, (3) X-ray crystallinities of SAPO-11, SAPO-31 and SAPO-5 obtained by programmed heating (rapid crystallization) were higher than those of the conventional samples.

Scanning electron micrographs revealed that the crystals of SAPO-39 were bundles of stick-like particles. Crystallites of SAPO-11 synthesized from aqueous and non-aqueous media were spherical, those of the non-aqueous samples being more uniform. Similarily, the crystallites of SAPO-31 synthesized from non-aqueous medium were more uniform than those synthesized from aqueous medium. SAPO-11(r) synthesized by rapid crystallization method was made up of rectangular crystallites (1.0 x 0.5 μm). Unlike the irregular stick-like crystals of SAPO-31(a) synthesized by the conventional method, the crystals of SAPO-31(r) (synthesized by rapid crystallization method) were of uniform rhombohedral shape (3.5 x 1.0 μm). Crystallites of conventionally synthesized SAPO-5(a) had mixed morphologies (5.0-8.0 μm) but those of the rapid crystallized SAPO-5(r) were regular hexagonal prisms (6.0 x 8.0 μm). Crystallites of MnAPO-11(na) synthesized from non-aqueous medium were more uniform than those of MnAPO-11(a) synthesized from aqueous medium.

TGA/DTA analysis of SAPO-11 and SAPO-31 revealed that there was more weight loss from the samples synthesized by rapid crystallization method and from non-aqueous medium than the conventional samples due to the larger amount of occluded water and template molecules in the former resulting from their higher crystallinity and higher surface areas. TGA of SAPO-39 showed greater weight loss than for MAPO-39 and $AlPO_4$-39 (more so at higher temperatures) implying higher crystallinity for the former than the latter two. TGA/DTA profiles of MnAPO-11(na) showed higher temperatures of decomposition (above 673 K) for MnAPO-11(na) compared to that for MnAPO-11(a) probably due to the larger substitution of Al(III) by Mn(II) in the MnAPO-11(na) resulting in larger charge build up of the framework and stronger adsorption of the organic molecules.

^{27}Al MAS-NMR spectra of SAPO-11 and SAPO-31 synthesized by the three methods showed similar spectra with an intense peak at δ = -39 ppm due to tetrahedral Al in the framework. However, the ^{29}Si MAS-NMR spectra were different for the samples. Conventionally synthesized SAPO-11(a), SAPO-31(a) and SAPO-5(a) samples showed a broad band in the region of δ = -90 to -110 ppm indicating the presence of large amounts of multiple Si environments and Si island formation. But SAPO-5(r), SAPO-11(r) and SAPO-31(r) synthesized by the rapid crystallization method and SAPO-11(na) and SAPO-31(na) synthesized from non-aqueous medium all showed low intensity signals in the δ = -100 to -110 ppm region in their ^{29}Si MAS-NMR spectra attributed to non-acidic silica islands, while they exhibited a very intense peak at around δ = -92 ppm indicating the presence of large amounts of Si as Si(4Al) type species in the framework.

Temperature programmed desorption of adsorbed pyridine showed that the acidities of SAPO-11 and SAPO-31 samples synthesized from ethylene glycol medium and by rapid crystallization method were higher than those of the conventionally synthesized samples.

X-band ESR spectra of MnAPO-11 reveal that Mn(II) is present as four types of species viz., isolated framework Mn sites in O_h coordination with reversible hydration-dehydration behaviour, isolated tetrahedral sites, small patches containing two or three nearby framework Mn(II) ions and as hydrated extraframework bulk manganese species. Mn is more homogeneously distributed in the sample prepared from ethylene glycol than the sample prepared from the aqueous medium.

6.3 CATALYTIC PROPERTIES

6.3.1 Isomerization of m-Xylene.

During the isomerization of m-xylene, p-xylene/o-xylene ratio for SAPO-11, SAPO-31, MeAPO-11 and MeAPSO-11 samples was well above the thermodynamic equilibrium value of 1.1 due to diffusion controlled product shape selectivity. This ratio over MeAPO-11 and MeAPSO-11 molecular sieves was higher than that over SAPO-11 which could be due to the partial pore blocking in MeAPO-11 and MeAPSO-11 due to some extraframework metal ions. 1,2,4-Trimethyl benzene was the only disproportionation product observed.

6.3.2 Transformation of methanol to hydrocarbons

Transformation of methanol to hydrocarbon over small pore SAPO-39 resulted in the formation of only lower hydrocarbons. SAPO-39 exhibited higher conversions and deactivated faster compared to MAPO-39 which could be due to the stronger Bronsted acidity of SAPO-39 than in MAPO-39.

6.3.3A Hydroisomerization of n-alkanes over SAPO-11 and SAPO-31

SAPO-11(na) and SAPO-31(na) synthesized in ethylene glycol possessed higher acidities and as a result they possessed greater isomerization activities. They also possessed greater isomerization selectivities. SAPO-11 produced more di (and multi-) branched isomers than SAPO-31 because of the larger effective diameter of its pores. Pore mouth reactions are more predominant over SAPO-31. A study of the cracking of larger alkanes suggests the presence of increasing diffusion constraints with an increase in the size of the molecule.

6.3.3B Hydroisomerization of n-hexane over MeAPO-11 and MeAPSO-11

MeAPO-11 samples exhibited similar conversions comparable to that of SAPO-11 suggesting that all the samples had nearly similar acidities. Even though the 2MP/3MP ratios in the products were close to the equilibrium values, the

MP/DMB ratios were very large and far from equilibrium values suggesting steric constraints and weak acidities of the samples.

LIST OF PUBLICATIONS

1. Preparation and Characterization of the silicoaluminophosphate SAPO-39.
   A.K. Sinha, S.G. Hegde, N.E. Jacob and S. Sivasanker, ***Zeolites***, **18** (1997) 350.

2. Hydroisomerization of n-alkanes over Pt-SAPO-11 and Pt-SAPO-31 synthesized from aqueous and non-aqueous media.
   A.K. Sinha, S. Sivasanker and P. Ratnasamy, ***Ind. Eng. Chem. Res.***, **37** (1998) 2208.

3. Synthesis, Characterization and Catalytic properties of SAPO-31 molecular sieves.
   A.K. Sinha, K.R. Kamble and S. Sivasanker, ***Stud. Surf. Sc. and Catal.*, 113** (1998) 659.

4. Hydroconversion of n-hexane over Pt-SAPO-31 and Pt-SAPO-11.
   A.K. Sinha and S. Sivasanker, ***Catalysis Today*** (In press).

5. Influence of synthesis methods on the acidic and catalytic properties of SAPO molecular sieves.
   S. Sivasanker and **A.K. Sinha**, ***National Seminar on Advances in Catalysis***, 9th May, 1998, p.21.

6. Synthesis, Characterization and Catalytic properties of SAPO-11.
   A.K. Sinha and S. Sivasanker, ***National Workshop on Catalysis***, Trivendrum, India, December, (1997), p.71.

7. Isomerization of long - chain hydrocarbons over SAPO-11: Application in the production of lube base oils.
   A.K. Sinha, K.J. Waghmare, K.R. Kamble, S. Sivasanker, A. Meenakshisundaram and K.S. Balaraman, ***14th National Symposium on Catalysis***, December (1998).

8. Crystallization of SAPO-11 and SAPO-31 from non-aqueous medium.
   A.K. Sinha and S. Sivasanker, ***Catalysis Letters*** (communicated).

9. An improved method for the synthesis of SAPO-5, SAPO-11 and SAPO-31.
   A.K. Sinha, S. Sainkar and S. Sivasanker, ***Microporous and Mesoporous Materials***, (communicated).

10. Transformation of n-hexane over microporous molecular sieves : studies over MeAPO-11 and MeAPSO-11.
    A.K. Sinha, S. Kaushik and S. Sivasanker, ***React. Kinet. Catal. Lett.*** (communicated).

11. Location of Mn in MnAPO-11: influence of synthesis from aqueous and non-aqueous media.
A.K. Sinha, D.Srinivas and S.Sivasanker, **Catalysis Letters**, (communicated)

PATENT:

(1) An improved process for the preparation of silicoaluminophosphate molecular sieve, **A.K. Sinha** and S. Sivasanker, ***Indian Patent*** (submitted).